INVESTIGATING DRUG INTERACTIONS: FROM THERMODYNAMIC DRIVING FORCES OF LIGAND BINDING TO *IN VIVO* MULTIPHOTON MICROSCOPY OF CHEMOTHERAPY DRUG INTRINSIC FLUORESCENCE

A Dissertation

Presented to the Faculty of the Graduate School

of Cornell University

in Partial Fulfillment of the Requirements for the Degree of

Doctor of Philosophy

by

Bethsabe Romero

January 2013

INVESTIGATING DRUG INTERACTIONS FROM THERMODYNAMIC DRIVING FORCES OF LIGAND BINDING TO *IN VIVO* MULTIPHOTON IMAGING OF DRUG INTRINSIC FLUORESCENCE

Bethsabe Romero, Ph.D.

Cornell University 2013

In 1905, Langley introduced the concept of a “receptive substance”. He theorized these substances were different in different species and together with the findings of Paul Ehrlich and A.J. Clark the field of receptor theory was born. Since then, biological, biophysical and biochemical methods of investigation have led us to identify not only “substances” but also their molecular targets, how they’re involved in physiological mechanisms, and the roles they play when a disease state develops. Pharmacological interactions can be dissected into basic thermodynamic forces that contribute to drug binding to receptor targets. Here we investigate the driving forces of ligand-binding to a soluble protein, GluA-s1s2 using displacement isothermal titration calorimetry. Langley was correct in his theory about the diversity of substances, and we exploit this diversity by investigating the effects of cocaine and cocaine metabolites on several neuronal nACh receptor subtypes using two-electrode voltage clamp and the *Xenopus laevis* oocyte expression system. Lastly, we utilize the intrinsic fluorescence of a chemotherapy drug to investigate its potential as a diagnostic tool *in vivo*.

BIOGRAPHICAL SKETCH

Bethsabe Romero was born in 1975 in the small city of Hawaiian Gardens, which is nowhere near Hawaii. She was raised alongside five siblings by two ambitious and loving parents who immigrated to southern California from the small towns of Jalpa and Huanusco, Mexico. Bethsabe's mother Eva, was courted by many young men in the town, but she daydreamed about moving to a big city in another country far, far away. She refused to marry a local farmer and continue scrubbing laundry against stones in the river. Bethsabe's father, Raul, also had big dreams. He taught Bethsabe the values of persistence, hard work and troubleshooting. Before becoming a U.S. citizen, he crossed the U.S./Mexican Border illegally three times in one night. Each time he was caught (by the same officer), the officer would ask incredulously, "Don't you get tired of trying"? It was this spirit of persistence and stubbornness in the face of defeat that sustained the author throughout graduate school.

Despite a 6th grade education, Bethsabe's mother understood the importance of assimilation. She treated her children to McDonald's every Friday evening, and allowed the author and her siblings to dance like monkeys on the couches while she played Blondie, Village People and Billy Joel records. During the California summers they attended Holy Mass every morning, and rode their Schwinns until sundown when it was time to pray the Holy Rosary. It was at this time the author learned college was the place with really big pools where you could swim for a dollar and buy a snack

with a quarter. The author taught herself to read when she was four years old. When she wasn't in the back yard torturing insects and building guns to play "Vietnam" with her brothers, she was immersed in a book. As she grew older she enjoyed the challenge of completing her older siblings' homework.

Bethsabe attended St. Paul High School where she was captain of the cheerleading squad and excelled in all of her honors and advanced placement courses. She loved anatomy lab. In the evenings she would escape to her bedroom to flip through university recruiting materials and daydreamed about attending a university far, far away. Instead, she attended UCLA where her interest in neuroscience came alive due to dynamic faculty members and student research projects. She felt at home in the lab and foolishly believed her mentors who said graduate school was "easy".

Upon visiting Cornell for the first time, Bethsabe fell in love with the cold weather and the waterfalls. The graduate school years were busy as Bethsabe became involved in departmental recruiting, administrative committees, science outreach and mental health advocacy. In the laboratory, experiments seemed to follow the all-or-none principle of neuronal conduction. Research oscillated between times of experimental failure and despair, followed by jubilation as the result of data and comforting potluck dinners with friends. Bethsabe's time in Ithaca was filled with learning, growth and healing. Of all the lessons she learned throughout

her graduate training, there was one that emerged as the most critical and poignant of all: after a good fall, despite bloody hands and knees, get up and come out swinging.

For My Grandparents

Isidoro Medina and Felicitas Romero,

Leon Romero and Josefina Salazar,

And

My nina, Lucy Salazar Romero,

May they rest in the loving peace of Christ.

ACKNOWLEDGMENTS

First and foremost I need to acknowledge and thank my advisor, Robert E. Oswald for being patient, understanding, and motivating me throughout this entire process. Words cannot express my gratitude. I am also very grateful to my committee members Drs. George Hess, Manfred Lindau, Linda Nicholson, and Greg Weiland who unknowingly taught me some critical lessons. I learned we should look to nature to understand scientific questions; that saying nothing is sometimes the best answer; resonance can be found when you least expect it, and I should've learned to play rugby. I acknowledge my additional committee member Dr. Warren Zipfel and his wife Dr. Becky Williams for hiring me and believing in me. My short time in the Zipfel/Williams research group was filled with many exciting discoveries, and fun and funny friendships. I acknowledge Avtar Singh for asking me daily if I was finished with my dissertation. Avtar's expansive wisdom gave me perspective when I needed it most. I acknowledge Dr. Ahmed H. Ahmed for his kindness, for treating me like a daughter and always respecting me. I acknowledge my lab mates and pseudo little sisters, Dr. Kinning Poon and Madeline Martinez. Sometimes I found them intolerable. Other times, I was shocked and humbled by their limitless kindness and compassion towards me. I learned how to perfectly prepare baby bok choy and much to my dismay, that I'm a kitchen Nazi. We giggled and laughed out loud, fought tears and ate juicy bison burgers. I acknowledge Drs. Jayasri and Ram who opened their home to me countless

times for tasty dinners and homemade chai over academic discussions. Jayasri has been a loyal friend to the end. I acknowledge Dr. Becky Marquez. Our dinner dates of Thai food and discussing dating will be one of my fondest memories of grad school. Thanks for forging the way, mentoring me, and bolstering my self-worth. I acknowledge Bergur Ragnarsson (Reykjavik, Iceland) who watched over me like a caring father when I had pneumonia and a fever of 106°F. I acknowledge Dr. Francesco Boldrin (Venice, Italy) who dragged me out of depressive periods with wine, good cheese, and even better pasta. I acknowledge Dr. Oliver Purwin aka Schnitz (Frankfurt, Germany) who countlessly comforted me with the simple phrase, "it's okay, honey bunny". I acknowledge Michael Letchworth who was my partner in crime and eating adventures while writing my dissertation. I acknowledge Dr. Fr. Dan McMullin, Dr. Sandy Bem and Dr. Robyn Robinson for spiritual direction, keeping me relatively sane, and helping me appreciate the arduous Ph.D. process. They were a constant reminder of my strength when I felt worthless and frail. I acknowledge my friends in the Cornell Catholic Community who are too numerous to name. I acknowledge my family: Mom, Dad, Raul, Eva, Danny, Julio, Emily, Jocelyn, Elijah, Ulysses, Soraya, Edgar and baby Abraham. I acknowledge my adorable nephew, Xavier, who is no longer a "bebito"—and helped me through a very difficult time period. My numerous visits home reminded me of the importance of my education. You guys inspire me and drive me crazy. You are what matters most in this world. The best part of living so far away from

home is that there is always a lobster and carne asada dinner awaiting me. I acknowledge my Nina Lucy who told me I was “purty” and had silky hair like a Barbie even though I was a fat and ugly kid. After losing her battle with cancer, she inspired me to move across the country to attend graduate school at Cornell. I acknowledge Dr. Caroline Coffey whose tragic death reminded me that the only way to live is with a fiery soul. I acknowledge my buddies St. Josemaria Escriva, St. Francis of Assisi, St. Padre Pio, St. Anthony, St. Teresa of Avila, St. Therese of Lisieux, St. Mother Cabrini, St. Marianne Cope, St. Joan of Arc, the Infant of Prague, and Fr. Bob Smith who were my pillars of strength and hope. Lastly, when there was no light at the end of a tunnel, nor a tunnel of any kind, I enlisted in divine intervention.

TABLE OF CONTENTS

Biographical Sketch	iii
Dedication	vi
Acknowledgments	vii
Table of Contents	x
List of Figures	xii
List of Tables	xiv
CHAPTER 1. Introduction	1
1.1 Ionotropic Glutamate Receptors	2
1.2 Neuronal Nicotinic Acetylcholine Receptors	5
1.3 *In vivo* Multiphoton Microscopy (MPM) and Second Harmonic Generation to Study Cancer	8
References	11
CHAPTER 2. Thermodynamic Forces that Drive Antagonist and Partial Agonist Binding to GluA2-s1s2.	16
Abstract	17
Introduction	18
Methods	26
Results	31
Discussion	40
Conclusion	55
References	58
CHAPTER 3. Electrophysiological Studies of Cocaine and Cocaine derivatives on Neuronal Nicotinic Acetylcholine Receptors.	63
Abstract	64

Introduction 66
Methods 70
Results 73
Discussion 79
Conclusion 85
References 86
CHAPTER 4. Investigating the use of Irinotecan as a tumor contrast agent in an *in vivo* Murine Mammary Cancer Model. 92
Abstract 93
Introduction 94
Methods 99
Results 105
Discussion 114
Conclusion 118
References 119
CHAPTER 5. Future Directions 122
5.1. Continuing studies of GluA2-s1s2 123
5.2. Future benzoylecgonine studies on neuronal nAChRs 125
5.3. Future in vitro Irinotecan experiments 126
References 128

LIST OF FIGURES

CHAPTER 1. Introduction

Figure 1.1 Glutamate Receptor Schematic.

Figure 1.2 Nicotinic Acetylcholine Receptor Schematic.

CHAPTER 2. Thermodynamic Studies of Antagonist and Willardiine Partial Agonist Binding to GluA2-s1s2.

Figure 2.1 GluA2 Antagonists, Glutamate, and the parent compound Willardiine.

Figure 2.2 Glutamate Displacement by DNQX.

Figure 2.3 Representative Isotherms for GluA2-s1s2 Displacement Experiments.

Figure 2.4 Representative Isotherms for Glutamate Displacement by Willardiine Derivatives.

Figure 2.5 Glutamate Displacement by Iodowillardiine is Endothermic.

Figure 2.6 Representative Isotherms for Glutamate Displacement by Iodowillardiine at 5°C, 10°C, and 15°C.

Figure 2.7. Binding pocket nomenclature.

Figure 2.8. Conserved interactions between glutamate and FW and the binding pocket of GluA2.

Figure 2.9. Nitrowillardiine forms interactions that may stabilize the closed-lobe conformation.

CHAPTER 3. Electrophysiological Studies of Cocaine and Cocaine derivatives on Neuronal Nicotinic Acetylcholine Receptor subtypes.

Figure 3.1 Cocaine Metabolic Pathway.

Figure 3.2 Oocyte Control and Inhibitory Responses of nAChR subtype α3β4.

Figure 3.3 Concentration Dependence of Cocaine Inhibition of nAChR subtypes, α4β2, α3β4, and α4β4.

Figure 3.4 Concentration Dependence of Cocaine Methiodide Inhibition of nAChR subtypes α4β2, α3β4, and α4β4.

Figure 3.5 Voltage-dependence of cocaine methiodide inhibition of α3β4 and cocaine inhibition of α4β2.

Figure 3.6 Cocaine, Cocaine Methiodide, and Benzoylecgonine inhibition of α4β2 nAChRs.

CHAPTER 4. Investigating the use of Irinotecan as a tumor contrast agent in an *in vivo* Murine Mammary Cancer Model.

Figure 4.1. Irinotecan structure and action cross-section.

Figure 4.2 Mammary Gland Transplantation of MCN2 cells.

Figure 4.3 *In vivo* Imaging Chamber.

Figure 4.4. Absorption normalized fluorescence spectra of Irinotecan and SN-38 at low and high pH.

Figure 4.5. *In vivo* Irinotecan intrinsic fluorescence in an MCN2-derived carcinoma.

Figure 4.6. *In vivo* Irinotecan intrinsic fluorescence in a mammary gland control sample.

Figure 4.7. Raw Data for *in vivo* tumor imaging after irinotecan injection.

Figure 4.8. Irinotecan intrinsic fluorescence in mammary carcinomas and mammary gland controls.

Figure 4.9. *In vivo* single cell intensity

Figure 4.10. Irinotecan intensity is concentration dependent *in vitro*.

Figure 4.11. *In vitro* Irinotecan intrinsic fluorescence time series.

Figure 4.12. General Overview of Irinotecan Metabolism.

LIST OF TABLES

CHAPTER 2. Thermodynamic Studies of Antagonist and Willardiine Partial Agonist Binding to GluA2-s1s2.

Table 2.1. Experimental Titration Conditions

Table 2.2. Antagonist binding parameters for Figure 2.3.

Table 2.3. Antagonist binding parameter summary.

Table 2.4. Thermodynamic Binding Parameters of Willardiine Derivatives as a Result of Glutamate Displacement at 10°C.

Table 2.5. Thermodynamic Binding Parameters of Glutamate Displacement by Iodowillardiine.

CHAPTER 3. Electrophysiological Studies of Cocaine and Cocaine derivatives on Neuronal Nicotinic Acetylcholine Receptor subtypes.

Table 3.1. IC_{50} values for cocaine and cocaine methiodide inhibition.

CHAPTER I.

Introduction

Pharmacological development and intervention has been facilitated by the development and use of an enormous number biochemical and biophysical techniques. We explore thermodynamic forces involved in ligand binding through isothermal titration calorimetry. We investigate the effect of cocaine and cocaine derivatives through two-voltage clamp electrophysiology. Lastly, we explore the ability of an anti-cancer drug as a tumor contrast agent using multiphoton microscopy. All three studies were performed in an effort to understand the underlying biological mechanisms involved in drug interactions which may lead to drug discoveries and improved pharmacological treatments.

1.1 Ionotropic Glutamate Receptors

Ionotropic glutamate receptors (iGluRs) are membrane-bound ligand-gated ion channels that mediate most excitatory synaptic transmission in the central nervous system (Watkins & Evans, 1981; Mayer & Westbrook, 1987; Collingridge & Lester, 1989). Initially, glutamate activation was thought to be a non-specific effect since most central neurons responded to glutamate (Curtis *et al.*, 1959). Later it was discovered that glutamate actually activates distinct receptor subtypes (Ascher and Nowak, 1988; Collingridge and Lester, 1989; Monaghan *et al.*, 1989).

Glutamate receptors can be structurally and pharmacologically categorized. Those consisting of four subunits organized around a central ion channel pore are also known as ionotropic glutamate receptors (iGluRs) (Dingledine *et al.*, 1999). Glutamate receptors that activate G-proteins are

known as metabotropic glutamate receptors (mGluRs) and show structural homology to the extracellular ligand-binding domains of iGluRs (O'Hara *et al.*, 1993). Glutamate receptors are categorized by agonist activation into three main groups known as kainate, NMDA (N-methyl-D-aspartic acid) and AMPA ((*S*)-*a*-amino-3-hydroxy-5-methylisoxazole-4-propionicacid) receptors.

AMPA receptors are encoded by three gene families and composed of GluA1-GluA4 subunits which assemble as tetramers. Each receptor subunit is composed of a large extracellular domain including the ligand-binding domains s1 and s2 (D1 and D2), three transmembrane helices, a pore helix, and an intracellular C-terminal domain (Mayer, 2011) (Figure 1.1).

The development of selective glutamate receptor antagonists was instrumental in identifying subtypes of glutamate receptors (Evans *et al.*, 1979), and an explosion in glutamate receptor studies followed over the next 30 years. Since then, glutamate receptors have been associated with several neurological disorders such as stroke, dementia, schizophrenia, Parkinson's disease and Alzheimer's disease (Mattson *et al.*, 1993; Sensi *et al.*, 2011; Ogden and Traynelis, 2011). The study of glutamate receptor antagonists as therapeutic tools emerged soon after. Lamotrigine, a glutamate receptor antagonist, has enjoyed prolonged success as an anticonvulsant and is currently being used off-label to treat bipolar disorders I and II, depression, and post-traumatic stress disorder to name a few, illustrating the importance of continued study of glutamate receptor antagonists (Gildengers, *et al.,* 2012; Zavodnick and Ali, 2012). Recently, the focus of

glutamate receptors as drug targets has shifted to the study of modulators (Ahmed and Oswald, 2010; Ahmed *et al.*, 2010; Thewlis *et al.*, 2010; Pøhlsgaard *et al.*, 2011; Krintel *et al.*, 2012) which may contribute to the development of drugs that fine-tune neuronal transmission.

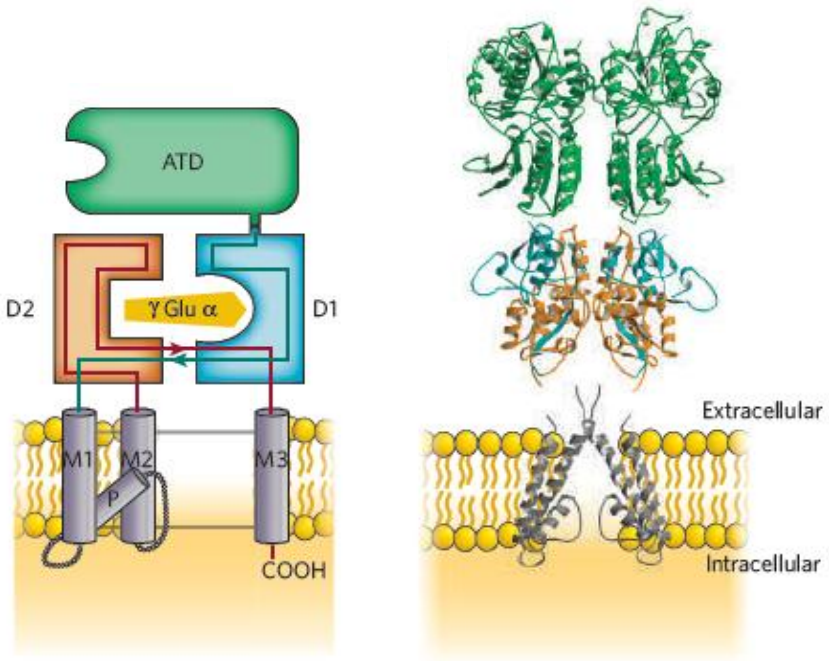

Figure 1.1 Glutamate Receptor Schematic. Modular diagram of a glutamate receptor subunit is illustrated. The amino terminal domain is in green, domains 2 and 1 of the ligand-binding domain are in orange and cyan, while the transmembrane segments are in grey with P representing the pore loop (modified with permission from Mayer 2006).

One of the challenges in studying iGluRs is that they are transmembrane receptors. Because 85% of the receptor structure is extracellular (Mayer, 2011), studies of the soluble ligand binding domain have led to a greater understanding of glutamate receptor structure and function through NMR and crystallographic studies. Interestingly, only a

handful of studies have utilized isothermal titration calorimetry to study glutamate receptors (Madden *et al.*, 2000; Kasper *et al.*, 2006; Ahmed *et al.*, 2009). The construction of the first ice calorimeter dates to 1782 by Antoine Lavoisier and Pierre-Simon Laplace; and since then, the development of isothermal titration calorimetry (ITC) has led to an incredibly powerful quantitative technique. In a single, well-planned and executed experiment one may determine several thermodynamic binding parameters. Furthermore, displacement experiments may be designed to circumvent issues involving molecular targets which are unstable in the presence of a ligand. While we cannot use ITC to directly study ion channel function, we can identify the relative contributions of thermodynamic parameters to the steps which initiate ion channel opening. Furthermore, identifying thermodynamic driving forces of ligand binding can guide us towards drug affinity optimization, and an understanding of how the energy of ligand binding translates to ion channel opening.

1.2 Neuronal Nicotinic Acetylcholine Receptors

Acetylcholine receptors (AChRs) are transmembrane receptors activated by the neurotransmitter acetylcholine (ACh). The two major subtypes of cholinergic receptors consist of metabotropic muscarinic receptors and ionotropic nicotinic receptors (Albuquerque *et al.* 2009). Metabotropic receptors are second messenger, G-protein coupled receptors capable of modulating cellular homeostasis of phospholipase C, inositol

triphosphate, cAMP and Ca^{2+} through slow activation (millisecond to second timescale) (Eglen, 2005). Ionotropic nAChR activation occurs on a faster timescale (micro- to sub microsecond) and they are permeable to monovalent (K^+, Na^+) and divalent (Ca^{2+}) cations.

Nicotinic acetylcholine receptors (nAChRs) are ionotropic and composed of five subunits organized around a central ion channel pore (Figure 1.2). Each subunit consists of a large (~200 amino acids) extracellular N-terminal domain with a cysteine-loop, three transmembrane domains, a variable cytoplasmic loop, and a fourth transmembrane domain with a short C-terminal sequence. Neuronal nAChRs may be homomeric or heteromeric subtypes based on their subunit composition. There are 12 types of vertebrate neuronal ACh subunits, α2-α10 and β2-β4 (Karlin, 2002). Initially these subtypes were described as neuronal because they were cloned from neuronal-like cells and brain-derived cDNA libraries. Since then, many neuronal nAChR subunits have been discovered in non-neuronal cell types of the body such as tegumental cells that line external and internal body surfaces (Conti-Fine *et al.*, 2000).

Nicotinic receptors have been intensely studied for over 40 years (Changeux, 2009). They are the initial molecular targets of the nicotine contained in tobacco smoke and 50% of individuals who smoke from early adulthood throughout their lifetimes are expected to die from diseases associated with smoking (World Health Organization, 2011). Two neuronal pathways have been identified which mediate the reinforcement and

withdrawal symptoms associated with nicotine addiction. The α4, β2 and α6 subunits are considered key players in the mesocorticolimbic pathway, which includes projections from the ventral tegmental area to the nucleus accumbens (Di Chiara 1999; Wise 2000; Berke *et al.*, 2000; Dani *et al.*, 2011). The α3, α5 and β4 subunits play critical roles in regulating nicotine dosing and withdrawal symptoms in the epithalamic habenular complex and the interpeduncular nucleus which are bridged together by the fasciculus retroflexus (Salas *et al.*, 2003; Salas *et al.*, 2004; Salas *et al.*, 2009). Other drugs of abuse such as cocaine can interact with nAChRs (Karpen *et al.*, 1982; Francis *et al.*, 2000; Francis *et al.*, 2001) highlighting the importance of continued study of this receptor superfamily.

Two-electrode voltage clamp can be a particularly powerful technique to evaluate drug interactions when coupled with the *Xenopus laevis* oocyte expression system. Biological membranes function as capacitors in which the potential across membranes may be controlled by voltage-clamping. In two-electrode voltage clamp, two electrodes which function as a voltage sensor and a current injector are inserted into an oocyte. If there is a change in the membrane potential as a result of drug application, current is injected into the oocyte to return to the holding membrane potential. Two-electrode voltage clamp provides a very exciting method by which to investigate how drugs affect ionic transmission when they interact with transmembrane receptors such as ligand-gated ion channels.

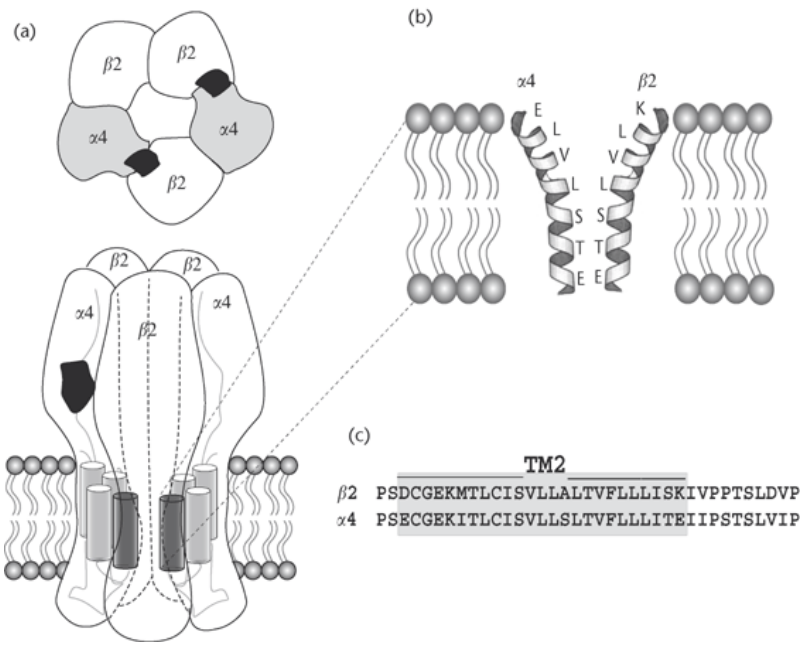

Figure 1.2 Nicotinic Acetylcholine Receptor Schematic including (a.) top view of an α4β2 receptor and side view in the membrane, (b.) magnified view of two α-helices of which face the inner ion channel pore, and (c.) alignment of amino acid sequences which line the pore of the ion channel for the α4 and β2 subunits (modified with permission from Hogg and Bertrand, 2007).

1.3 *In vivo* Multiphoton Microscopy (MPM) and Second Harmonic Generation (SHG) to Study Cancer

Multiphoton microscopy (MPM) is a non-linear optical imaging process by which two photons of the same energy simultaneously excite a molecule leading to the emission of a single photon of higher energy (Denk *et al.*, 1990). Second Harmonic Generation (SHG) is also non-linear, however, in SHG photons are not absorbed by the specimen but instead scattered and photons having twice the energy of the incident photon are collected as signal as long as the specimen is non-centrosymmetric. Collagen is an example of a biological structure which produces a strong SHG signal in

MPM imaging (Zipfel *et al.*, 2003). We've begun to explore the use of MPM and collagen SHG with chemotherapy drugs which exhibit strong intrinsic fluorescence.

Intrinsic fluorescence may be due to intracellular or extracellular molecules. Intracellular sources of intrinsic fluorescence are primarily due to NAD(P)H, flavins, retinol and indoleamines such as serotonin and melatonin while extracellular fluorescence is due to structural proteins such as elastin, collagen and keratin. The intrinsic fluorescence of tissue fluorophores can be attributed to aromatic amino acids such as tryptophan, tyrosine and phenylalanine (Zipfel *et al.*, 2003). In translational cancer studies, clinical investigators have searched for intrinsic molecular markers associated with different types of cancer. Several studies have evaluated the reorganization of collagen during cancer development as it is a key structural component of the extracellular matrix (Brown *et al*, 2003; Han *et al.*, 2008; Hopland *et al.*, 2008; Wolf *et al.*, 2009).

While MPM has been used to investigate biological processes associated with cancer progression including the tumor microenvironment, angiogenesis, and tumor metabolism, most pre-clinical studies have been performed on biopsied samples. Only a handful of studies have progressed towards MPM imaging *in vivo* to investigate cancer progression (Brown *et al.*, 2001; Ahmed *et al.*, 2002; Williams *et al.*, 2010). Moreover, chemotherapy drugs which exhibit intrinsic fluorescence may be used to identify tumor tissue and tumor margins *in vivo,* but may be dependent upon tissue

specificity. Chemotherapy drugs exhibiting intrinsic fluorescence may also be advantageous in studying *in vivo* drug metabolism and cellular localization of metabolites. Using both MPM and SHG simultaneously, we can directly visualize cell morphology, cell metabolism, and alterations due to diseased states.

REFERENCES

Ahmed AH, Thompson MD, Fenwick MK, Romero B, Loh AP, Jane DE, Sondermann H, Oswald RE. Mechanisms of antagonism of the GluR2 AMPA receptor: structure and dynamics of the complex of two willardiine antagonists with the glutamate binding domain. *Biochemistry.* 2009 May 12;48(18):3894-903.

Ahmed AH, Oswald RE. Piracetam defines a new binding site for allosteric modulators of alpha-amino-3-hydroxy-5-methyl-4-isoxazole-propionic acid (AMPA) receptors. *J Med Chem.* 2010 Mar 11;53(5):2197-203.

Ahmed AH, Ptak CP, Oswald RE. Molecular mechanism of flop selectivity and subsite recognition for an AMPA receptor allosteric modulator: structures of GluA2 and GluA3 in complexes with PEPA. *Biochemistry.* 2010 Apr 6;49(13):2843-50.

Ahmed F, Wyckoff J, Lin EY, Wang W, Wang Y, Hennighausen L, Miyazaki J, Jones J, Pollard JW, Condeelis JS, Segall JE. GFP expression in the mammary gland for imaging of mammary tumor cells in transgenic mice. *Cancer Res.* 2002 Dec 15;62(24):7166-9.

Albuquerque EX, Pereira EF, Alkondon M, Rogers SW. Mammalian nicotinic acetylcholine receptors: from structure to function. *Physiol Rev.* 2009 Jan;89 (1):73-120.

Ascher P, Nowak L. Quisqualate- and kainate-activated channels in mouse central neurones in culture. *J Physiol.* 1988 May;399: 227-45.

Berke JD, Hyman SE. Addiction, dopamine, and the molecular mechanisms of memory. *Neuron.* 2000; 25:515–32.

Brown EB, Campbell RB, Tsuzuki Y, Xu L, Carmeliet P, Fukumura D, Jain RK. In vivo measurement of gene expression, angiogenesis and physiological function in tumors using multiphoton laser scanning microscopy. *Nat Med.* 2001 Jul;7(7):864-8.

Brown E, McKee T, diTomaso E, Pluen A, Seed B, Boucher Y, Jain RK. Dynamic imaging of collagen and its modulation in tumors in vivo using second-harmonic generation. *Nat Med.* 2003 Jun;9(6):796-800.

Changeux JP. Nicotinic receptors and nicotine addiction. *C R Biol.* 2009 May;332 (5):421-5.

Collingridge GL, Lester RA. Excitatory amino acid receptors in the vertebrate central nervous system. *Pharmacol Rev.* 1989 Jun;41(2):143-210.

Conti-Fine BM, Navaneetham D, Lei S, Maus AD. Neuronal nicotinic receptors in non-neuronal cells: new mediators of tobacco toxicity? *Eur J Pharmacol* 393: 279–294, 2000.

Cooper E, Couturier S, Ballivet M. Pentameric structure and subunit stoichiometry of a neuronal nicotinic acetylcholine receptor. *Nature.* 1991 Mar 21;350(6315):235-8.

Curtis DR, Phillis JW, Watkins JC. Chemical excitation of spinal neurones. *Nature.* 1959 Feb 28;183(4661):611-2.

Dani JA, Jenson D, Broussard JI, De Biasi M. Neurophysiology of Nicotine Addiction. *J Addict Res Ther.* 2011 Apr 20;S1(1). pii: 001.

Denk W, Strickler JH, Webb WW. Two-photon laser scanning fluorescence microscopy. *Science.* 1990 Apr 6;248 (4951):73-6.

Di Chiara G. Drug addiction as dopamine-dependent associative learning disorder. *Eur J Pharmacol.* 1999; 375:13–30.

Dingledine R. New wave of non-NMDA excitatory amino acid receptors. *Trends Pharmacol Sci.* 1991 Oct;12 (10):360-2. Review.

Eglen RM. Muscarinic receptor subtype pharmacology and physiology. *Prog Med Chem.* 2005;43:105-36.

Elgoyhen AB, Johnson DS, Boulter J, Vetter DE, Heinemann S. Alpha 9: an acetylcholine receptor with novel pharmacological properties expressed in rat cochlear hair cells. *Cell.* 1994 Nov 18;79 (4):705-15.

Elgoyhen AB, Vetter DE, Katz E, Rothlin CV, Heinemann SF, Boulter J. alpha10: a determinant of nicotinic cholinergic receptor function in mammalian vestibular and cochlear mechanosensory hair cells. *Proc Natl Acad Sci U S A.* 2001 Mar 13;98 (6):3501-6.

Evans RH, Francis AA, Hunt K, Oakes DJ, Watkins JC. Antagonism of excitatory amino acid-induced responses and of synaptic excitation in the isolated spinal cord of the frog. *Br J Pharmacol.* 1979 Dec;67(4):591-603.

Francis MM, Vazquez RW, Papke RL, Oswald RE. Subtype-selective inhibition of neuronal nicotinic acetylcholine receptors by cocaine is determined by the alpha4 and beta4 subunits. *Mol Pharmacol.* 2000 Jul;58(1):109-19.

Francis MM, Cheng EY, Weiland GA, Oswald RE. Specific activation of the alpha 7 nicotinic acetylcholine receptor by a quaternary analog of cocaine. *Mol Pharmacol.* 2001 Jul;60(1):71-9.

Gildengers A, Tatsuoka C, Bialko C, Cassidy KA, Al Jurdi RK, Gyulai L, Mulsant BH, Young RC, Sajatovic M. Correlates of treatment response in depressed older adults with bipolar disorder. *J Geriatr Psychiatry Neurol.* 2012 Mar; 25(1):37-42.

Jean-Pierre Changeux. Allosteric Receptors: From Electric Organ to Cognition. *Annu. Rev. Pharmacol. Toxicol.* 2010. 50:1–38.

Han X, Burke RM, Zettel ML, Tang P, Brown EB. Second harmonic properties of tumor collagen: determining the structural relationship between reactive stroma and healthy stroma. *Opt Express.* 2008 Feb 4;16(3):1846-59.

Hogg RC and Bertrand D. Receptors and Human Disorders. Published Online: 16 APR 2007. DOI: 10.1002/9780470015902.a0005164.pub2

Karlin A. Emerging structure of the nicotinic acetylcholine receptors. *Nat Rev Neurosci.* 2002 Feb;3(2):102-14.

Karpen JW, Aoshima H, Abood LG, Hess GP. Cocaine and phencyclidine inhibition of the acetylcholine receptor: analysis of the mechanisms of action based on measurements of ion flux in the millisecond-to-minute time region. *Proc Natl Acad Sci* U S A. 1982 Apr; 79(8):2509-13.

Kasper C, Pickering DS, Mirza O, Olsen L, Kristensen AS, Greenwood JR, Liljefors T, Schousboe A, Wätjen F, Gajhede M, Sigurskjold BW, Kastrup JS. The structure of a mixed GluR2 ligand-binding core dimer in complex with (S)-glutamate and the antagonist (S)-NS1209. *J Mol Biol.* 2006 Apr 7;357(4):1184-201.

Krintel C, Frydenvang K, Olsen L, Kristensen MT, de Barrios O, Naur P, Francotte P, Pirotte B, Gajhede M, Kastrup JS. Thermodynamics and structural analysis of positive allosteric modulation of the ionotropic glutamate receptor GluA2. *Biochem J.* 2012 Jan 1;441(1):173-8.

Le Novère N, Zoli M, Changeux JP. Neuronal nicotinic receptor alpha 6 subunit mRNA is selectively concentrated in catecholaminergic nuclei of the rat brain. *Eur J Neurosci.* 1996 Nov;8(11):2428-39.

Madden DR, Abele R, Andersson A, Keinänen K. Large-scale expression and thermodynamic characterization of a glutamate receptor agonist-binding domain. *Eur J Biochem.* 2000 Jul;267(13):4281-9.

Mattson MP, Rydel RE, Lieberburg I, and Smith-Swintosky VL. Altered calcium signaling and neuronal injury: stroke and Alzheimer's disease as examples. *Ann N Y Acad Sci.* 1993 May 28; 679:1-21.

Mayer ML. Glutamate receptors at atomic resolution. *Nature.* 2006 Mar 23; Vol 440: 456-452.

Mayer ML. Emerging models of glutamate receptor ion channel structure and function. *Structure.* 2011 Oct 12;19(10):1370-80.

Mayer ML & Westbrook GL. The physiology of excitatory amino acids in the vertebrate central nervous system.1987. *Prog. Neurobiol.* 28, 197-276.

Monaghan DT, Olverman HJ, Nguyen L, Watkins JC, Cotman CW. Two classes of N-methyl-D-aspartate recognition sites: differential distribution and differential regulation by glycine. *Proc Natl Acad Sci U S A.* 1988 Dec;85 (24):9836-40.

Ogden KK, Traynelis SF. New advances in NMDA receptor pharmacology. *Trends Pharmacol Sci.* 2011 Dec; 32(12):726-33. Epub 2011 Oct 11. Review.

O'Hara PJ, Sheppard PO, Thøgersen H, Venezia D, Haldeman BA, McGrane V, Houamed KM, Thomsen C, Gilbert TL, Mulvihill ER. The ligand-binding domain in metabotropic glutamate receptors is related to bacterial periplasmic binding proteins. *Neuron.* 1993 Jul;11 (1):41-52.

Pøhlsgaard J, Frydenvang K, Madsen U, Kastrup JS. Lessons from more than 80 structures of the GluA2 ligand-binding domain in complex with agonists, antagonists and allosteric modulators. *Neuropharmacology.* 2011 Jan;60 (1):135-50.

Ramirez-Latorre J, Yu CR, Qu X, Perin F, Karlin A, Role L. Functional contributions of alpha5 subunit to neuronal acetylcholine receptor channels. *Nature.* 1996 Mar 28;380(6572):347-51.

Salas R, Cook KD, Bassetto L, De Biasi M. The alpha3 and beta4 nicotinic acetylcholine receptor subunits are necessary for nicotine-induced seizures and hypolocomotion in mice. *Neuropharmacology*. 2004; 47:401–407.

Salas R, Orr-Urtreger A, Broide RS, Beaudet A, Paylor R, et al. The nicotinic acetylcholine receptor subunit alpha 5 mediates short-term effects of nicotine in vivo. *Mol Pharmacol.* 2003; 63:1059–1066.

Salas R, Pieri F, De Biasi M. Decreased signs of nicotine withdrawal in mice null for the beta4 nicotinic acetylcholine receptor subunit. *J Neurosci*. 2004; 24:10035–10039.

Salas R, Sturm R, Boulter J, De Biasi M. Nicotinic receptors in the habenulo-interpeduncular system are necessary for nicotine withdrawal in mice. *J Neurosci.* 2009; 29:3014–3018.
Sensi SL, Paoletti P, Koh JY, Aizenman E, Bush AI, Hershfinkel MJ. The neurophysiology and pathology of brain zinc. *Neurosci.* 2011 Nov 9; 31(45):16076-85.

Thewlis KM, Aldegheri L, Harries MH, Mookherjee C, Oliosi B, Ward SE. N-substituted pyrrolidines and tetrahydrofurans as novel AMPAR positive modulators. *Bioorg Med Chem Lett.* 2010 Dec 1;20(23):7116-9.

Vernallis AB, Conroy WG, Berg DK. Neurons assemble acetylcholine receptors with as many as three kinds of subunits while maintaining subunit segregation among receptor subtypes. *Neuron.* 1993 Mar;10(3):451-64.

Watkins, JC & Evans, RH. Excitatory amino acid transmitters. *Ann. Rev. Pharmacol. Toxicol.* 1981; 21, 165-204.

Williams RM, Flesken-Nikitin A, Ellenson LH, Connolly DC, Hamilton TC, Nikitin AY, Zipfel WR. Strategies for high-resolution imaging of epithelial ovarian cancer by laparoscopic nonlinear microscopy. *Transl Oncol.* 2010 Jun 1;3(3):181-94.

Wise RA. Interactions between medial prefrontal cortex and mesolimbic components of brain reward circuitry. *Prog Brain Res.* 2000; 126:255–262.

Wolf K, Alexander S, Schacht V, Coussens LM, von Andrian UH, van Rheenen J, Deryugina E, Friedl P. Collagen-based cell migration models in vitro and in vivo. *Semin Cell Dev Biol.* 2009 Oct;20 (8):931-41.

World Health Organization, 2011.
http://www.who.int/tobacco/global_report/en/index.html

Zavodnick AD, Ali R. Lamotrigine in the Treatment of Unipolar Depression with and Without Comorbidities: A Literature Review. *Psychiatr Q.* 2012 Feb 10. [Epub ahead of print]

Zipfel WR, Williams RM, Christie R, Nikitin AY, Hyman BT, Webb WW. Live tissue intrinsic emission microscopy using multiphoton-excited native fluorescence and second harmonic generation. *Proc. Natl. Acad. Sci.* U S A. 2003 Jun 10; 100 (12):7075-80.

CHAPTER 2.

Thermodynamic Forces that Drive Antagonist and Partial Agonist Binding to GluA2-s1s2.

ABSTRACT

Ionotropic glutamate receptors (iGluRs) mediate fast synaptic transmission in the central nervous system (Oswald, 2004), and have been implicated in neurodegenerative diseases and epilepsy (Gillessen *et al.*, 2002) leading to the investigation of subtype specific antagonists. Here we investigate the thermodynamic driving forces of antagonist and partial agonist binding to the soluble ligand binding domain (LBD), GluA2-s1s2. Glutamate binds to the apo state of GluA4-s1s2 with favorable changes in entropy and enthalpy (Madden *et al.*, 2000). Using displacement isothermal titration calorimetry (ITC), we investigate the changes in enthalpy and entropy with the displacement of glutamate by antagonists CNQX and DNQX, and the displacement of the antagonists UBP277 and UBP282 by glutamate. Antagonist binding relative to glutamate is entropically unfavorable and enthalpically favored. We also investigate partial agonist binding relative to glutamate. With the exception of nitrowillardiine (NW), iodowillardiine (IW), fluorowillardiine (FW), and chlorowillardiine (ClW) binding relative to glutamate is entropically favorable and enthalpically unfavorable. Identifying thermodynamic driving forces of antagonist and partial agonist binding to GluA2-s1s2 may help us develop a greater understanding of how these ligands interact with a receptor family that is responsible for mediating neuronal function.

INTRODUCTION

Two major breakthroughs occurred in the mid-late 1990s which propelled the field of glutamate receptors toward its first structural perspective. The first finding, that structural similarities existed between the glutamate receptor and bacterial amino acid binding proteins (Nakanishi *et al.*, 1990; O'Hara *et al.*, 1993), led to the prediction of the kainate receptor homology model of Wo and Oswald (1994). The next breakthrough occurred a year later when Keinänen's group developed a method to express soluble forms of the GluA4 agonist binding site in sf21 (*Spodoptera frugiperda*) insect cells (Kuusinen *et al.*, 1995), however, protein expression was relatively low. A high yield protein expression system was subsequently developed by Chen and Gouaux (1997) in which they expressed a denatured form of GluA2 protein in bacteria and then refolded it into its native state. These breakthroughs led to structural determinations of GluA2-s1s2. Most significantly, the binding properties of the soluble LBD were identical to the intact transmembrane receptor—thus providing a powerful experimental tool by which to study GluA2 receptor properties and activity.

Competitive antagonists bind to the same site as agonists but fail to induce channel opening and signal propagation. High resolution crystal structures of GluA2-s1s2 bound to antagonists have led to a greater understanding about the mechanism and the structural basis of antagonist action (Armstrong and Gouaux, 2000; Hogner *et al.*, 2003; Frølund *et al.*, 2003; Kasper *et al.*, 2006; Pentikäinen *et al.*, 2006; Ritz *et al.*, 2008; Ahmed

et al., 2009). Antagonism appears to be dependent on overall lobe orientation as well as specific interactions or lack of interactions within the LBD. Some of the interactions between antagonists and amino acids within the binding domain are similar to those of agonists within the binding pocket. Antagonist moieties mimic interactions of agonists with domain 1; however, antagonist interactions with domain 2 and the degrees of domain closure vary significantly. Upon antagonist binding, the lobes of the LBD do not induce the same degree of domain closure as full agonists, resulting in a smaller distance between the linkers (Menuz, *et al.*, 2007). Despite a wealth of information about the binding interactions between agonists and GluA2-s1s2, there is little information about the driving forces that lead to antagonist binding. Interpretation of thermodynamic driving forces coupled with known crystal structures may help us better understand the functional differences between antagonists and agonists. Thermodynamic characterization of glutamate receptor antagonists is also of interest in designing high affinity, subtype-specific antagonists for use in the treatment of neuronal disorders.

The antagonists, DNQX (6, 7-dinitroquinoxaline-2, 3-dione) and CNQX (6-cyano-7-nitroquinoxaline-2, 3-dione) (Figure 2.1A) potently and selectively block AMPA receptors (Menuz *et al.*, 2007). The IC_{50} value for displacement of ^{3}H-AMPA (α-amino-3-hydroxy-5-methyl-4-isoxazolepropionic acid) by the antagonists is between 0.38 μM and 1.0 μM for DNQX, and 0.68 μM for CNQX (Kasper *et al.*, 2006; Ahmed *et al.*, 2009). Armstrong

and Gouaux's crystal structure of GluA2-s1s2 bound to DNQX reveals that two carbonyl groups of the antagonist mimic the α-carboxyl group common to agonists by forming hydrogen bonds to the negatively charged Arg485 and the hydroxyl and backbone amide of Thr480. An amide nitrogen of DNQX forms a hydrogen bond to the backbone carbonyl of Pro478, which plays a role in the tetrahedral interaction between the binding pocket and the α-amino group of agonists. When a sulfate is modeled into the crystal structure of GluA2-s1s2 bound to DNQX, it coordinates binding to the protein and solvent molecules just as the anionic "R" groups of agonists. While DNQX mimics some of the interactions between agonists and the ligand binding domain, it does not induce domain closure to the same extent as full agonists—making it an excellent antagonist for thermodynamic studies. CNQX differs from DNQX by a single moiety: it has a nitrile group at the 6' position of the quinoxalinedione, while DNQX has a nitro group in the same position. The nitrile group is fairly unreactive compared to the nitro group which may hydrogen-bond to sidechains within the binding pocket. Studies of these two compounds will give us some indication of the effect of a single moiety change on thermodynamic parameters of antagonist binding.

The natural product willardiine (Figure 2.1C) can be converted from an agonist to an antagonist by adding substituents to the N3 position of the uracil ring that increase the interacidic moiety chain length by two methylene groups (More *et al.*, 2003). The benzyl moiety of UBP282 (Figure

2.1A) is equivalent to approximately three or four methylene groups; UBP277 (Figure 2.1A) has a chain length of two methylene groups and the terminal carboxylic acid groups of both derivatives interact with different binding sites (More *et al.*, 2003; Ahmed, *et al.*, 2009). UBP282 is a more potent AMPA receptor antagonist compared to the N3-carboxyalkyl-substituted willardiine derivatives, and UBP277 is the most potent of these analogues (More *et al.*, 2003). The thermodynamics of the binding of the antagonists (*RS*)-NS1209, DNQX, and (*S*)-ATPO to GluA2-s1s2 have been studied previously using displacement ITC (Kasper *et al.*, 2006) and all three bind with similar affinities. The IC_{50} values of UBP277 and UBP282 are at least 100-fold greater (More *et al.*, 2003; Ahmed *et al.*, 2009) than DNQX and CNQX allowing us to investigate the relationship between antagonist affinity and thermodynamic binding parameters.

Investigating the balance between enthalpic and entropic contributions of antagonist binding may also provide information about how to optimize affinities of medically relevant antagonists (Velázquez-Campoy and Freire, 2004; Crespo and Fernandez, 2008). Overactivation of glutamate receptors is associated with many neurological diseases and disorders such as ischemic stroke, epilepsy, Parkinson's disease, and Aids-related dementia (Dingledine *et al.*, 1999). The GluA2 antagonist (*S*)-NS1209 has shown robust anticonvulsant and neuroprotective effects in clinical trials (Kasper *et al.*, 2006).

Thermodynamic studies of the binding of four competitive antagonists, DNQX, CNQX, UBP277, and UBP282 (Figure 2.1) are presented here. While structurally dissimilar antagonists such as DNQX, (*S*)-NS1209, and ATPO make some of the same contacts as agonists with s1s2, their binding is a result of additional distinct interactions leading to differences in binding affinities and free energies of binding (Armstrong and Gouaux, 2000; Hogner *et al.*, 2003; Kasper *et al.*, 2006). Crystal structures of antagonists bound to GluA2-s1s2 have identified specific hydrogen bond, dipole-dipole and ion pair interactions that take place upon binding; however the relative contributions of enthalpy and entropy to antagonist binding have not been characterized in depth. Understanding the driving forces behind these interactions may aid in the development of high-affinity, subtype-specific antagonists as therapeutic tools in the treatment of neurological disorders.

Similar to antagonists, partial agonists bind to the same site as full agonists, and mimic some of the interactions that take place between full agonists and amino acid side chains within the binding pocket. Despite the similarities in binding interactions, a long-standing question in iGluR studies involves the mechanism by which partial agonists can fully occupy the ligand binding sites of these tetrameric receptors, yet elicit only submaximal responses at saturating ligand concentrations. Based on the Monod-Wyman-Changeux (MWC) model of allosteric proteins, partial agonists and full agonists can stabilize the same receptor conformations;

however, partial agonists do not shift the equilibrium towards the activated state as efficiently as full agonists (Monod, *et al.*, 1965). An alternative theory, the Koshland-Nemethy-Filmer (KNF) model, proposes that different ligands induce specific receptor conformations, and each ligand-receptor conformation differs in its ability to elicit a response (Koshland, *et al.*, 1966). Recently Patneau and Mayer (1992) have proposed that differences in responses between full and partial agonists are due to the relative affinities of each type of ligand for the active and desensitized states of the iGluR.

High-resolution crystal structures of GluA2-s1s2 complexed with several partial agonists have been solved and based on these results another model has been proposed (Armstrong *et al.*, 1998; Jin *et al*, 2003; Jin and Gouaux, 2003). According to this structure-based model of partial agonism, the extent of activation is correlated with the degree of lobe closure (Armstong and Gouaux, 2000; Armstrong *et al.*, 2003; Jin *et al.*, 2003). NMR experiments of receptors in solution have led to yet another theory to explain partial agonists: partial agonism may arise from a decreased proportion of time spent in a conformation permissive to channel opening (Fenwick and Oswald, 2008; Maltsev, *et al.*, 2008). Additionally, functional and mutational studies have suggested that the stability of the interface between the lobes determines both ligand efficacy and binding affinity (Robert *et al.*, 2005). Single channel studies have demonstrated that full and partial agonists induce three or four conductance levels and higher conductance levels are observed more often for full agonists (Jin *et al.*,

2003; Poon *et al.*, 2010). More recently, Ahmed *et al.* (2011) proposed that the fully closed LBD would trigger the opening of the channel gate and efficacy is based on the probability of producing a fully closed LBD.

In order to continue to address some of these long-standing questions about partial agonism, we have performed displacement isothermal titration calorimetry (ITC) experiments in which the full agonist, glutamate (Figure 2.1B), is displaced by a series of structural analogues halogenated or nitrated in the 5-position of willardiine (Figure 2.1C) that function as partial agonists at AMPA receptors (More *et al.*, 2003). One of the reasons 5-substituted willardiines have been intensely studied is that they bind to the resting and desensitized states of the receptor with different affinities (Patneau *et al.*, 1992). These compounds differ by a single atom yet result in graded degrees of domain and extent of activation and desensitization (Jin *et al.*, 2003). This is the first study to adopt a thermodynamic approach to address the differences between full and partial agonist binding to GluA2-s1s2. Thermodynamic characterization of 5-substituted willardiines such as iodowillardiine (IW), fluorowillardiine (FW), chlorowillardiine (ClW), and nitrowillardiine (NW) may help us understand why partial agonists produce submaximal responses. Our results may lead to structure-based predictions of ligand binding energies and facilitate future drug design.

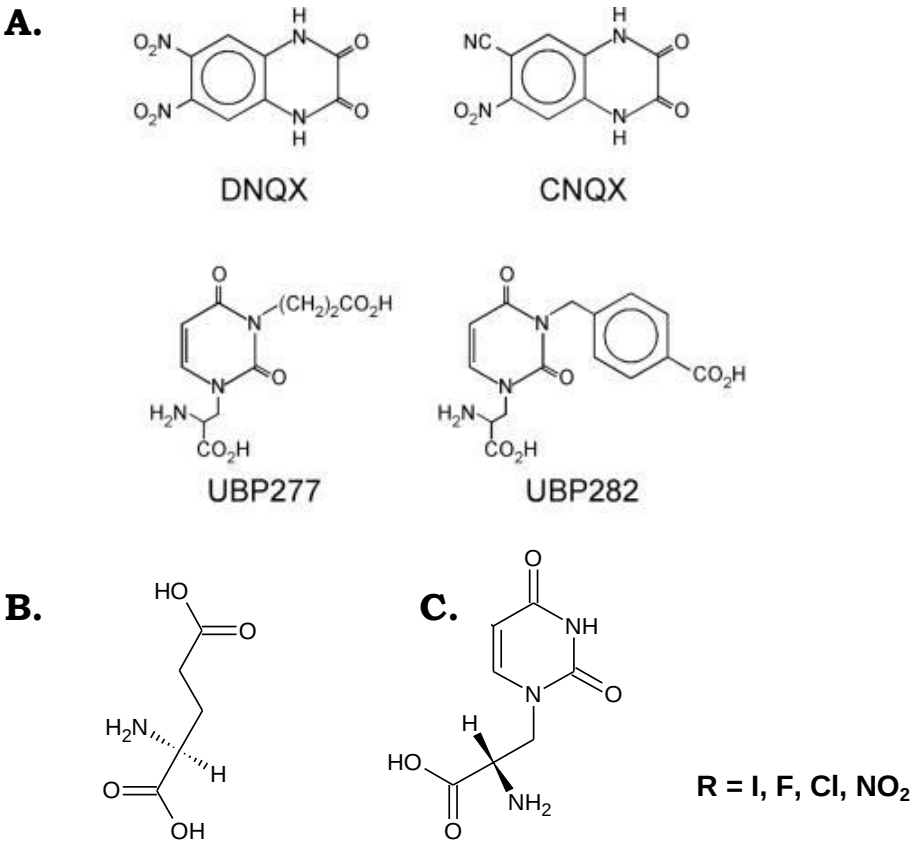

Figure 2.1. GluA2 antagonists (A.), glutamate (B.), and the parent compound, willardiine (C.), of the partial agonist structures iodowillardiine (I), chlorowillardiine (Cl), fluorowillardiine (F) and nitrowillardiine (NO_2).

METHODS

Materials. A 262 residue fragment of the rat flop isoform (Hollmann and Heinemann, 1994) of the GluA2 LBD, s1s2, was provided by Dr. Eric Gouaux (Vollum Institute of Oregon Health & Science University). GluA2-s1s2 consists of residues N392 - K506, P632 - S775, a 'GA' segment at the N-terminus, and a 'GT' linker connecting K506 and P632 (Armstrong and Gouaux, 2000). DNQX, iodowillardiine and fluorowillardiine were purchased from Tocris (Ellisville, MO); and CNQX was purchased from Ascent Scientific (Princeton, NJ). UBP277, UBP282, chlorowillardiine and nitrowillardiine were synthesized by Dr. David E. Jane (University of Bristol) as previously described (Jane *et al.,* 1997; Dolman *et al.*, 2005).

Protein Purification and Expression. Inclusion bodies [BL-21(DE3) Escherichia coli) expressing the s1s2 plasmid were grown in LB broth medium supplemented with 100 μg/mL kanamycin. Cultures were expanded from a 3 mL inoculated sample to 3 L over 36 hours at 37°C. When the culture reached an OD_{560} of approximately 0.8, protein expression was induced with 700 μM IPTG overnight. Cells were harvested by centrifugation for 15 minutes at 6K rpm and resuspended in 75 mL of Buffer A: 50 mM Tris-HCl, pH 8.0, 1 mM EDTA, and 100 mM NaCl). PMSF, lysozyme, and deoxycholic acid were added to a final concentration of 1 mg/mL. Cells were incubated at room temperature for 20 minutes until highly viscous (determined empirically). After addition of 3 mLs of 1 mg/mL

of DNAse in 1 M $MgCl_2$ viscosity retreated and was similar to that of water (determined empirically). The lysate was centrifuged at 32K rpm for 25 minutes, and the pellet resuspended in 50 mL of Buffer B (50 mM Tris-HCl, pH 8.0, 10 mM EDTA, 100 mM NaCl, and 0.5% Triton X-100) supplemented with 1 mM PMSF (supernatant was discarded). The pellet was subsequently centrifuged and resuspended in 50 mL Buffer C (20 mM Tris-HCl, pH 7.4, 1 mM EDTA, and 200 mM NaCl) also supplemented with 1 mM PMSF. After another collection by centrifugation the material was solubilized in 6.0 M GuHCl, 100 mM Tris-HCl, pH 8.0, and 2 mM BME, centrifuged, and applied to a nickel column. The volume of recovered material was increased to 100 mL with buffer containing 4 M GuHCl, 20 mM NaOAc, 10 mM BME, and 1 mM DTT, pH 4.5, and dialyzed for 12 hours against 4 L of folding buffer: 0.65 M arginine, 20 mM Tris-HCl, pH 8.5, 1 mM EDTA, 10 mM NaCl, 2 mM KCl, and 1 mM glutamate. Recovered material was subsequently dialyzed for 12 hours in buffer 4: 20 mM Tris-HCl, pH 7.4, 200 mM NaCl, 1 mM EDTA, and 1 mM glutamate. This two-step dialysis procedure was repeated twice to maximize protein recovery.

Recovered protein was centrifuged, concentrated to ~10 mL, and run over a XK-26/100 Superose sizing column at a flow rate of 2 mL/min. Fractions containing GluA2-s1s2 were collected and concentrated for trypsin cleavage (1: 250). Digestion was evaluated by SDS-PAGE. Trypsin was inactivated with PMSF and the digested material was dialyzed against SP column buffer overnight (20 mM NaOAc, pH 6.0, 1 mM EDTA, 1 mM

glutamate). The sample was loaded onto a 5 mL HiTrap SP column and equilibrated with SP column buffer. The SP column was first washed with 50 mL of 5% S-column buffer B: 20 mM NaOAc, pH 6.0, 1 mM EDTA, 1 mM glutamate, and 500 mM NaCl. A second wash of 50 mL 10% S-column buffer B was performed before elution with a linear gradient of 150 mL 10% - 30% S-column buffer B. Fractions containing s1s2 were confirmed through SDS-PAGE, pooled and concentrated.

Spectroscopic Characterization. UV absorbance spectra were determined using a Beckman DU 640B spectrophotometer (Beckman, Fullerton, CA) in a quartz cuvette with a 1-cm path length. Absorbance values were measured at 280 nm and normalized against a reference cuvette containing buffer.

Displacement Isothermal Titration Calorimetry (ITC). Ligand solutions were prepared in glutamate-free ITC phosphate buffer (20 mM NaH_2PO_4, 50 mM NaCl, 1 mM NaN_3, pH 7.3). GluA2-s1s2 stock solutions (0.19-0.35 mg/mL of protein in 20 mM NaOAc, pH 6.0, 1 mM EDTA, 1 mM glutamate) were exchanged with glutamate-free ITC phosphate buffer over 4-5 cycles of centrifugation using Amicon® Ultra-4 Centrifugal Filter Devices (Millipore Corp, MA) until the concentration of free glutamate in the protein sample was sub-picomolar. During exchange, samples were centrifuged at 3.4K rpm for 20 min. at 4°C and maintained on ice or below experimental temperature (10°C). The resultant protein solution was again exchanged with ITC buffer containing either 2 μM glutamate, 190 μM UBP277, or 500 μM UBP282. For

experiments in which the competing ligands, CNQX and DNQX were injected (360-400 µM, #40-6 µl injections), s1s2 was pre-bound with 2 µM glutamate during buffer exchange. In our UBP277 and UBP282 experiments the competing ligand injected was glutamate (500 µM, #40-6 µl injections) and s1s2 was pre-bound with 190 µM UBP277 or 500 µM UBP282. The final protein concentration (5-25 µM), was determined from the absorbance at 280 nm using a molar extinction coefficient of 1.0 mL/mg (28600 M^{-1}). Experiments were performed using a VP-ITC Microcalorimeter (MicroCal, LLC, Northampton, MA) and parameters were 306 rpm stirring speed, 0.5 µl/sec injection rate, and 10 µCal/sec reference power. Experimental titration conditions are described in Table 2.1.

Raw data were analyzed using Origin® v7.0301 software supplied by MicroCal, LLC (Northampton, MA). Isotherms were fit with the competitive binding model as described by Sigurskjold (2000). The protein concentration was adjusted by the best fit to the data with a stoichiometric value N = 1.0. One glutamate molecule binds per site and s1s2 is a monomer in solution up to a concentration of 20 mg/mL, which is far above the concentration of protein used in these studies (Chen and Gouaux, 1997; Abele *et al.*, 1998; Abele, *et al.*, 1999; Madden *et al.*, 2000). The value of $\Delta\Delta H$ for binding of glutamate to apo protein was set to zero as a reference. For displacement experiments in which CNQX, and DNQX were the competing ligands and glutamate was bound to s1s2 in the cell, data were fit using an equilibrium association constant of 1.0×10^6 M^{-1} for glutamate. The data were fit by

iteratively varying the equilibrium association constant of the antagonist until the association constant of glutamate was 1.0×10^6 M^{-1}. The value of the association constant for the unknown ligand was subsequently refit and iterated until convergence of both fittings.

Table 2.1. Experimental Titration Conditions

Ligand titrated into cell	Concentration of titrant (μM)	Ligand prebound to GluA2-s1s2 in ITC cell	Concentration of prebound ligand in ITC cell (μM)
CNQX	363	Glutamate	2
DNQX	397	Glutamate	2
Glutamate	500	UBP277	500
Glutamate	500	UBP282	500
Iodowillardiine	500	Glutamate	2
Chlorowillardiine	500	Glutamate	2
Fluorowillardiine	644	Glutamate	2
Nitrowillardiine	500	Glutamate	2

RESULTS

Direct titration of glutamate into the apo form of GluA2-s1s2 at 10-25°C produced a weak or undetectable signal which is consistent with other studies of glutamate receptor thermodynamics (Kasper *et al.*, 2006; Madden *et al.*, 2000). In order to acquire full thermodynamic characterization, each injection of ligand should evolve or adsorb at least an average of 3-5 µcal of heat from the binding reaction (Doyle, 1999; Freyer and Lewis, 2008; MicroCal™ User's Manual). The heat evolved from glutamate binding to the apo form of GluA2-s1s2 was similar in magnitude to the heat of dilution of glutamate (data not shown) leading us to believe the heat signal from glutamate binding to the apo form of GluA2-s1s2 is too small to resolve relative to the heat of dilution of glutamate. When the binding enthalpy of a reaction is small, the reaction can be optimized by varying the temperature to amplify the heat signal from binding (Doyle, 1999; Freyer and Lewis, 2008); however, the apo form of GluA2-s1s2 is unstable at higher temperatures (Ahmed *et al.*, 2007). Another difficulty with direct titration is that glutamate removal from the protein prep is incomplete despite extensive dialysis against glutamate-free buffer (4 L every 6 hours for 48 hours). Lastly, protein saturation may have also occurred sooner due to loss of protein as a result of precipitation in the absence of ligand.

Despite the experimental difficulties in direct titration experiments, useful data can be obtained through displacement ITC. In our antagonist studies, GluA-s1s2 was bound with ligand prior to the experiment. CNQX

and DNQX were titrated into glutamate-bound s1s2 and the glutamate-bound state was used as the reference state. UBP277 and UBP282 have lower affinities for GluA2-s1s2 relative to glutamate; therefore, experiments were performed by titrating glutamate into UBP277- and UBP282-bound s1s2. In our partial agonist studies, GluA-s1s2 was bound with glutamate prior to the experiment and displaced by IW, ClW, FW and NW. Experimental titration conditions are summarized in Table 2.1.

DNQX and CNQX binding to GluA2-s1s2 relative to glutamate were exothermic with favorable enthalpies and unfavorable entropy changes (Fig. 2.2). UBP277 and UBP282 displacement by glutamate were also exothermic, however, with a smaller enthalpy decrease for UBP282. The entropic changes of displacement of UBP277 and UBP282 by glutamate were very unfavorable. The free energies of glutamate displacement by DNQX and CNQX were favorable and displacement of UBP277 and UBP282 by glutamate was favorable. The binding affinities determined from the fits to the data for DNQX and CNQX were ($1.05 \times 10^6 \pm 1.50 \times 10^5$ M^{-1}) and ($8.18 \times 10^5 \pm 8.29 \times 10^4$ M^{-1}). UBP277 and UBP282 bind with lower affinities: ($1.31 \times 10^5 \pm 2.95 \times 10^4$ M^{-1}) and ($9.49 \times 10^3 \pm 1.97 \times 10^3$ M^{-1}) (Fig. 2.3). Thermodynamic results for experiments in Figure 2.3 are listed in Table 2.2 while average results (2 trials for each antagonist) are listed in Table 2.3.

Displacement of glutamate by the partial agonists ClW and FW was endothermic and entropically favorable at 10°C, while glutamate displacement by the partial agonist NW was exothermic and entropically

unfavorable (Table 2.4). The changes in free energy relative to glutamate were favorable: $\Delta\Delta G^{obs}$ = -2.81 kcal/mol (ClW); $\Delta\Delta G^{obs}$ = -2.74 kcal/mol (FW); and $\Delta\Delta G^{obs}$ = -2.94 kcal/mol (NW). The binding affinities for the willardiine derivatives determined from fits to the data were: $1.24 \times 10^8 \pm 1.01 \times 10^8$ M^{-1} (ClW), $1.32 \times 10^8 \pm 1.04 \times 10^8$ M^{-1} (FW), and $1.86 \times 10^8 \pm 2.50 \times 10^8$ M^{-1} (NW) (Figure 2.4).

Displacement of glutamate by the partial agonist iodowillardiine was endothermic and entropically favorable (Figure 2.5), while the changes in free energy relative to glutamate were unfavorable. The binding affinities for iodowillardiine determined from the fits to the data were: $3.51 \times 10^5 \pm 7.34 \times 10^4$ M^{-1} (5°C), $2.40 \times 10^5 \pm 6.42 \times 10^4$ M^{-1} (10°C), and $7.92 \times 10^4 \pm 1.15 \times 10^4$ M^{-1} (15°C) (Figure 2.6). Thermodynamic results for glutamate displacement by iodowillardiine are summarized in Table 2.5.

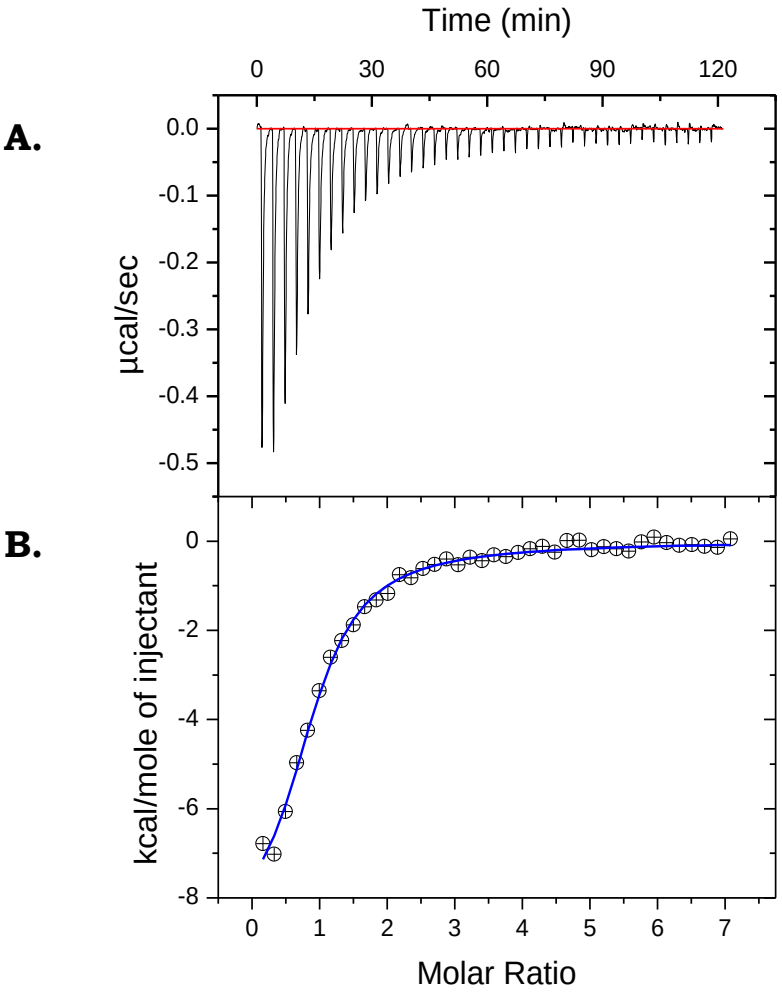

Figure 2.2. Glutamate displacement by DNQX. (A) Thermogram for titration of 397 µM DNQX into 9 µM GluA2-s1s2 with 2 µM glutamate at 10°C, pH 7.3. Raw data is reported as µcal/sec versus time. **(B)** Integrated heats plot, illustrating amount of heat measured as a result of each injection normalized to the number of moles of DNQX injected (kcal/mol) versus molar ratio of total DNQX added per mol of GluA2-s1s2. Data were fit by least-squares nonlinear regression analysis for displacement titration calorimetry: $\Delta Q_i = V_0[P_0](\Delta H_A\{x_{PA,i}\text{-}f_i x_{PA,i-1}\} + \Delta H_B\{x_{PB,i}\text{-}f_i x_{PB,i-1}\}) + q_d$ (Sigurskjold, 2000); and yielded $\Delta\Delta H^{obs}$= -8.3 ± 0.3 kcal/mol DNQX. $\Delta\Delta S$ was calculated using $\Delta\Delta G = \Delta\Delta H^{obs} - T\Delta\Delta S$ and $\Delta\Delta G$ was calculated using the observed binding constant K_a = 1.05 x 10^6 M^{-1} ± 1.50 x 10^5 M^{-1}.

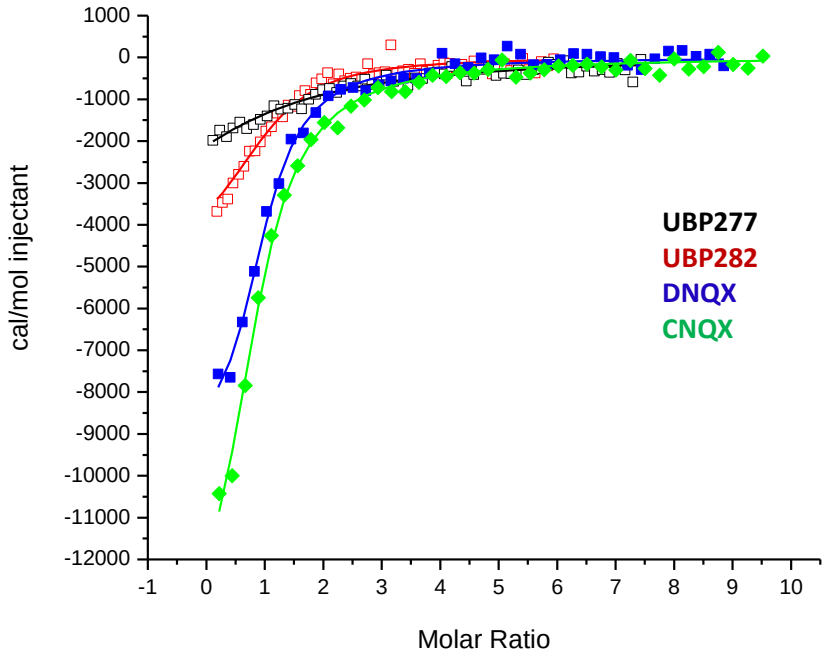

Figure 2.3. Representative isotherms for GluA2-s1s2 displacement experiments. Isotherms for glutamate displacement by titration with DNQX, CNQX; and UBP277, UBP282 displacement by titration with glutamate. Data were fit using the competitive binding 2 model as described by Sigurskjold (2000). Iterations were performed until the protein to antagonist ratio was ~1.0. The binding affinities determined from the fits to the data were: 1.05 x 10^6 M^{-1} (DNQX), 8.18 x 10^5 M^{-1} (CNQX), 1.31 x 10^5 M^{-1} (UBP277), and 9.49 x 10^3 M^{-1} (UBP282).

Table 2.2. Antagonist binding parameters for Figure 2.3.

Antagonist	$\Delta\Delta H^{obs}$ (kcal/mol)	$\Delta\Delta S^{obs}$ (cal/mol•K)	$-T\Delta\Delta S^{obs}$ (kcal/mol)	$\Delta\Delta G^{obs}$ (kcal/mol)
CNQX	-14.2 ± 0.52	-23.1	6.54	-7.66
DNQX	-9.26 ± 0.32	-9.75	2.76	-6.50
UBP277	-6.44 ± 2.7	0.657	-0.186	-6.63
UBP282	-5.96 ± 0.32	-2.86	0.81	-5.15

Table 2.3. Antagonist binding parameter summary.

Antagonist	$\Delta\Delta H^{obs}$ (kcal/mol)	$\Delta\Delta S^{obs}$ (cal/mol•K)	$-T\Delta\Delta S^{obs}$ (kcal/mol)	$\Delta\Delta G^{obs}$ (kcal/mol)	K_a^{obs} (M^{-1})
CNQX	-11.1 ± 3.06	-24.2	6.85	-4.25	$2.24 \times 10^6 \pm 1.42 \times 10^6$
DNQX	-7.80 ± 1.02	-12.7	3.59	-4.21	$2.08 \times 10^6 \pm 1.03 \times 10^6$
UBP277	-6.50 ± 0.0552	-1.48	0.42	-6.08	$9.05 \times 10^4 \pm 4.05 \times 10^4$
UBP282	-7.38 ± 1.01	-6.18	1.75	-5.63	$1.59 \times 10^4 \pm 2.55 \times 10^3$

Table 2.4. Thermodynamic binding parameters of willardiine derivatives as a result of glutamate displacement at 10°C.

Ligand	$\Delta\Delta H^{obs}$ (kcal/mol)	$\Delta\Delta S^{obs}$ (cal/mol•K)	$-T\Delta\Delta S^{obs}$ (kcal/mol)	$\Delta\Delta G^{obs}$ (kcal/mol)	K_a^{obs} (M^{-1})
IodoW	5.12 ± 0.69	15	-4.24	0.88	$2.40 \times 10^5 \pm 6.42 \times 10^4$
ChloroW	5.85 ± 0.33	31	-8.66	-2.81	$1.24 \times 10^8 \pm 1.01 \times 10^8$
FluoroW	1.28 ± 0.07	14	-4.02	-2.74	$1.32 \times 10^8 \pm 1.04 \times 10^8$
NitroW	-3.87 ± 0.59	-3.3	0.93	-2.94	$1.86 \times 10^8 \pm 2.50 \times 10^8$

Table 2.5. Thermodynamic binding parameters of glutamate displacement by iodowillardiine.

Temp (°C)	$\Delta\Delta H^{obs}$ (kcal/mol)	$\Delta\Delta S^{obs}$ (cal/mol•K)	$-T\Delta\Delta S^{obs}$ (kcal/mol)	$\Delta\Delta G^{obs}$ (kcal/mol)	K_a^{obs} (M^{-1})
5	4.56 ± 0.49	14	-3.89	0.67	$3.51 \times 10^5 \pm 7.34 \times 10^4$
10	5.12 ± 0.69	15	-4.24	0.88	$2.40 \times 10^5 \pm 6.42 \times 10^4$
15	7.99 ± 2.43	23	-6.62	1.37	$7.92 \times 10^4 \pm 1.15 \times 10^4$

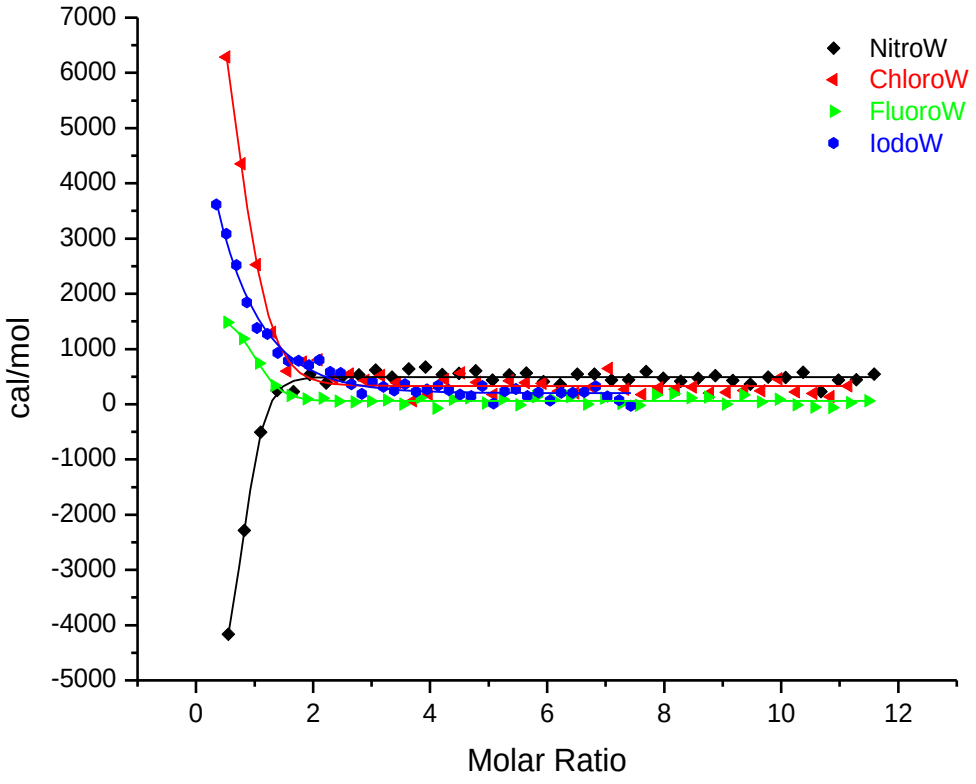

Figure 2.4. Representative isotherms for glutamate displacement by willardiine derivatives. Isotherms for glutamate displacement by titration with IW, FW, ClW, and NW. Data were fit using the competitive binding 2 model as described by Sigurskjold (2000). Iterations were performed until the protein to antagonist ratio was ~1.0. The binding affinities determined from the fits to the data were: 2.40 x 10^5 M^{-1}(IW), 1.32 x 10^8 M^{-1} (FW), 1.24 x 10^8 M^{-1} (ClW), and1.86 x 10^8 M^{-1} (NW).

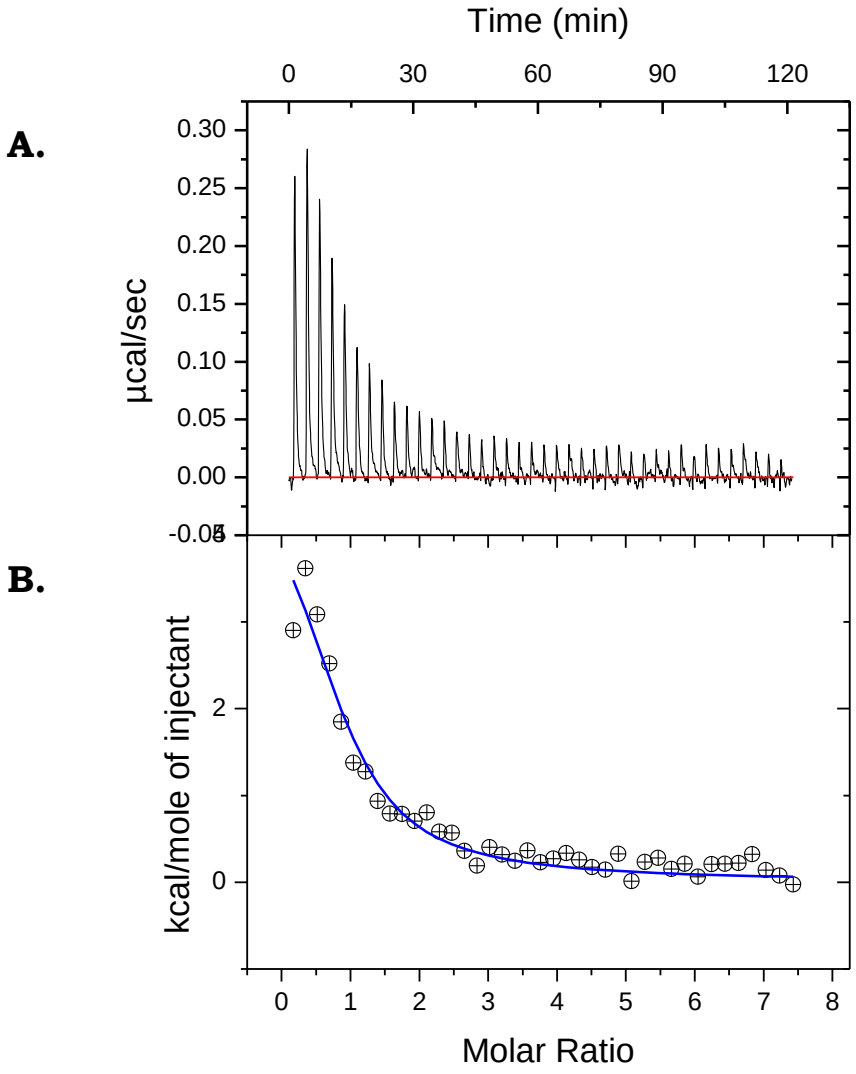

Figure 2.5. Glutamate displacement by iodowillardiine is endothermic. **(A)** Thermogram for titration of 500 µM iodowillardiine into 10 µM GluR2-s1s2 with 2 µM glutamate at 10°C, pH 7.3. Raw data is reported as µcal/sec versus time. **(B)** Integrated heats plot illustrating amount of heat measured as a result of each injection normalized to the number of moles of iodowillardiine injected (kcal/mol) versus molar ratio of total iodowillardiine added per mol of GluR2-s1s2. Data was fit by least-squares nonlinear regression analysis for displacement titration calorimetry (Sigurskjold, 2000) and yielded $\Delta\Delta H^{obs}$= 5.12 ± 0.69 kcal/mol, and an observed binding constant K_a^{obs}= 2.40 x 10^5 ± 6.42 x 10^4 M^{-1}.

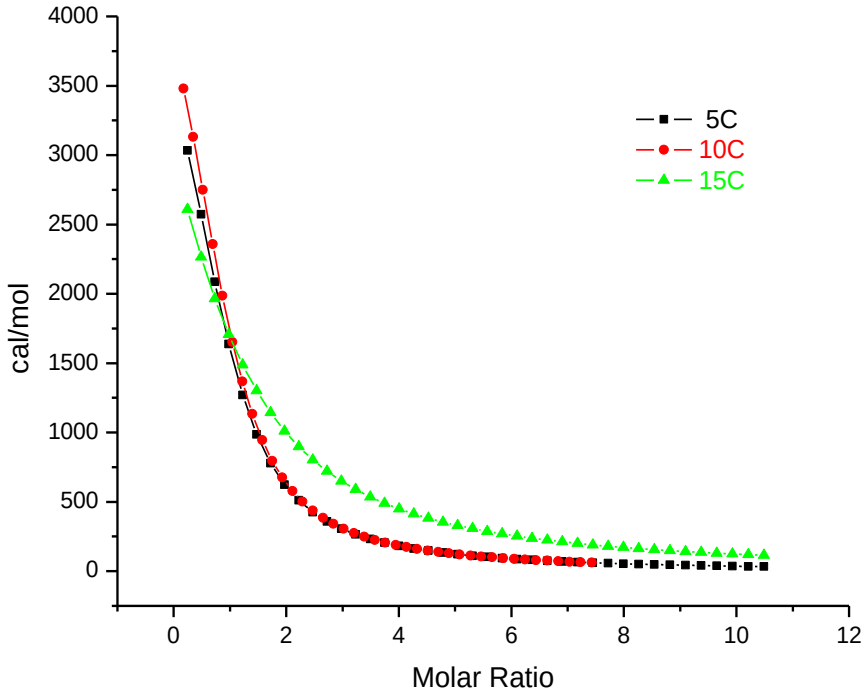

Figure 2.6. Representative isotherms for glutamate displacement by iodowilardiine at 5°C, 10°C, and 15°C. Isotherms for glutamate displacement by titration with 500 µM iodowillardiine. Data were fit as previously described (Sigurskjold, 2000). The binding affinities determined from the fits to the data were: 3.51 x 10^5 M^{-1} (5°C), 2.40 x 10^5 M^{-1} (10°C), 7.92 x 10^4 M^{-1} (15°C).

DISCUSSION

Glutamate receptor ion channel opening results from agonist-induced conformational changes leading to lobe closure, and individual interactions between the agonist and amino acid side chains within the binding pocket. Most antagonists bind to GluA2 without inducing lobe closure and stabilize the lobes in an open conformation or lead to domain extension relative to the glutamate-bound state (Armstrong and Gouaux, 2000; Hogner *et al.*, 2003; Kasper *et al.*, 2006; Ahmed *et al.*, 2009). Domain closure leading to channel activation has been extensively studied with GluA2-s1s2 (Armstrong and Gouaux, 2000); however, thermodynamic forces that drive antagonist binding have not been as well characterized.

Antagonist binding relative to glutamate is dominated by entropic penalties. Displacement of glutamate by DNQX and CNQX, and displacement of UBP277 and UBP282 by glutamate are entropically unfavorable (Table 2.3). Entropic penalties may be due to losses in conformational entropy when the motions of lobes 1 and 2 are restricted upon antagonist binding. The quinoxalinediones, DNQX and CNQX induce ~17.5° and~13.4° lobe opening relative to the glutamate-bound state (Armstrong & Gouaux, 2000; Menuz *et al.*, 2007). Conformational entropic penalties may also be due to stabilization of the antagonists within the binding pocket. UBP277 and UBP282 make more extensive interactions with lobe 2 relative to DNQX and CNQX, and the position of their uracil

rings may be responsible for a greater degree of lobe separation. In the UBP277-GluA2 crystal structure the uracil ring of UBP277 is rotated by ~22° relative to the unsubstituted willardiine and positioned deeper in the binding cleft resulting in a large-scale rotation of lobe 2 (Ahmed *et al.*, 2009). The uracil ring of UBP282 is rotated to a greater extent than UBP277 (~33°), and the carboxylbenzyl group leads to a greater degree of lobe opening relative to the glutamate-bound state resulting in the largest hyperextension of the lobes reported (Ahmed, *et al.*, 2009).

Additional entropic penalties may arise from solvent-mediated interactions. Solvent molecules may lose degrees of freedom as they rearrange around the surface of the antagonist-bound complex. Conformational entropy and entropies of solvation and desolvation are primary sources of entropies of binding. Due to the open-lobe conformations of s1s2 leading to an increase in the surface area of the antagonist-bound complex, antagonist binding may result in partial desolvation or insufficient solvation entropy to overcome the entropic penalties incurred from solvent rearrangement. Glutamate binding to apo GluA4-s1s2 is entropically favorable due to solvent molecule exclusion from the binding pocket upon agonist binding (Madden *et al.*, 2000; Kasper *et al.*, 2006; Ahmed *et al.*, 2009). Solvent molecule exclusion into the bulk solvent may not occur to the same extent in antagonist binding. Several water molecules coordinate binding of antagonists to side chains within the binding pocket. The 6-nitro of DNQX interacts with Tyr732 and a protein-bound water molecule

(Armstrong and Gouaux, 2000), and a water molecule bridges the hydroxyl of Thr655 and the α-carboxylate of UBP277 (Ahmed *et al.*, 2009).

Antagonist binding relative to glutamate is enthalpically favorable. Despite the entropic penalties incurred by antagonist binding to GluA2-s1s2, antagonist binding is exothermic and thus enthalpically favorable. A common source of favorable enthalpies results from hydrogen bonding and van der Waals contacts between antagonists and sidechains within the binding pocket. Individual interactions between antagonists and GluA2-s1s2 are described in detail by Armstrong and Gouaux (2000), and Ahmed *et al.* (2009). Interactions that stabilize the three-dimensional structure of GluA2-s1s2 may be another source of favorable enthalpies. In side chain methyl dynamics studies, the antagonist-bound state of GluA2-s1s2 shows less chemical exchange compared to the glutamate-bound state of GluA2-s1s2 (Maltsev and Oswald, 2010). Favorable changes in enthalpy may also be due to solvent interactions upon antagonist binding as solvent molecules maximize their hydrogen bonding potential by forming hydration shells around the antagonist-protein complex.

The large entropic penalties incurred with DNQX and CNQX binding relative to glutamate are offset by favorable enthalpy decreases leading to changes in free energy that are near zero. Our results for DNQX are consistent with the results of Kasper *et al.* (2006) where the change in free energy of (*S*)-glutamate displacement by DNQX was also found to be near zero. While UBP277 and UBP282 binding to GluA2-s1s2 results in greater

degrees of lobe opening; DNQX and CNQX are more potent inhibitors and bind with higher affinities to GluA2-s1s2. Entropic penalties dominate the displacement of UPB277 and UBP282 by glutamate, and these entropy decreases are even more unfavorable than for CNQX or DNQX. As a result, UPB277 and UBP282 binding relative to glutamate lead to unfavorable increases in free energy. Despite the favorable enthalpy decreases of antagonist binding relative to glutamate the enthalpy changes are not sufficient to generate favorable decreases in free energy since the enthalpic gains are neutralized by the entropic penalties.

Our results with CNQX and DNQX may be of interest for several reasons. The structure of CNQX bound to GluA2 is very similar to the DNQX-bound structure (Menuz *et al.*, 2007) and differs only at the 6' moiety of the quinoxalinedione ring. CNQX has a nitrile moiety at this position which is fairly unreactive under our experimental conditions, while the nitro moiety of DNQX at this position interacts with Tyr732 and a protein bound water molecule. The difference in the 6' moiety did not make a significant difference in the observed thermodynamic values. Moreover, CNQX and DNQX can act as weak AMPA receptor partial agonists on a subset of interneurons in the presence of transmembrane AMPA receptor regulatory proteins (TARPs) which are auxiliary subunits responsible for receptor trafficking to the membrane (Menuz, *et al.*, 2007). These authors suggest the presence of TARPs enhance the degree of domain closure thus strengthening the coupling between domain closure and channel opening.

In light of these results, antagonism and activation may result from a mechanistic property of the ligand-binding domain, rather than individual interactions that stabilize the ligand within the binding pocket. UBP277, for instance, binds to GluA2-s1s2 through many of the same non-covalent interactions as the agonist glutamate, yet it is not activating. When a single point mutation is made in GluR1 (A636T), CNQX converts from an antagonist to a potent agonist (Taverna *et al.*, 2000). Moreover, Ahmed *et al.* (2011) crystallized a CNQX-bound GluA2 ligand-binding domain mutant in the fully closed state—suggesting that it may be the probability of attaining a fully closed ligand-binding domain which determines efficacy. The versatility of these antagonists highlights the importance of their thermodynamic characterization and further study.

IW, FW, and ClW partial agonist binding relative to glutamate is endothermic and enthalpically unfavorable. Perhaps the most exciting and unexpected observation from our partial agonist studies was that displacement of glutamate by iodowillardiine (IW), fluorowillardiine (FW), and chlorowillardiine (ClW) was endothermic and thus enthalpically unfavorable (Table 2.3). The electron-withdrawing groups of IW, ClW, and FW are expected to increase the concentration of the negatively charged species of each molecule at physiological pH (Patneau *et al.*, 1992). The enthalpic cost of desolvating them by binding to s1s2, may not be as energetically favorable compared to IW, FW, and ClW remaining in solution and glutamate remaining in the binding pocket. Interestingly, the most

electronegative willardiine compound, nitrowillardiine, had enthalpically favorable binding. Although FW binding relative to glutamate was endothermic, it was the least unfavorable of the endothermic compounds and also more electronegative than ClW and IW.

Several interactions within the binding pocket may be contributing to the observed unfavorable enthalpy increases. The binding pocket can be divided into nine positions (A-E, F1 and F2, G-H) based on the terminology by Armstrong and Gouaux (2000) (Figure 2.7). Historically, subsite F is the site that distinguishes full agonists from partial agonists and it can be further subdivided into subsites F1 and F2. In the FW and IW-bound crystal structures of GluA2-s1s2, site F2 moves ~1.4 Å away from F1 and closer to domain 2, thus increasing the distance between sites F1 and F2 and the distance between the lobes of s1s2 (Jin *et al.*, 2003). Atoms that occupy sites F1 and F2 interact with the backbone nitrogen of Glu705. Glu705 is located in the binding pocket and upon agonist binding undergoes rearrangement which may facilitate lobe closure by directly interacting with Tyr732. Mamanova *et al.* (2008) suggest this interaction is part of a larger electrostatic network which stabilizes lobe closure as a result of agonist binding. Increasing the distances between sites F1 and F2 and the distance between the lobes may weaken the interactions between atoms in these sites including Glu705 which may be partly responsible for facilitating and stabilizing lobe closure. Moreover, full agonists occupy subsite F1, and in the glutamate-bound structure of GluA2-s1s2, F1 is occupied by a water

molecule (W4). In the willardiine-bound structures of s1s2, F1 is unoccupied and the F2 subsite is occupied by the 4-carbonyl oxygen of the willardiine structures positioning the ligand farther from domain 1 (Figure 2.8). The differences in atomic interactions involving sites F1 and F2 between full and partial agonists may be contributing to net observed endothermic enthalpies of binding.

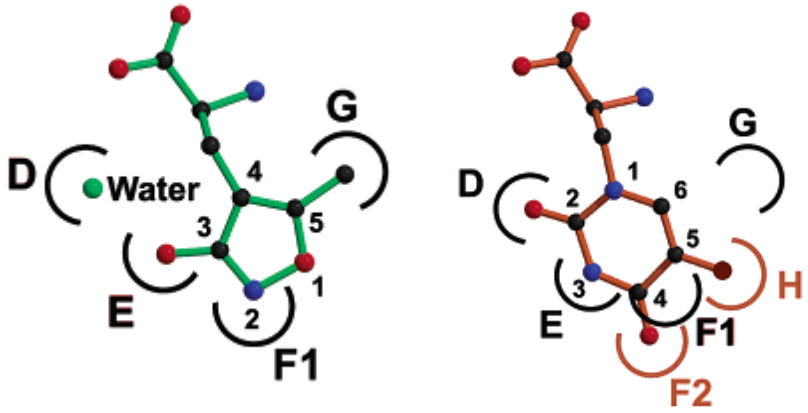

Figure 2.7. Binding pocket nomenclature. Sites D-H of agonist molecules illustrating differences in F-binding sites between full agonist, AMPA (green) and partial agonist, FW (orange) (adapted from Jin and Gouaux, 2003, with permission).

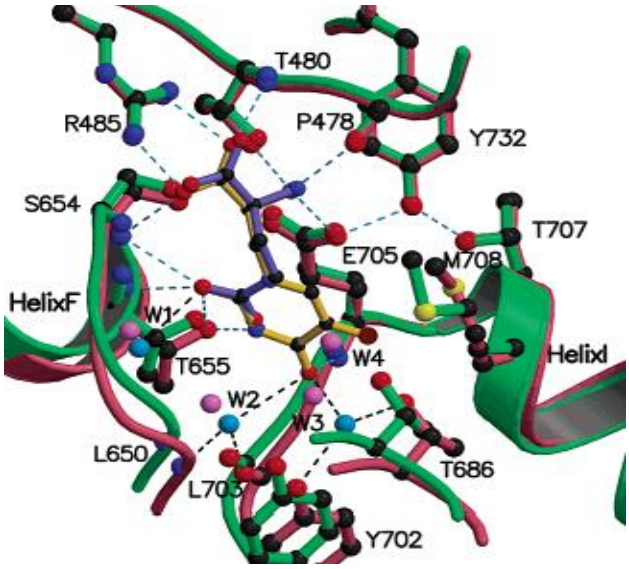

Figure 2.8. Conserved interactions between glutamate and FW and the binding pocket of GluA2. Stereoview of glutamate (purple) in complex with GluA2-s1s2 (green) and FW (yellow) in complex with GluA2-s1s2 (strawberry). Conserved interactions (turquoise dashes) include those between S654, R485, and T480 with the α-carboxyl groups of glutamate and FW; and the interactions between T480, Pro478, and Glu705 with the α-amino groups of glutamate and FW (adapted from Jin and Gouaux, 2003, with permission).

Disruption of water-mediated interactions may contribute to unfavorable enthalpies of binding for FW, IW and ClW relative to glutamate. Endothermic enthalpies of binding may also be due to differences or disruption of water-mediated interactions that are critical for full agonist binding to GluA2-s1s2. In the full agonist-bound state, a water molecule (W2) coordinates interactions between Leu650 and Leu703 and agonist atoms occupying subsite E (Figure 2.8). In the willardiine-bound structures, the increasing distance between lobes 1 and 2 changes the position of W2 and disrupts this interaction. Instead of W2 bridging interactions between the agonist and Leu650 and Leu703, W2 forms a

hydrogen bond with the 4-carbonyl oxygen of FW. In one of the IW structures (PDB 1mqg_A), W2 is ~3.8 Å away from the 4-carbonyl oxygen atom and this interaction is completely abolished (Jin and Gouaux, 2003). This interaction may not be abolished in the IW-GluA2-s1s2 Zn crystal structure which results in a smaller degree of lobe opening of ~3.6° (PDB 1my4). Lastly, the water-mediated interaction (W1) between O2 of glutamate and the NH of Glu705 is also absent in the willardiine bound structures (Armstrong and Gouaux, 2000). Moreover, sites G and H of s1s2 exist in a partially hydrophobic pocket and agonist atoms which occupy site G directly interact with Tyr405 and Met708. The willardiine partial agonists do not occupy site G but instead, the halogen atoms of the willardiines occupy site H leading to a conformational change of Thr707 that may not be as enthalpically favorable especially when we consider the energetic cost of occupying the partially hydrophobic pocket with electronegative halogen atoms. In the AMPA-bound structure, a methyl group of the full agonist occupies site G. In addition to disruption of water-mediated interactions, local structural changes may help explain why IW, FW and ClW binding to GluA2-s1s2 relative to glutamate is endothermic and enthalpically unfavorable.

IW, FW and ClW partial agonist binding relative to glutamate is driven by favorable entropy increases. In our studies, IW, FW, and ClW binding relative to glutamate is primarily driven by favorable entropy changes indicating an increase in degrees of freedom of the protein-ligand

complex, solvent molecules, or free ligand. A net increase in entropy indicates that any entropic penalties incurred from either stabilization of lobes or restriction of side chains as a result of binding are overcome by an increase in solvation or conformational entropy. The 5-substituted willardiines induce small degrees of lobe opening relative to glutamate and may not incur conformational penalties similar to GluA2-s1s2 antagonists (Ahmed *et al.*, 2009). Binding pocket interactions in glutamate-bound GluA2-s1s2 that stabilize lobe closure are not seen between s1s2 and IW and FW. As a result, displacing glutamate and water molecules that coordinate glutamate binding may lead to more structural degrees of freedom within the binding pocket and an increase in solvation entropy. Moreover, partial agonists can bind to GluA2-s1s2 and sample a range of conformations as evidenced by crystal structures and NMR studies (Jin *et al.*, 2003; Maltsev *et al.*, 2008; Ahmed *et al.*, 2011).

Functional and structural studies of the 5-substituted willardiines show that an increase in the size of the substituent leads to a smaller current response and a larger degree of lobe opening relative to glutamate (Jin *et al.*, 2003). Moreover, lobe closure may involve more extensive motions than a simple opening and closing around a single hinged axis. Rocking and twisting motions around two additional screw axes of the binding domains have been observed in molecular dynamics studies for full and partial agonists in complex with GluA2-s1s2 (Bjerrum and Biggin, 2008). These authors argue that partial agonists specifically induce a

distinct twisting motion which may affect efficacy by moving the receptor closer to an inactive state. If partial agonist binding by the 5-substituted willardiines results in a range of motions and open states, we may expect an increase in entropy as a result of binding to GluA2-s1s2.

Other sources of positive entropy may be due to motion observed by NMR studies of the 5-substituted willardiines in complex with GluA2-s1s2. Solution NMR experiments on the ligand-binding core of GluA2-s1s2 in complex with FW and IW show chemical exchange on the μs-ms timescale at the base of helix K in GluA2-s1s2. The function of helix K has not been thoroughly investigated; however, it is associated with the disulfide bond and may be involved in the hinge region of s1s2. The glutamate-bound GluA2-s1s2 structure shows no significant chemical exchange at this position, while another partial agonist, kainate, shows increased chemical exchange in this region (Fenwick and Oswald, 2008). Increased chemical exchange in the hinge region is seen with the 5-substituted willardiines and another partial agonist, kainate, and may contribute to positive entropy changes.

Nitrowillardiine binding relative to glutamate is driven by favorable enthalpy changes but is entropically unfavorable. Antagonists and partial agonists studied thus far had shown similar thermodynamic profiles based on their functional significance; therefore, we expected the willardiine partial agonist, NW, to exhibit an endothermic

enthalpy and a favorable entropy of binding relative to glutamate. Interestingly, NW binding to GluA2-s1s2 relative to glutamate was exothermic and enthalpically favorable (Table 2.4). This may be due to additional interactions between NW and the binding pocket of GluA2-s1s2. Of the 5-substituted willardiine derivatives studied, NW is the most electronegative (Norinder and Högberg, 1992). The NO_2 group of nitrowillardiine may induce less electron delocalization than the halogen-substituted willardiines and become more attractive as an electron donor. Based on the crystal structure of NW in complex with GluA2-s1s2, one of the oxygen atoms (O1) of the 5-nitro group of NW forms a putative hydrogen bond with the backbone nitrogen of Glu705. The other oxygen atom (O2) of the 5-nitro group of NW forms a putative hydrogen bond with the hydroxyl of Thr686 (Figure 2.9). A water molecule, W2, bridges Leu650 and Leu703 with full agonist atoms at subsite E (Jin and Gouaux, 2003) (Figure 2.7). In the NW crystal structure, W2 also bridges Leu650 and Leu703 while interacting with the 4-carbonyl oxygen of NW. Two pairs of residues believed to form contacts across the binding cleft in the glutamate-bound state of GluA2-s1s2 (Mamonova *et al.*, 2008) also interact in the NW-bound s1s2 structure. Thr686 interacts with Glu402 via a water molecule and Ser652 interacts with the backbone nitrogen of Gly451. Many of these interactions between NW and the binding pocket of GluA2-s1s2 are also seen with full agonist binding to GluA2-s1s2. In some cases, these interactions are not direct in the NW-GluA2-s1s2 structure, but instead mediated by water

molecules. These water-mediated interactions and additional hydrogen bonds may partly explain why NW binding to GluA2-s1s2 relative to glutamate is enthalpically favorable.

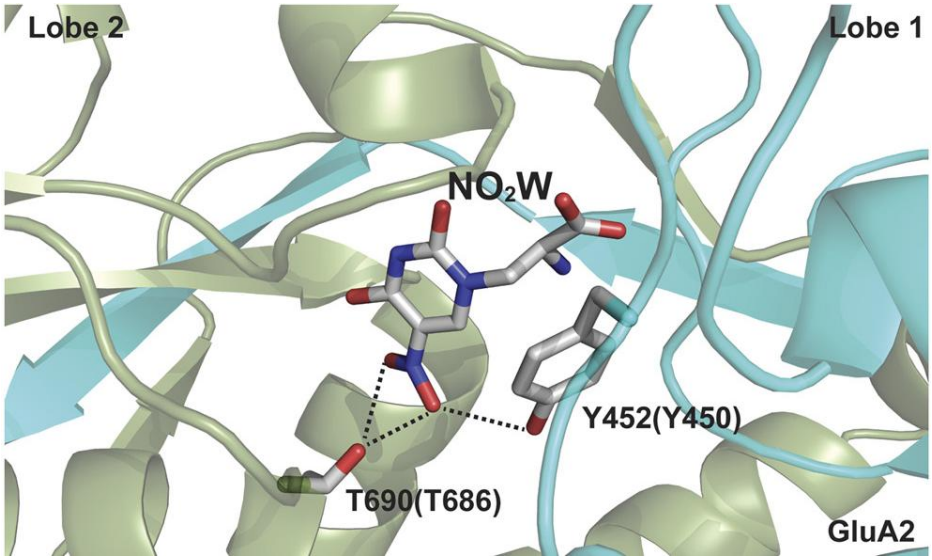

Figure 2.9. Nitrowillardiine forms interactions that may stabilize the closed-lobe conformation. Crystal structure of NW-bound GluA2-s1s2 with GluA3 residue numbering and GluA2 numbering in parentheses. The nitro group of NW is capable of forming hydrogen bonds with T686 and Y450 of GluA2-s1s2 (modified from Poon *et al.,* 2011, with permission)

Nitrowillardiine binding relative to glutamate exhibits small entropic penalties. Nitrowillardiine binding to GluA2-s1s2 relative to glutamate also leads to a small entropic penalty decrease. The same interactions which stabilize NW within the bonding pocket may also contribute to entropic penalties not seen in IW and FW binding relative to glutamate. In the NW-bound structures of GluA2 and GluA3, the nitro group is accommodated in the binding pocket through a change in the

rotameric state of the M712 sidechain at the β carbon. Furthermore, displacing and solvating glutamate may not overcome the conformational entropic penalties induced by NW binding to GluA2-s1s2. While it is possible that NW binding relative to glutamate may lead to changes in solvation and in the structure of GluA2-s1s2 that are entropically favorable, those changes were not sufficiently positive to result in a net increase in entropy. Despite the unfavorable entropy of binding relative to glutamate, NW binding to GluA2-s1s2 is driven by a larger and negative enthalpy of binding resulting in a favorable increase in free energy of binding relative to glutamate.

Iodowillardiine binding relative to glutamate at 5°C and 15°C. In addition to the NW, FW, ClW and IW experiments performed at 10°C, displacement ITC experiments were performed at 5°C and 15°C for glutamate displacement by IW (Figure 2.6). Iodowillardiine displacement of glutamate was endothermic at all three temperatures and became more unfavorable as the temperature increased (Table 2.5). The favorable entropy of binding relative to glutamate also increased with increasing temperatures but not sufficiently to result in favorable changes in free energy of binding relative to glutamate ($\Delta\Delta G^{obs}$ = 0.88 kcal/mol). Similar to the other partial agonists, iodowillardiine is interesting in that it may bind GluA2-s1s2 and, based on crystal structures, sample a variety of conformations (Jin *et al.*, 2003; Ahmed *et al.*, 2011). The heat capacity is proportional to the non-polar surface area of the solute molecule exposed to water (Creighton,

1992), and a comparison of enthalpy values at different temperatures for both the IW-bound complex and the glutamate-bound complex would allow us to determine how much of the IW-bound GluA2-s1s2 complex is exposed to solution versus the glutamate bound GluA2-s1s2 structure.

With the exception of IW, binding of all of the 5-substituted willardiines examined resulted in changes in free energy relative to glutamate that were favorable (Table 2.4). Favorable changes in free energy despite endothermic enthalpies of binding relative to glutamate for IW, FW, and ClW, were primarily due to increases in entropy. Fluorowillardiine, NW, and ClW bind with high affinities to GluA2-s1s2 which are not reflective of their abilities to induce channel opening (Figure 2.4). Jin and Gouaux (2003) attribute their high binding affinities to the interactions they make with side chains in lobe 1 of GluA2-s1s2 which are also shared by full agonists. In our studies, partial agonist binding to GluA2-s1s2 relative to glutamate is driven by either favorable entropies (IW, ClW, and FW) or favorable enthalpy (NW).

CONCLUSION

Competitive antagonists and partial agonists bind to the same site on the glutamate receptor as full agonists; however, antagonist binding does not induce channel opening leading to signal propagation. Partial agonist binding can lead to signal propagation, but single channel studies indicate that openings tend to populate lower conductance levels compared to full agonists in which higher conductance levels are more prevalent. Agonists, antagonists and partial agonists share interactions with lobe 1 of GluA2-s1s2 that are considered essential for locking the ligand into place; however, the driving forces that dominate binding to both lobes vary significantly between these functionally distinct ligands.

The full agonist, glutamate, binds to the apo state of GluA4-s1s2 with a favorable enthalpy and entropy at 10°C. Antagonist binding to GluA2-s1s2 relative to glutamate is characterized by favorable enthalpies and entropic penalties at 10°Cthat lead to near-zero or unfavorable changes in free energy. In the only other study of AMPA receptor antagonists using displacement ITC, antagonists (*RS*)-NS1209 and (*S*)-ATPO also bind with large entropic penalties and are primarily driven by favorable enthalpy changes of binding (Kasper *et al.,* 2006). DNQX and CNQX were selected for thermodynamic studies based on their ability to potently and selectively block AMPA receptors (Menuz *et al.*, 2007). The willardiine derivatives, UBP277 and UBP282, result in a greater degree of lobe opening relative to

the glutamate-bound state, yet bind with lower affinity than DNQX and CNQX.

One underlying theory of partial agonism is that the receptor exists in equilibrium between two states: active and resting. Fenwick and Oswald (2010) have recently suggested that partial agonists' shift the equilibrium towards open domain conformations. Open domain conformations may be less restricted which would correlate with our experimental results of increasing entropy as a result of partial agonist binding to GluA2-s1s2 relative to glutamate. It was previously suggested by Jin *et al.* (2003) that partial agonists such as FW and do not use their binding energy in gating or opening the ion channel. Based on our ITC studies, partial agonists may not be able to couple the energy of binding to opening of the ion channel because the interactions or lack of interactions between IW, FW, ClW and the binding pocket may not provide sufficient enthalpic energy. This is the first study to use a thermodynamic approach to evaluate the differences between full and partial agonist binding.

Investigating the balance between enthalpic and entropic contributions of antagonist and partial agonist binding may provide clues about how to optimize affinities of medically relevant ligands. The GluA2 antagonist (*S*)-NS1209 has shown robust anticonvulsant and neuroprotective effects in clinical trials (Kasper *et al.*, 2006). Future studies of these compounds that identify individual contributions to net observed entropy and enthalpy values may lead to more detailed information about

how to develop high affinity, subtype-specific GluA2 antagonists for use in clinical studies. While it is evident that more detailed ITC studies are needed, an expansive view of partial agonism is emerging. The mechanism by which partial agonist binding leads to channel opening is still unresolved and our results may contribute to an understanding of the thermodynamic basis of partial agonist binding.

REFERENCES

Abele R, Lampinen M, Keinänen K, Madden DR. Disulfide bonding and cysteine accessibility in the alpha-amino-3-hydroxy-5-methylisoxazole-4-propionic acid receptor subunit GluRD. Implications for redox modulation of glutamate receptors. *J Biol Chem.* 1998 Sep 25; 273 (39):25132-8.

Abele R, Svergun D, Keinänen K, Koch MH, Madden DR. A molecular envelope of the ligand-binding domain of a glutamate receptor in the presence and absence of agonist. *Biochemistry*. 1999 Aug 24; 38 (34):10949-57.

Ahmed AH, Loh AP, Jane DE, Oswald RE. Dynamics of the S1S2 glutamate binding domain of GluR2 measured using 19F NMR spectroscopy. *J Biol Chem*. 2007 Apr 27; 282 (17):12773-84.

Ahmed AH, Thompson MD, Fenwick MK, Romero B, Loh AP, Jane DE, Sondermann H, Oswald RE. Mechanisms of antagonism of the GluR2 AMPA receptor: structure and dynamics of the complex of two willardiine antagonists with the glutamate binding domain. *Biochemistry.* 2009 May 12;48 (18):3894-903.

Ahmed AH, Wang S, Chuang HH, Oswald RE. Mechanism of AMPA receptor activation by partial agonists: disulfide trapping of closed lobe conformations. *J Biol Chem.* 2011 Oct 7; 286 (40):35257-66.

Armstrong N, Sun Y, Chen GQ, Gouaux E. Structure of a glutamate-receptor ligand-binding core in complex with kainate. *Nature*. 1998 Oct 29; 395 (6705): 913-7.

Armstrong N, and Gouaux E. Mechanisms for activation and antagonism of an AMPA-sensitive glutamate receptor: crystal structures of the GluR2 ligand binding core. *Neuron.* 2000 Oct;28 (1):165-81.

Armstrong N, Mayer M, Gouaux E. Tuning activation of the AMPA-sensitive GluR2 ion channel by genetic adjustment of agonist-induced conformational changes. *Proc Natl Acad Sci U S A.* 2003 May 13;100(10):5736-41.

Bjerrum EJ, Biggin PC. Rigid body essential X-ray crystallography: distinguishing the bend and twist of glutamate receptor ligand binding domains. *Proteins.* 2008 Jul; 72 (1):434-46.

Chen GQ, Gouaux E. Overexpression of a glutamate receptor (GluR2) ligand binding domain in Escherichia coli: application of a novel protein folding screen. *Proc Natl Acad Sci* U S A. 1997 Dec 9;94 (25):13431-6.

Creighton, TE. Proteins: Structures and Molecular Properties. W. H. Freeman; Second Edition edition (August 15, 1992).

Crespo A, Fernández A. Induced disorder in protein-ligand complexes as a drug-design strategy. *Mol Pharm.* 2008 May-Jun;5 (3):430-7.

Dingledine R, Borges K, Bowie D, Traynelis SF.The glutamate receptor ion channels. *Pharmacol Rev.* 1999 Mar;51 (1):7-61.

Doyle ML. Characterization of binding interactions by isothermal titration calorimetry. *Current Opinion in Biotechnology.* 1997, 8:31-35

Dolman NP, Troop HM, More JC, Alt A, Knauss JL, Nistico R, Jack S, Morley RM, Bortolotto ZA, Roberts PJ, Bleakman D, Collingridge GL, Jane DE. Synthesis and pharmacology of willardiine derivatives acting as antagonists of kainate receptors. *J Med Chem*. 2005 Dec 1;48 (24):7867-81.

Fenwick MK and Oswald RE. NMR spectroscopy of the ligand-binding core of Ionotropic Glutamate Receptor 2 Bound to 5-Substituted Willardiine Partial Agonists. J Mol Biol.2008 May 2;378(3):673-85.

Fenwick MK, and Oswald RE. On the mechanism of the AMPA Receptor Binding to Glutamate and Kainate. *J Biol Chem.* 2010 Apr 16;285 (16):12334-43.

Freyer MW, Lewis EA. Isothermal titration calorimetry: experimental design, data analysis, and probing macromolecule/ligand binding and kinetic interactions. *Methods Cell Biol.* 2008; 84: 79-113.

Frølund B, Tagmose L, Jørgensen AT, Kristiansen U, Stensbøl TB, Liljefors T, Krogsgaard-Larsen P.Design and synthesis of a new series of 4-alkylated 3-isoxazolol GABA A antagonists. *Eur J Med Chem*. 2003 Apr;38 (4):447-9.

Gillessen T, Budd SL, Lipton SA. Excitatory amino acid neurotoxicity. *Adv Exp Med Biol*. 2002; 513:3-40. Review.

Hansen KB, Yuan H, Traynelis SF. Structural aspects of AMPA receptor activation, desensitization and deactivation. *Curr Opin Neurobiol.* 2007 Jun;17(3):281-8.

Hogner A, Greenwood JR, Liljefors T, Lunn ML, Egebjerg J, Larsen IK, Gouaux E, Kastrup JS. Competitive antagonism of AMPA receptors by ligands of different classes: crystal structure of ATPO bound to the GluR2 ligand-binding core, in comparison with DNQX. *J Med Chem.* 2003 Jan 16; 46(2):214-21.

Hollmann M, Heinemann S. Cloned glutamate receptors. *Annu Rev Neurosci.* 1994; 17:31-108.

Jane DE, Hoo K, Kamboj R, Deverill M, Bleakman D, Mandelzys A. Synthesis of willardiine and 6-azawillardiine analogs: pharmacological characterization on cloned homomeric human AMPA and kainate receptor subtypes. *J Med Chem.* 1997 Oct 24; 40 (22):3645-50.

Jin R, Gouaux E. Probing the function, conformational plasticity, and dimer-dimer contacts of the GluR2 ligand-binding core: studies of 5-substituted willardiines and GluR2 s1s2 in the crystal. *Biochemistry*. 2003 May13;42 (18):5201-13.

Jin R, Banke TG, Mayer ML, Traynelis SF, Gouaux E. Structural basis for partial agonist action at ionotropic glutamate receptors. *Nat Neurosci*. 2003 Aug;6 (8): 803-10.

Kasper C, Pickering DS, Mirza O, Olsen L, Kristensen AS, Greenwood JR, Liljefors T, Schousboe A, Wätjen F, Gajhede M, Sigurskjold BW, Kastrup JS. The structure of a mixed GluR2 ligand-binding core dimer in complex with (S)-glutamate and the antagonist (S)-NS1209. *J Mol Biol*. 2006 Apr 7;357 (4):1184-201.

Koshland DE Jr, Némethy G, Filmer D. Comparison of experimental binding data and theoretical models in proteins containing subunits. *Biochemistry*. 1966 Jan;5 (1):365-85.

Kuusinen, A., Arvola, M., and Keina¨nen, K. Molecular dissection of the agonist binding site of an AMPA receptor. *EMBO J.* 1995. 14, 6327–6332.
Madden DR, Abele R, Andersson A, Keinänen K. Large-scale expression and thermodynamic characterization of a glutamate receptor agonist-binding domain. *Eur J Biochem.* 2000 Jul; 267(13):4281-9.

Maltsev AS, Ahmed AH, Fenwick MK, Jane DE, Oswald RE. Mechanism of partial agonism at the GluR2 AMPA receptor: Measurements of lobe orientation in solution. *Biochemistry.* 2008 Oct 7;47 (40):10600-10.

Maltsev AS, Oswald RE. Hydrophobic side chain dynamics of a glutamate receptor ligand binding domain. *J Biol Chem*. 2010 Mar 26;285 (13):10154-62.

Mamonova T, Yonkunas MJ, Kurnikova MG. Energetics of the cleft closing transition and the role of electrostatic interactions in conformational rearrangements of the glutamate receptor ligand binding domain.*Biochemistry.* 2008 Oct 21; 47(42):11077-85. Epub 2008 Sep 30.

Mayer ML, Armstrong N. Structure and function of glutamate receptor ion channels.Annu Rev Physiol.2004;66:161-81.

Menuz K, Stroud RM, Nicoll RA, Hays FA. TARP auxiliary subunits switch AMPA receptor antagonists into partial agonists. *Science.* 2007 Nov 2;318 (5851):815-7.

Monod J, Wyman J, Changeux JP. On the nature of allosteric transitions: a plausible model. *J. Mol Biol* . 1965 May;12:88-118.

More JC, Troop HM, Dolman NP, Jane DE.Structural requirements for novel willardiine derivatives acting as AMPA and kainate receptor antagonists. *Br J Pharmacol.* 2003 Mar;138 (6):1093-100.

Nakanishi, N., Schneider, N. A., and Axel, R. A family of glutamate receptor genes: Evidence for the formation of heteromultimeric receptors with distinct channel properties. *Neuron.* 1990. 5, 569–581.

Norinder U, Högberg T. A quantitative structure-activity relationship for some dopamine D2 antagonists of benzamide type. *Acta Pharm Nord.* 1992;4(2):73-8.

O'Hara, P. J., Sheppard, P. O., Thøgersen, H., Venezia, D., Haldeman, B. A., McGrane, V., Houamed, K. M., Thomsen, C., Gilbert, T. L., and Mulvihill, E. R. The ligand-binding domain in metabotropic glutamate receptors is related to bacterial periplasmic binding proteins. *Neuron* 1993. 11, 41–52.

Oswald RE. Ionotropic glutamate receptor recognition and activation. *Adv Protein Chem.* 2004; 68:313-49. Review.

Patneau DK, Mayer ML, Jane DE, Watkins JC. Activation and desensitization of AMPA/kainite receptors by novel derivatives of willardiine. *J Neurosci.* 1992 Feb; 12(2): 595-606.

Pentikäinen U, Settimo L, Johnson MS, Pentikäinen OT. Subtype selectivity and flexibility of ionotropic glutamate receptors upon antagonist ligand binding. *Org Biomol Chem.* 2006 Mar 21;4 (6):1058-70.

Poon K, Nowak LM, Oswald RE. Characterizing single-channel behavior of GluA3 receptors. *Biophys J.* 2010 Sep 8;99(5):1437-46.

Poon K, Ahmed AH, Nowak LM, Oswald RE. Mechanisms of modal activation of GluA3 receptors. *Mol Pharmacol.* 2011 Jul; 80(1):49-59. Epub 2011 Apr 4. Ritz M, Micale N, Grasso S, Niu L.Mechanism of inhibition of the GluR2 AMPA receptor channel opening by 2,3-benzodiazepine derivatives. *Biochemistry.* 2008 Jan 22; 47 (3):1061-9.

Robert A, Armstrong N, Gouaux JE, Howe JR. AMPA receptor binding cleft mutations that alter affinity, efficacy, and recovery from desensitization. *J Neurosci*. 2005 Apr 13;25 (15):3752-62.

Sigurskjold BW. Exact analysis of competition ligand binding by displacement isothermal titration calorimetry. *Anal Biochem*. 2000 Jan 15; 277 (2):260-6.

Taverna F, Xiong ZG, Brandes L, Roder JC, Salter MW, MacDonald JF. The Lurcher mutation of an alpha-amino-3-hydroxy-5-methyl- 4-isoxazolepropionic acid receptor subunit enhances potency of glutamate and converts an antagonist to an agonist. *J Biol Chem*. 2000 Mar 24; 275(12):8475-9.

Velázquez Campoy A, Freire E. ITC in the post-genomic era...? Priceless. *Biophys Chem.* 2005 Apr 1;115 (2-3):115-24. Epub 2004 Dec 25.

Wo, Z. G., and Oswald, R. E. Transmembrane topology of two kainate receptor subunits revealed by N-glycosylation. *Proc. Natl. Acad. Sci. USA* 1994. 91, 7154–7158.

CHAPTER 3.

Electrophysiological Studies of Cocaine and Cocaine Derivatives on Neuronal Nicotinic Acetylcholine Receptors.

ABSTRACT

Neuronal nicotinic acetylcholine receptors (nAChRs) are ligand-gated ion channels that mediate fast excitatory synaptic transmission in the central and peripheral nervous systems. They are expressed on neurons and mediate learning, reward and memory formation (Wonnacott, 1997). The role of nAChRs in nicotine addiction has been extensively studied. Interestingly, another drug of addiction, cocaine, also interacts with nAChRs as a non-competitive inhibitor (Karpen *et al.*, 1982; Swanson and Albuquerque, 1987). Using two-electrode voltage clamp and the oocyte expression system we tested the ability of cocaine and the cocaine derivatives to inhibit neuronal nicotinic subtypes α4β2, α3β4 and α4β4. Cocaine and cocaine methiodide inhibit all three subtypes in a dose-dependent manner. Inhibition of α4β2 and α3β4 by cocaine and cocaine methiodide is also voltage dependent indicating these drugs may bind to a site within the ion channel pore. Lastly, we tested the effects of benzoylecgonine on the α4β2 subtype which plays a central role in nicotine addiction (Schwartz and Kellar, 1983; Flores *et al.*, 1992; Tapper *et al.*, 2004). This is the first study to demonstrate that benzoylecgonine interacts with nAChRs and is more potent at the α4β2 subtype than cocaine. Characterizing the effects of cocaine and cocaine metabolites on nAChR subtypes illustrate the complexity of the molecular mechanism of cocaine addiction as it can interact with several targets. The primary method of treatment for cocaine addiction is behavioral therapy and nAChR receptor

modulation may be a promising avenue of pharmacological intervention for cocaine addiction.

INTRODUCTION

Neuronal nicotinic acetylcholine receptors (nAChRs) are ligand-gated ion channels that mediate fast excitatory synaptic transmission in the central and peripheral nervous systems (Wonnacott, 1997). They are involved in cognitive deficits resulting from neurodegenerative disorders such as schizophrenia, Alzheimer's disease, and Parkinson's disease (Kem, 2000; Leonard *et al.*, 1996; Quik and Jeyarasasingam, 2000); and are expressed on synaptic boutons, neurites, cell bodies, and axons of neurons (Bertrand, 2010), thus, perfectly positioning them for their critical role in regulating pre- and post-synaptic neurotransmitter release. Activation and resultant desensitization of nAChR subtypes by nicotine is considered the molecular basis of behavioral nicotine addiction (Dani and Heinemann, 1996). While the molecular basis of cocaine addiction has been primarily associated with inhibition of dopamine reuptake by blocking dopamine transporters (Ritz *et al.*, 1987; Carroll *et al.*, 1999); nicotinic receptors may also play a role in cocaine addiction, as the cholinergic system is directly involved in reward, learning, and memory (Williams and Adinoff, 2008).

Cocaine is a central nervous system stimulant, local anesthetic and illegal drug of abuse. It shares structural motifs with other local anesthetics such as an ionizable amine group and a hydrophobic moiety (Swanson and Albuquerque, 1987; Niu *et al.*, 1995). Similar to other local anesthetics, cocaine acts on voltage-gated sodium channels and its effects as a local anesthetic have been well characterized [Ragsdale *et al.*, 1994; Li *et al.*,

1999]. There is increasing evidence that cocaine interacts with multiple targets (Ye *et al.*, 1997; Xiao *et al.*, 1998; Breitinger *et al.*, 2001) and its interaction at dopamine transporters may be only one of several interactions that lead to cocaine addiction.

Cocaine is a non-competitive inhibitor of nAChRs (Karpen *et al.*, 1982; Swanson and Albuquerque, 1987). Francis *et al.* (2000) demonstrated cocaine's effects to be subtype specific and differences in apparent affinity for cocaine were caused by independent contributions from α- and β-subunits. Subsequent work on the interaction between cocaine and nAChRs led to the generation of small molecules which would prevent cocaine inhibition of nAChRs (Chen *et al.*, 2004), and the proposal of a minimum mechanism for inhibition of muscle-type nAChRs (Hess *et al.*, 2000).

Here we test the ability of cocaine and the cocaine derivatives, cocaine methiodide and benzoylecgonine, to inhibit neuronal nicotinic subtypes α4β2, α3β4 and, α4β4. Benzoylecgonine is one of several products generated *in vivo* as a result of cocaine metabolism, and until now, its effect on neuronal nAChR subtypes had not been investigated (Fig. 3.1). Nicotinic receptor subtypes that include the α3 subunit predominate in the peripheral nervous system where they mediate neurotransmission within autonomic ganglia (Luo *et al.*, 1998; Quick *et al.*, 1999; Whiteaker *et al.*, 2002). Cocaine inhibition of α3β4 may allow us to characterize the peripheral nervous system effects of cocaine. The α4β2 subtype is of interest in cocaine

addiction since it is widely expressed in the brain and has a high affinity binding site for another highly addictive drug, nicotine (Flores *et al.,* 1992).

Cocaine methiodide is of particular interest for several reasons. It acts as a homomeric α7 nAChR agonist, 6-fold more potent than acetylcholine at this subtype, but is an antagonist at heteromeric nAChR subtypes (Francis *et al.*, 2001). The quaternary amine of cocaine methiodide is charged preventing it from crossing the blood brain barrier (Schindler *et al.*, 1992). In addition to the reinforcing feelings of euphoria elicited by cocaine use, cocaine is also responsible for physiological effects such as locomotor stimulation and myocardial ischemia (Kalivas, 2007; Koob and Kreek, 2007). The toxic effects of cocaine methiodide are similar to those of cocaine but the stable charge on cocaine methiodide allows us to investigate peripheral nervous system effects. Cocaine methiodide can also be a useful probe to investigate extracellular allosteric binding sites or sites within the ion channel pore since it can't cross the cell membrane. Concentration-response curves for cocaine methiodide will allow us to further characterize its inhibitory effects on heteromeric neuronal nicotinic receptor subtypes.

Studies of the mechanism by which inhibitors interact with nAChRs have been ongoing since the late 1970's. Non-competitive inhibitors may act by binding to extracellular allosteric sites, blocking the ion channel, or stabilizing a desensitized state of the receptor (Hansen and Taylor, 2007). The site where non-competitive inhibitors, such as cocaine, interact with heteromeric nicotinic receptors appears to be similar to the modulating site

of benzodiazepines on $GABA_A$ receptors (Hansen and Taylor, 2007), thus underscoring the importance of characterizing cocaine's interactions at these receptors. Moreover, increasing evidence suggests the cholinergic system is involved in cocaine addiction (Williams and Adinoff, 2008). Characterization of cocaine and cocaine derivatives on neuronal nicotinic receptor subtypes may contribute to a greater understanding of non-competitive inhibition, and provide the impetus for future drug development as there is presently no treatment or cure for cocaine addiction.

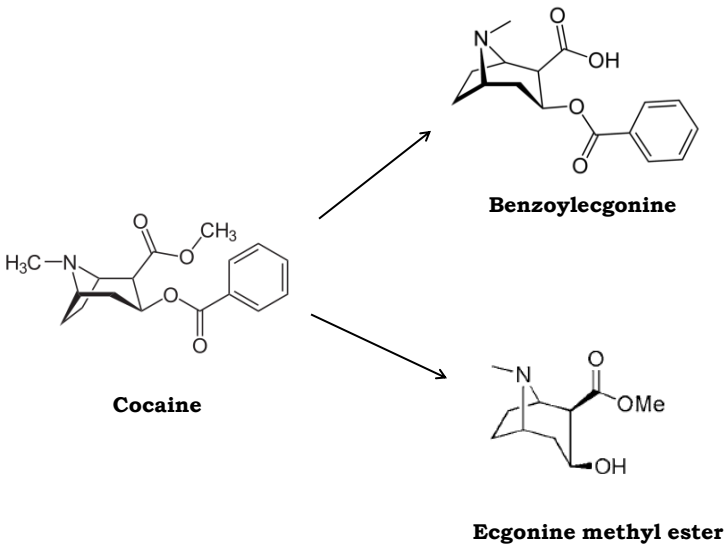

Figure 3.1 Cocaine Metabolites. One of several cocaine degradation pathways: cocaine is hydrolyzed in the liver, lungs, kidneys, and brain by carboxylesterases (hCE-1) to form benzoylecgonine and ecgonine methyl ester [Dean et al., 1991; Brzezinski et al., 1997; Toennes, et al., 2003].

METHODS

Materials. Cocaine, cocaine methiodide, and benzoylecgonine were provided by the National Institute on Drug Abuse (Bethesda, MD). Drug stock solutions were prepared daily prior to electrophysiological experiments and diluted to working concentrations in oocyte saline solution (82.5 M NaCl, 2.5 M KCl, 1 mM NaH_2PO_4, 15 mM Hepes, 1 mM $MgCl_2$, pH 7.4). Cell culture reagents were purchased from Invitrogen (Carlsbad, CA). All other chemical reagents were purchased from Sigma-Aldrich (St. Louis, MO). Rat cDNA for nAChR subtypes was provided by Dr. Steve Heinnemann (Salk Institute, La Jolla, CA) and Dr. Jim Boulter (Semel Institute at UCLA, Los Angeles, CA).

RNA preparation and oocyte expression system. cDNA for nAChR subtypes was linearized and purified for mRNA generation. mRNA transcripts were generated using the mMessage mMachine in vitro RNA transcription kit (Ambion, TX). RNA transcription was confirmed through agarose gel electrophoresis under denaturing conditions and visualized with ethidium bromide as previously described [Francis *et al.*, 2000]. RNA stocks were diluted to 500ng/mL and stored in ribonuclease-free water at -80°C. Adult female *Xenopus laevis* frogs were anesthetized prior to surgery and an incision was made through the abdominal cavity of each frog. Ovarian lobes were gently tugged out of the cavity, and lobules were snipped off of the parent lobe, sliced open and placed immediately in collagenase solution (1

mg/mL collagenase, 82.5 M NaCl, 2.5 M KCl, 1mM NaH_2PO_4, 15 mM Hepes, 1mM $MgCl_2$, pH 7.4). Incisions were sutured and female frogs were monitored until waking and subsequently transported to the animal care facility. Ovarian tissue was digested at room temperature for 1-2 hours on a rocker at low speed. Healthy stage IV oocytes were sorted (3-5 hrs), washed and placed in oocyte storage medium (oocyte saline solution with 1.8 mM $CaCl_2$, 5 U/mL penicillin, 5 μg/mL streptomycin, and 5% fetal calf serum) overnight at 37°C. Healthy oocytes were injected with 50 nl of RNA for specific subtypes (*i.e.* 1:1 for the α4β2 subtype), stored at 37°C and media was changed daily.

Electrophysiology. Two-electrode voltage-clamp experiments were performed at room temperature with a Turbo Tec 01C amplifier (Adams & List, Westbury, NY) at a holding potential of -50 mV. Recording electrodes were backfilled with 3 M KCl and were pulled with tips having resistances from 1-3 MΩ. Recording solution (oocyte saline solution supplemented with 1.8 mM $CaCl_2$) was perfused 0.5 mm above the oocyte at a rate of 5 mL/min. through a Lucite recording chamber. Data were collected on a Gateway personal computer at a sampling rate of 100 Hz using pClamp 5.5.1 (Axon Instruments, Foster City, CA) and filtered at 30 Hz using a low pass filter in the amplifier. After each drug application 2 min. of data were acquired for each oocyte. Oocyte responses to substances tested were normalized to an agonist-induced response 3 min prior to the experimental response. Before and after each drug application, the oocyte and chamber were perfused for 3

min with oocyte saline solution. After each drug application, a second control application of agonist was applied to assess receptor rundown (Fig. 3.2). Oocyte responses to the second control application of agonist that were not within 10% of the peak current amplitude of the primary control application were excluded from analysis. IC_{50} values were calculated with Origin© 7.0 (Northampton, MA) using non-linear least-squares fit to the equation:

$$\text{Response} = (\text{Response}_{max}) \frac{[IC_{50}]^n}{[\text{antagonist}]^n + [IC_{50}]^n}$$

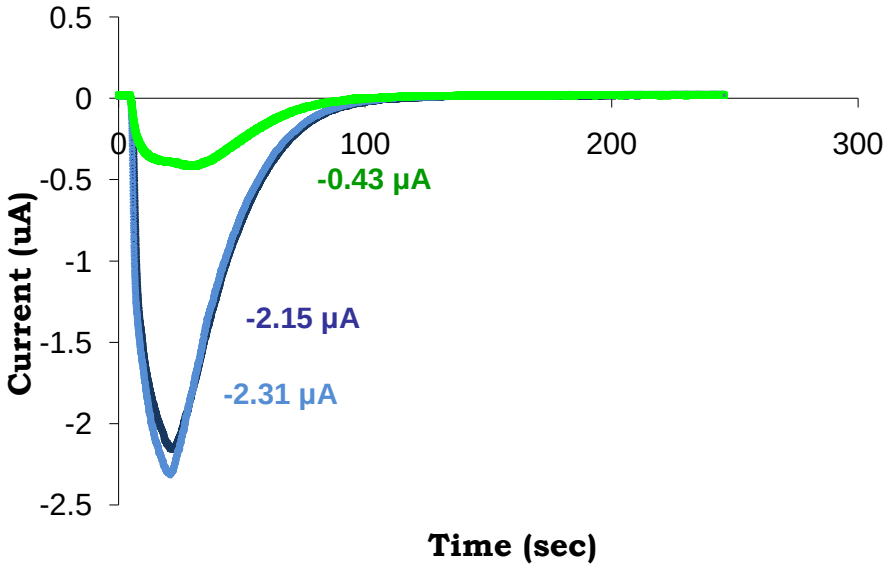

Figure 3.2 Oocyte Control and Inhibitory Responses of nAChR subtype α3β4. Agonist application of 50 µM ACh (light blue trace) results in a peak current of -2.31 µA. A second co-application of cocaine (100 µM) and 50 µM ACh (light green trace) results in a peak current of -0.43 µA. A final control application of 50 µM ACh alone (dark blue trace) leads to a -2.15 µA peak current. Each drug application was followed by a 3 minute wash with oocyte saline solution.

RESULTS

One of the advantages of using the *Xenopus laevis* oocyte expression system to study ligand-gated ion channels is that it allows us characterization of pharmacological effects for specific nicotinic receptor subunit combinations. When cocaine is co-applied with 50 μM ACh, cocaine inhibits neuronal nicotinic α4β2, α3β4 and α4β4 subtypes with IC_{50} values of 28 ± 2.9 μM, 7.1 ± 0.33 μM, and 5 ± 0.76 μM, respectively. Based on the concentration-inhibition curves, cocaine binds to the α4β4 subtype with a greater affinity than the α4β2 and α3β4 subtypes. The IC_{50} value for the α3β4 subtype was two-fold greater than the IC_{50} value for α4β4, while the IC_{50} value for the α4β2 subtype was eight-fold greater than the α4β4 subtype, indicating a eight-fold lower affinity of cocaine compared to the α4β4 subtype. Concentration-inhibition curves are shown in Figure 3.3 and IC_{50} values are summarized in Table 3.1.

In addition to cocaine, inhibition by cocaine methiodide inhibition was evaluated on the α4β2, α3β4 and α4β4 subtypes. Similar to cocaine, cocaine methiodide inhibits all three subtypes in a concentration-dependent manner, indicating a direct interaction with each of the receptor subtypes. Based on concentration-inhibition curves, the cocaine derivative, cocaine methiodide inhibited the α4β2, α3β4 and α4β4 subtypes with IC_{50} values of 11 ± 0.56 μM, 24 ± 1.6 μM and 1.1 ± 0.18 μM, respectively (Fig. 3.4). Cocaine methiodide inhibition of all three subtypes exhibited a similar trend to cocaine inhibition in that cocaine inhibited α4β4 with the greatest affinity

and α4β2 with the lowest affinity. The IC_{50} value for α3β4 was two-fold greater than that of α4β4, indicating a two-fold lower affinity of cocaine methiodide for the α3β4 subtype. IC_{50} values for cocaine methiodide inhibition of these subtypes have not been previously published. Table 3.1 summarizes these values, in comparison with previously published cocaine inhibition results.

In order to determine whether cocaine methiodide was inhibiting α3β4 by binding to a site within the ion channel pore, we determined the voltage dependence of the inhibition on the α3β4 subtype. Whole cell oocyte recordings were performed at a holding potential range from -50 mV to -10 mV. Co-application of 10 μM cocaine methiodide with 25 μM ACh at a holding potential of -50 mV resulted in 30% inhibition. Application of the same concentrations of cocaine methiodide and ACh at a holding potential of -20 mV resulted in 11% inhibition, while raising the holding potential to -10 mV resulted in outward current (Fig. 3.5A). Similar to cocaine inhibition of this subtype, cocaine methiodide inhibition of α3β4 appears linear over the holding potential range tested. Subsequently, we tested the voltage dependence of cocaine inhibition on the α4β2 subtype at a holding potential range between -100 mV and -40 mV. Co-application of 30 μM cocaine with 50 μM ACh resulted in 63% inhibition at a holding potential of -100 mV. Co-application of cocaine and ACh at the same concentrations and at a holding potential of -40 mV resulted in 26%, inhibition. Similar to cocaine

methiodide inhibition of α3β4cocaine inhibition of α4β2 appears linear over the holding potential range tested (Figure 3.5C).

Lastly we tested the ability of the cocaine metabolite, benzoylecgonine, to inhibit the α4β2 subtype which plays a critical role in nicotine addiction. Cocaine and cocaine methiodide inhibition at 10 µM were compared to benzoylecgonine inhibition at the same concentration. When co-applied with 50 µM ACh, benzoylecgonine inhibited the response to ACh by 69% while cocaine and cocaine methiodide inhibited the response to ACh by 31% and 47% respectively (Fig. 3.6).

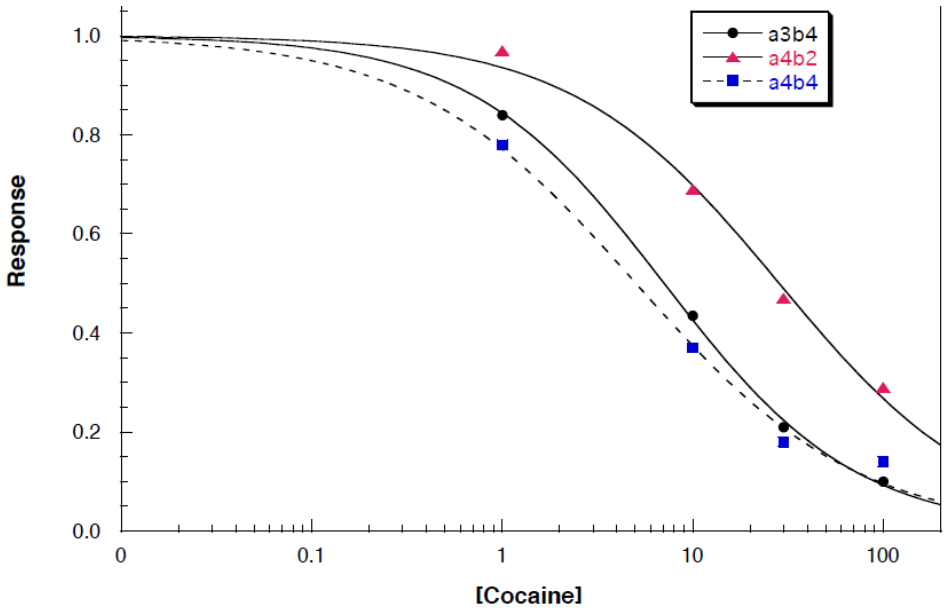

Figure 3.3 Concentration Dependence of Cocaine Inhibition of nAChR subtypes, α4β2, α3β4, and α4β4. Data were normalized to an initial response to 50 µM ACh alone. Each data point represents the mean of three oocyte responses. IC_{50} values were calculated using a nonlinear, least-squares fit as previously described and yielded IC_{50} values of 28 ± 2.9 µM for α4β2 (n=0.79), 7.1 ± 0.33 µM for α3β4 (n=0.86), and 5.0 ± 0.76 µM for α4β4 (n=0.75).

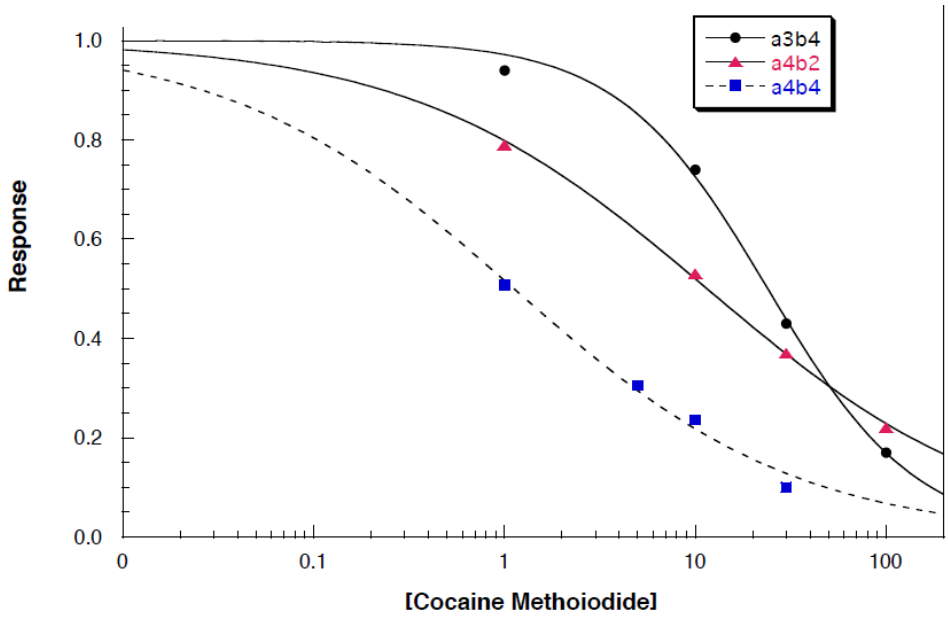

Figure 3.4 Concentration Dependence of Cocaine Methiodide Inhibition of nAChR subtypes α4β2, α3β4, and α4β4. Data were normalized to an initial response to 50 µM ACh alone. Each data point represents the mean of three oocyte responses. IC_{50} values were calculated using a nonlinear, least-squares fit as previously described and yielded IC_{50} values of 11 ± 0.56 µM for α4β2 (n=0.56), 24 ± 1.6 µM for α3β4 (n=1.1) and 1.1 ± 0.18 µM for α4β4 (n=0.58).

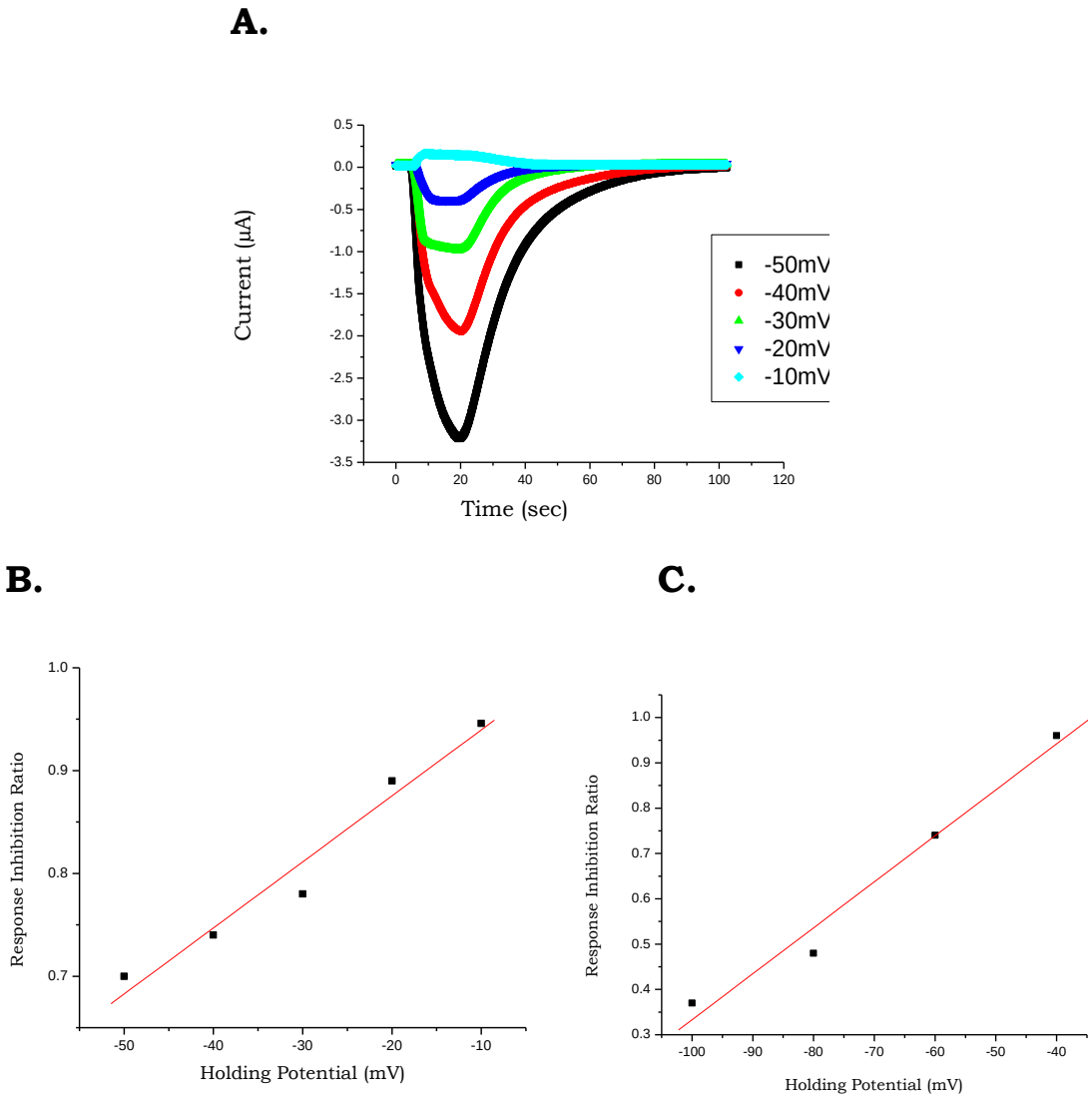

Figure 3.5 Voltage-dependence of cocaine methiodide inhibition of α3β4 and cocaine inhibition of α4β2. (A) Oocyte whole cell currents generated by co-application of 25 µM ACh and 10 µM cocaine methiodide at holding potentials from -50 mV to -10 mV for the α3β4 subtype (B). Data represent ratio of current responses in the presence and absence of inhibitor versus membrane holding potential. (C.) Data for α4β2 was generated by co-application of 50 µM ACh and 30 µM cocaine at holding potentials between -100 mV and -40 mV. Data for both subtypes represent a single series of recordings.

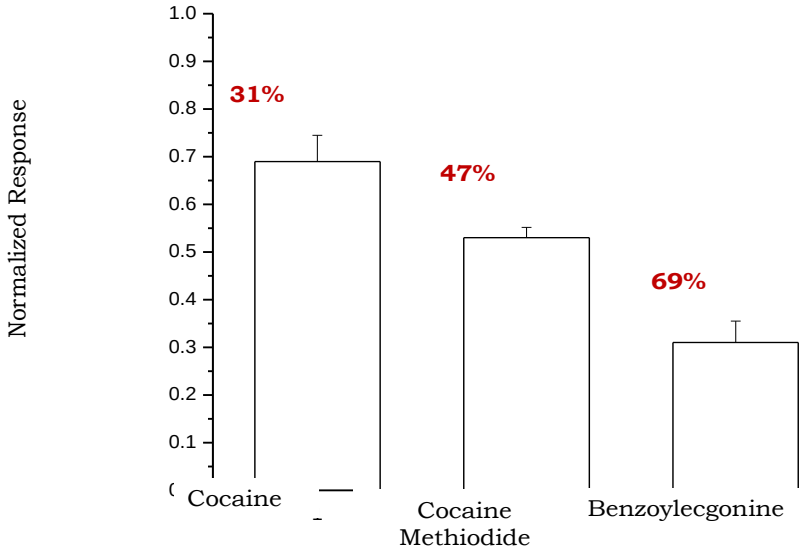

Figure 3.6 Cocaine, Cocaine Methiodide, and Benzoylecgonine inhibition α4β2 nAChRs. Comparison of cocaine, cocaine methiodide and benzoylecgonine inhibition when co-applied with 50 μM ACh. Cocaine and cocaine derivatives were tested at a concentration of 10 μM. Oocyte responses (3 for each inhibitor tested) were normalized responses to agonist alone. Percentages are the inhibition produced by each compound.

Table 3.1. *IC50* values for cocaine and cocaine methiodide inhibition.

nAChR Subtype	Cocaine (Francis *et al.*, 2000)	Cocaine (μM)	Cocaine Methiodide
α4β2	15 ± 1	28 ± 2.9	11 ± 0.56
α3β4	6 ± 1	7.1 ± 0.33	24 ± 1.6
α4β4	2 ± 1	5 ± 0.76	1.1 ± 0.18

DISCUSSION

Cocaine inhibited all three nicotinic receptor subtypes in a concentration-dependent manner. Based on the IC_{50} values, cocaine binds to the α4β4 subtype with a greater affinity than the α4β2 and α3β4 subtypes. Comparing the IC_{50} values between α4β4 and α4β2, the β4 subunit causes an 8-fold increase in cocaine affinity. Francis *et al.* (2000) demonstrated that the β4 subunit in the α4β4 subtype led to a 7-fold increase in cocaine affinity compared to the α4β2 subtype, leading to the conclusion that the β4 subunit may contribute to a high-affinity allosteric site for cocaine. This is also supported by evidence from the x-ray crystallography study of Hansen and Taylor (2007) in which the soluble acetylcholine binding protein (AChBP) was co-crystallized with cocaine and galanthamine, a nAChR positive modulator. AChBP is a soluble homopentamer which is homologous to the binding domain of nAChRs (Smit *et al.*, 2001; Hansen *et al.*, 2004). Hansen and Taylor (2007) substituted amino acid residues in loop C of AChBP so that the subunit resembled the β subunit of neuronal nAChRs. As a result, cocaine displaced [^{3}H]-strychnine with a K_d value of 2.1 ± 0.7 μM indicating a high affinity binding site for cocaine may exist on the β subunit. The α4 subunit may also contribute to a high affinity binding site for non-competitive inhibitors. The IC_{50} value of α3β4 is over 2-fold greater than that of α4β4, indicating a 2-fold decrease in affinity is associated with the difference in alpha subunit. This was also

seen in the study by Francis *et al.* (2000) in which the cocaine affinity of α4β2 was 4-fold higher compared to the α3β2 subunit combination.

Cocaine methiodide inhibition was also characterized on the α4β2, α3β4 and α4β4 subunit combinations. Based on our inhibition curves (Fig. 3.4), cocaine methiodide inhibited the α4β4 subtype with the highest affinity and α4β2 with the lowest, similar to what was seen with cocaine. Francis *et al.* (2001) tested the effects of a single concentration of cocaine methiodide (30 μM) on these subtypes and found that at this concentration, cocaine methiodide inhibited the α3β4 subtype 5-10% more than cocaine. In contrast we found cocaine 2-3 fold more potent than cocaine methiodide on α3β4. The differences between our data may be due to their use of a 30 sec pre-incubation with the inhibitor prior to agonist application, while no prior incubation with inhibitors was performed in this study. Our results may also differ because of the different agonist concentrations co-applied with the inhibitors. For this study 50 μM ACh was co-applied with cocaine methiodide (EC_{50} value for α3β4 43 ± 4 μM; Francis *et al.*, 2000); while Francis *et al.* (2001) used 30 μM ACh with a single concentration of 30 μM cocaine methiodide.

Our interest in testing cocaine methiodide stemmed in part from its ability to act as an agonist at α7 homomeric receptors but as an antagonist at heteromeric nAChRs. Cocaine methiodide is formed by the addition of a methyl group to the amine moiety of cocaine, converting it from a tertiary to a quaternary amine (Francis *et al.*, 2001). Neher and Steinbach (1978) have

shown that quaternization of local anesthetics that act as nAChR inhibitors affect the state-dependence of inhibition, and inhibitory effects are limited to the open channel state of the receptor. Since cocaine methiodide is positively charged, inhibitory effects seen in our experiments would be the result of binding to an extracellular allosteric site, or a site within the ion channel pore exposed when the channel is in the open state. Cocaine methiodide inhibition appears linear over the holding potential range tested and based on our results, cocaine methiodide appears to be inhibiting α3β4 by binding to a site within the ion channel or by blocking the ion channel pore (Fig. 3.5). When we tested the voltage dependence of cocaine inhibition of α4β2 at a range of holding potentials between -100 mV and -40 mV, there was also a linear dependence.

Francis *et al.* (2000) had previously tested the voltage-dependence of cocaine inhibition of the α3β4 and α4β2 subtypes and found that the α4β2 subtype exhibited weaker voltage-dependence than α3β4 at equipotent concentrations and similar holding potentials. This led the authors to conclude that cocaine was inhibiting α3β4 and α4β2 by two distinct mechanisms. Since we only have a single series of data for each subtype we cannot make similar comparisons; however, since inhibition of both subtypes by cocaine methiodide and cocaine are voltage dependent, these drugs appear to be inhibiting by binding to a site within the ion channel pore. Local anesthetics such as tetracaine and cocaine inhibit voltage-gated sodium channels by binding to sites within the ion channel pore (Ragsdale

et al., 1994; Li *et al.*, 1999). Interestingly, inhibition of sodium channels by local anesthetics is frequency and voltage-dependent, and local anesthetics bind with a higher affinity when sodium channels are in open or inactivated states. Moreover, local anesthetics such as lidocaine, procaine, and tetracaine non-competitively inhibit the α3β4 nAChR subtype in a manner consistent with open-channel blockade (Gentry and Lukas, 2001; Papke *et al.*, 2001). Since α3β4 subtype receptors are expressed in autonomic ganglia in the peripheral nervous system, they may also be contributing to the peripheral effects of cocaine.

As early as 1986, a high-affinity site for non-competitive inhibitors was localized to the membrane-spanning helix, M2, of the membrane-bound nicotinic acetylcholine receptor from *Torpedo marmorata* (Giraudat, *et al.*, 1986). Each acetylcholine receptor subunit is formed by four transmembrane domains, and the M2 transmembrane α-helix is of particular interest since it lines the ion channel pore (Miyazawa *et al.*, 2003; Unwin, 2005). The binding sites for several non-competitive inhibitors such as barbiturates, dissociative anesthetics, and anti-depressants have more recently been localized to regions along the M2 α-helix (Arias *et al.*, 2006). Specifically, the leucine at position 9' contributes to a binding site shared by all of these non-competitive inhibitors in the desensitized state of nAChRs. Based on our voltage dependence studies of cocaine methiodide inhibition of α3β4, and voltage dependence studies of cocaine inhibition of α3β4 and

α4β2 by Francis *et al.*, 2000, the M2 transmembrane domain may contain a major site of cocaine and cocaine methiodide action.

Benzoylecgonine is one of the major urinary metabolites and a diagnostic tool for detecting cocaine use (Ambre *et al.*, 1985). Cocaine is converted to benzoylecgonine through two distinct pathways in the liver, kidney, lungs and brain (Dean *et al.*, 1985; Toennes, *et al.*, 2003). Human carboxylesterase-1 (hCE-1) hydrolyzes cocaine to benzoylecgonine (Dean *et al.*, 1991; Brzezinski *et al.*, 1997) and hydrolytic cleavage of the methyl ester of cocaine occurs spontaneously at body temperature to form benzoylecgonine (Inaba, 1989). Because the α4β2 subtype plays a central role in nicotine addiction (Schwartz and Kellar, 1983; Flores *et al.*, 1992; Tapper *et al.*, 2004) we tested the effects of benzoylecgonine on this neuronal subtype.

Ten μM benzoylecgonine inhibited 69% of the response of the α4β2 subtype to 50 μM ACh, while cocaine and cocaine methiodide only inhibited the response by 31% and 47% respectively (Fig. 3.6). Historically benzoylecgonine has been considered an inactive metabolite since it has no effect on the re-uptake of monoamine neurotransmitters (Jatlow, 1988). This is the first study demonstrating that benzoylecgonine can inhibit nicotinic receptor subtypes which is of interest for several reasons. Cocaine itself is eliminated rapidly from the body (30 minutes to 1 hour—dependent upon route of administration), while the half-life of benzoylecgonine, one of its major metabolites, is 4.5-5 hours and can be detected for up to 48 hours

after cocaine use (Ambre *et al.*, 1984; Chow *et al.*, 1985; Hawks and Chiang, 1986; Ambre *et al.*, 1988). It is therefore possible for benzoylecgonine to inhibit neuronal α4β2 receptors long after cocaine has been eliminated from the body. The effect of benzoylecgonine on nicotinic receptors and nicotinic receptors' subsequent involvement in cocaine addiction is difficult to interpret since nAChRs modulate the release of both excitatory and inhibitory neurotransmitters in several areas of the brain associated with addiction and reward (Adinoff *et al.*, 2010). It is significant interest to further characterize benzoylecgonine inhibition on α4β2 receptors since this subtype is widely expressed in the brain and plays a critical role in nicotine addiction. It may also be of interest to determine whether benzoylecgonine acts as a competitive antagonist, and whether it inhibits other heteromeric receptor subtypes, or perhaps even activates homomeric nicotinic receptors similar to cocaine methiodide.

CONCLUSION

Cocaine and cocaine methiodide are non-competitive inhibitors of neuronal α4β2, α3β4 and α4β4 receptor subtypes. nAChR subtypes are differentially expressed throughout the central nervous system, allowing us to investigate brain region-specific effects. Similar to cocaine inhibition of α3β4 by cocaine methiodide is voltage-dependent indicating both compounds may bind to sites within the ion channel pore similar to other non-competitive nAChR inhibitors and local anesthetics. The cocaine metabolite, benzoylecgonine, inhibits the α4β2 subtype with higher potency than cocaine or cocaine methiodide. This is the first study to demonstrate that benzoylecgonine interacts with nAChRs. Since neuronal nicotinic receptors are expressed on neurons that play a role in reward, learning, and memory, it should be of interest to further investigate benzoylecgonine inhibition of neuronal AChRs. As there is no current treatment for cocaine addiction aside from behavioral therapy, nAChR receptor modulation could prove to be a promising avenue of pharmacological intervention for cocaine addiction.

REFERENCES

Adinoff B, Devous MD Sr, Williams MJ, Best SE, Harris TS, Minhajuddin A, Zielinski T, Cullum M. Altered neural cholinergic receptor systems in cocaine-addicted subjects. Neuropsychopharmacology. 2010 Jun;35(7):1485-99.

Ambre J, Fischman M, Ruo TI. Urinary excretion of ecgonine methyl ester, a major metabolite of cocaine in humans. J Anal Toxicol. 1984 Jan-Feb; 8(1):23-5.

Ambre J, Ruo TI, Nelson J, Belknap S. Urinary excretion of cocaine, benzoylecgonine, and ecgonine methyl ester in humans. J Anal Toxicol. 1988 Nov-Dec;12(6):301-6.

Arias HR, Bhumireddy P, Bouzat C. Molecular mechanisms and binding site locations for noncompetitive antagonists of nicotinic acetylcholine receptors. Int J Biochem Cell Biol. 2006;38(8):1254-76.

Bertrand D. Neurocircuitry of the nicotinic cholinergic system. Dialogues Clin Neurosci. 2010;12 (4):463-70.

Breitinger HG, Geetha N, Hess GP. Inhibition of the serotonin 5-HT3 receptor by nicotine, cocaine, and fluoxetine investigated by rapid chemical kinetic techniques. Biochemistry. 2001 Jul 27;40(28):8419-29. Erratum in: Biochemistry 2002 Jul 9;41(27):8784.

Brzezinski MR, Spink BJ, Dean RA, Berkman CE, Cashman JR, Bosron WF. Human liver carboxylesterase hCE-1: binding specificity for cocaine, heroin, and their metabolites and analogs. Drug Metab Dispos. 1997 Sep;25(9):1089-96.

Carroll FI, Izenwasser S, French D, Kunko PM. Continuous infusion of selective dopamine uptake inhibitors or cocaine produces time-dependent changes in rat locomotor activity. Behav Brain Res. 1999 Mar;99(2):201-8.

Chen Y, Banerjee A, Hess GP. Mechanism-based discovery of small molecules that prevent noncompetitive inhibition by cocaine and MK-801 mediated by two different sites on the nicotinic acetylcholine receptor. Biochemistry. 2004 Aug 10;43(31):10149-56.

Chow MJ, Ambre JJ, Ruo TI, Atkinson AJ Jr, Bowsher DJ, Fischman MW. Kinetics of cocaine distribution, elimination, and chronotropic effects. Clin Pharmacol Ther. 1985 Sep;38(3):318-24.

Dani JA, Heinemann S. Molecular and cellular aspects of nicotine abuse. Neuron. 1996 May;16(5):905-8.

Dean RA, Christian CD, Sample RH, Bosron WF. Human liver cocaine esterases: ethanol-mediated formation of ethylcocaine. FASEB J. 1991 Sep;5(12):2735-9.

Flores CM, Rogers SW, Pabreza LA, Wolfe BB, Kellar KJ. A subtype of nicotinic cholinergic receptor in rat brain is composed of alpha 4 and beta 2 subunits and is up-regulated by chronic nicotine treatment. *Mol Pharmacol.* 1992 Jan;41(1):31-7.

Francis MM, Vazquez RW, Papke RL, Oswald RE. Subtype-selective inhibition of neuronal nicotinic acetylcholine receptors by cocaine is determined by the alpha4 and beta4 subunits. Mol Pharmacol. 2000 Jul;58(1):109-19.

Francis MM, Cheng EY, Weiland GA, Oswald RE. Specific activation of the alpha 7 nicotinic acetylcholine receptor by a quaternary analog of cocaine. Mol Pharmacol. 2001 Jul;60(1):71-9.

Gentry CL, Lukas RJ. Local anesthetics noncompetitively inhibit function of four distinct nicotinic acetylcholine receptor subtypes. J Pharmacol Exp Ther. 2001 Dec;299(3):1038-48.

Giraudat J, Dennis M, Heidmann T, Chang JY, Changeux JP. Structure of the high-affinity binding site for noncompetitive blockers of the acetylcholine receptor: serine-262 of the delta subunit is labeled by [3H]chlorpromazine. Proc Natl Acad Sci U S A. 1986 Apr;83(8):2719-23.

Giraudat J, Dennis M, Heidmann T, Haumont PY, Lederer F, Changeux JP. Structure of the high-affinity binding site for noncompetitive blockers of the acetylcholine receptor: [3H] chlorpromazine labels homologous residues in the beta and delta chains. Biochemistry. 1987 May 5; 26(9):2410-8.

Hansen SB, Talley TT, Radic Z, Taylor P. Structural and ligand recognition characteristics of an acetylcholine-binding protein from Aplysia californica. J Biol Chem. 2004 Jun 4;279(23):24197-202.

Hansen SB, Taylor P. Galanthamine and non-competitive inhibitor binding to ACh-binding protein: evidence for a binding site on non-alpha-subunit interfaces of heteromeric neuronal nicotinic receptors. J Mol Biol. 2007 Jun 15;369(4):895-901.

Hawks RL, Chiang CN. Implications of drug levels in body fluids: basic concepts. NIDA Res Monogr. 1986;73:62-83.

Hess GP, Ulrich H, Breitinger HG, Niu L, Gameiro AM, Grewer C, Srivastava S, Ippolito JE, Lee SM, Jayaraman V, Coombs SE. Mechanism-based discovery of ligands that counteract inhibition of the nicotinic acetylcholine receptor by cocaine and MK-801. Proc Natl Acad Sci U S A. 2000 Dec 5;97(25):13895-900.

Inaba T. Cocaine: pharmacokinetics and biotransformation in man. Can J Physiol Pharmacol. 1989 Sep; 67(9):1154-7.

Jatlow P. Cocaine: analysis, pharmacokinetics, and metabolic disposition. Yale J Biol Med. 1988 Mar-Apr;61(2):105-13.

Kalivas PW. Neurobiology of cocaine addiction: implications for new pharmacotherapy. Am J Addict. 2007 Mar-Apr;16(2):71-8.

Kalivas PW. Cocaine and amphetamine-like psychostimulants: neurocircuitry and glutamate neuroplasticity. Dialogues Clin Neurosci. 2007;9(4):389-97.

Karpen JW, Aoshima H, Abood LG, Hess GP. Cocaine and phencyclidine inhibition of the acetylcholine receptor: analysis of the mechanisms of action based on measurements of ion flux in the millisecond-to-minute time region. Proc Natl Acad Sci U S A. 1982 Apr;79(8):2509-13.

Kem WR. The brain alpha7 nicotinic receptor may be an important therapeutic target for the treatment of Alzheimer's disease: studies with DMXBA (GTS-21). Behav Brain Res. 2000 Aug;113(1-2):169-81.

Koob G, Kreek MJ. Stress, dysregulation of drug reward pathways, and the transition to drug dependence. Am J Psychiatry. 2007 Aug;164(8):1149-59.

Leonard S, Adams C, Breese CR, Adler LE, Bickford P, Byerley W, Coon H, Griffith JM, Miller C, Myles-Worsley M, Nagamoto HT, Rollins Y, Stevens KE, Waldo M, Freedman R. Nicotinic receptor function in schizophrenia. Schizophr Bull. 1996;22(3):431-45.

Li HL, Galue A, Meadows L, Ragsdale DS. A molecular basis for the different local anesthetic affinities of resting versus open and inactivated states of the sodium channel. Mol Pharmacol. 1999 Jan;55(1):134-41.

Luo S, Kulak JM, Cartier GE, Jacobsen RB, Yoshikami D, Olivera BM, McIntosh JM. alpha-conotoxin AuIB selectively blocks alpha3 beta4 nicotinic acetylcholine receptors and nicotine-evoked norepinephrine release. J Neurosci. 1998 Nov 1;18(21):8571-9.

Miyazawa A, Fujiyoshi Y, Unwin N. Structure and gating mechanism of the acetylcholine receptor pore. Nature. 2003 Jun 26;423(6943):949-55.

Neher E, Steinbach JH. Local anaesthetics transiently block currents through single acetylcholine-receptor channels. J Physiol. 1978 Apr;277:153-76.

Niu L, Abood LG, Hess GP. Cocaine: mechanism of inhibition of a muscle acetylcholine receptor studied by a laser-pulse photolysis technique. Proc Natl Acad Sci U S A. 1995 Dec 19;92(26):12008-12.

Papke RL, Horenstein BA, Placzek AN. Inhibition of wild-type and mutant neuronal nicotinic acetylcholine receptors by local anesthetics. Mol Pharmacol. 2001 Dec;60(6):1365-74.

Quick MW, Ceballos RM, Kasten M, McIntosh JM, Lester RA. Alpha3beta4 subunit-containing nicotinic receptors dominate function in rat medial habenula neurons. Neuropharmacology. 1999 Jun;38(6):769-83.

Quik M, Jeyarasasingam G. Nicotinic receptors and Parkinson's disease. Eur J Pharmacol. 2000 Mar 30;393(1-3):223-30.

Ragsdale DS, McPhee JC, Scheuer T, Catterall WA. Molecular determinants of state-dependent block of Na+ channels by local anesthetics. Science. 1994 Sep 16;265(5179):1724-8.

Ritz MC, Lamb RJ, Goldberg SR, Kuhar MJ. Cocaine receptors on dopamine transporters are related to self-administration of cocaine. Science. 1987 Sep 4;237(4819):1219-23.

Schindler CW, Tella SR, Katz JL, Goldberg SR. Effects of cocaine and its quaternary derivative cocaine methiodide on cardiovascular function in squirrel monkeys. Eur J Pharmacol. 1992 Mar 17;213(1):99-105.

Schwartz RD, Kellar KJ. [3H]acetylcholine binding sites in brain. Effect of disulfide bond modification. Mol Pharmacol. 1983 Nov;24(3):387-91.

Schwartz RD, Kellar KJ. Nicotinic cholinergic receptor binding sites in the brain: regulation in vivo. Science. 1983 Apr 8;220(4593):214-6.

Smit AB, Brejc K, van Dijk WJ, Klaassen RV, Schuurmans M, van Der Oost J, Sixma TK. Crystal structure of an ACh-binding protein reveals the ligand-binding domain of nicotinic receptors. *Nature*. 2001 May 17;411(6835):269-76.

Swanson KL, Albuquerque EX. Nicotinic acetylcholine receptor ion channel blockade by cocaine: the mechanism of synaptic action. J Pharmacol Exp Ther. 1987 Dec;243(3):1202-10.

Tapper AR, McKinney SL, Nashmi R, Schwarz J, Deshpande P, Labarca C, Whiteaker P, Marks MJ, Collins AC, Lester HA. Nicotine activation of alpha4* receptors: sufficient for reward, tolerance, and sensitization. Science. 2004 Nov 5;306(5698):1029-32.

Toennes SW, Thiel M, Walther M, Kauert GF. Studies on metabolic pathways of cocaine and its metabolites using microsome preparations from rat organs. Chem Res Toxicol. 2003 Mar;16(3):375-81.

Unwin N. Refined structure of the nicotinic acetylcholine receptor at 4A resolution. J Mol Biol. 2005 Mar 4;346(4):967-89.

Whiteaker P, Peterson CG, Xu W, McIntosh JM, Paylor R, Beaudet AL, Collins AC, Marks MJ. Involvement of the alpha3 subunit in central nicotinic binding populations. J Neurosci. 2002 Apr 1;22(7):2522-9.

Williams MJ, Adinoff B. The role of acetylcholine in cocaine addiction. Neuropsychopharmacology. 2008 Jul;33(8):1779-97.

Wonnacott S. Presynaptic nicotinic ACh receptors. Trends Neurosci. 1997 Feb;20(2):92-8.

Xiao YF, Morgan JP. Cocaine blockade of the acetylcholine-activated muscarinic K+ channel in ferret cardiac myocytes. J Pharmacol Exp Ther. 1998 Jan;284(1):10-8.

Xu W, Gelber S, Orr-Urtreger A, Armstrong D, Lewis RA, Ou CN, Patrick J, Role L, De Biasi M, Beaudet AL. Megacystis, mydriasis, and ion channel defect in mice lacking the alpha3 neuronal nicotinic acetylcholine receptor. Proc Natl Acad Sci U S A. 1999 May 11;96 (10):5746-51.

Ye JH, Liu PL, Wu WH, McArdle JJ. Cocaine depresses GABAA current of hippocampal neurons. Brain Res. 1997 Oct 3;770 (1-2):169-75.

Ye H, Hiroi N, Brown JR, Haile CN, Greenberg ME, Nestler EJ. FosB mutant mice: loss of chronic cocaine induction of Fos-related proteins and heightened sensitivity to cocaine's psychomotor and rewarding effects. Proc Natl Acad Sci U S A. 1997 Sep 16;94(19):10397-402.

CHAPTER 4

Investigating the use of Irinotecan as a tumor contrast agent in an *in vivo* Murine Mammary Cancer Model.

ABSTRACT

Despite ongoing active breast cancer research and an overall decrease in the incidence of breast cancer since 2003, 39,520 women were expected to die from the disease (American Cancer Society, 2010-2011). Early detection and complete removal of cancerous tissue is critical for survival. Here we investigate the use of an FDA-approved chemotherapy drug, Irinotecan, as a tumor contrast agent in an *in vivo* Murine Mammary Cancer Model using multiphoton microscopy. Multiphoton microscopy offers significant advantages over other imaging modalities providing high resolution imaging with greater depth and more efficient emission collection (Zipfel *et al.*, 2003). The results presented here that a chemotherapy drug exhibiting intrinsic fluorescence can be used as a contrast agent to identify cancer cells *in vivo,* and thus may be useful clinical tools for more effective surgical resection.

INTRODUCTION

Despite an overall decrease in breast cancer incidence since 2003, approximately 230,480 new cases of invasive breast cancer were expected to emerge in 2011 and over 39,000 women were expected to die from the disease. In addition, men are not immune to the disease and over 2,000 cases of male breast cancer were expected to emerge, with over 400 men expected to die from breast cancer in 2011 (American Cancer Society, 2010-2011).

Cancer mortality can be prevented in most cases with early detection and complete removal of cancerous tissue (Zivanovic *et al.*, 2009). Accurate tumor margin detection during resection is critical and improved intraoperative methods for discriminating between normal and cancer cells are needed. Although endogenous fluorophores targeted with cancer cell specific antibodies or aptamers can be added to provide contrast, FDA (Food and Drug Administration) approvals for these approaches are difficult to achieve and have been limited. Tumor border detection is currently based on white light macro-imaging of the tissue and the surgeon's judgment. Interestingly, chemotherapeutic drugs exhibiting intrinsic fluorescence can be used as contrast agents to identify cancer cells *in vivo,* and thus may provide a clinical tool for more effective surgical resection. These drugs are already FDA approved and in common use. Many of these compounds accumulate in tumor cells and have strong UV (ultraviolet) absorptions and fluorescence in the UV, blue and green region. For this reason multiphoton

microscopy (MPM) offers important advantages as a high resolution imaging modality for this purpose. These include the ability to excite UV absorbing species using NIR (near infrared) light in the 700 to 800 nm region in a three-dimensionally localized fashion and deeper imaging due to both the use of NIR light and with the more efficient emission collection optical design that MPM affords (Zipfel *et al.*, 2003). To explore the use of multiphoton microscopy for this purpose, seven chemotherapy drugs known to possess single photon excited intrinsic UV fluorescence were evaluated (McMullen, 2010). These were: Ellipticine, Aminoacridine, Camptothecin, Irinotecan, Doxorubicin, Dipyramidole, and Protoporphryn IX. Of these drugs, Irinotecan was selected for further study based on its relatively large action cross-section (Figure 4.1). Irinotecan in solution has a two-photon action cross-section (product of the fluorescence quantum yield times the two photon absorption cross-section) that is as large as many commonly used imaging dyes, and is at least a 1000-times brighter than typical intrinsic fluorophores such as NADH.

As an anti-neoplastic agent, Irinotecan (7-ethyl-10[4-(1piperidino)-1-piperidino] carbonyloxycamptothecin; Figure 4.1A) has been used to treat advanced and recurrent forms of colorectal cancer, small cell lung carcinoma, ovarian and cervical cancer, and ocular melanoma (Ohno *et al.*, 1990; Fukuoka *et al.*, 1992; Shimada *et al.*, 1993). Irinotecan is a semi-synthetic derivative of Camptothecin (CPT), an alkaloid extract derived from the bark of a tree native to south China (Wall *et al.,* 1966). CPT was found to

be active against a spectrum of animal tumor models but its clinical use was mitigated by poor solubility and severe toxicity leading to reversible myelosuppression and hemorrhagic cystitis (Wall *et al.,* 1966; Muggia *et al.*, 1972; Kunimoto *et al.*, 1987). Subsequently, Irinotecan was developed which is both more soluble and exhibits a higher LD_{50} (median Lethal Dose) of 178 mg/kg compared to 56 mg/kg for CPT (Nitta *et al.*, 1985; Kunimoto *et al.*, 1987). Irinotecan is metabolized by Liver carboxylesterase 1 to form SN-38 which is 2-20,000 times more potent in cytotoxicity assays in vitro. Both Irinotecan and SN-38 exist in an active lactone form and an inactive hydroxy acid anion form. A pH-dependent equilibrium exists between the two forms and acidic pH shifts the equilibrium towards the formation of the lactone (Mathijssen *et al.*, 2001).

Initial experiments investigating the use of Irinotecan as a tumor contrast agent were carried out using an ascites tumor model of ovarian cancer metastasis (McMullen, 2010). Mice in this model develop uterine horn and intestinal tumors similar to those found in ovarian cancer patients with metastatic disease (Williams *et al.*, 2010). To evaluate Irinotecan-mediated tumor contrast enhancement mice with palpable peritoneal tumors were injected intraperitoneally with 80 mg/kg Irinotecan, sacrificed after 4 hours, and tissues were immediately excised and imaged using multiphoton microscopy using 760 nm excitation. For tumors growing on the uterine horn, Irinotecan injection led to a four-fold increase in tissue contrast enhancement compared to non-injected tissue, and showed

preference for tumor cells over control tissue. In tumors located on the exterior intestinal wall, a drug uptake as evidenced by drug fluorescence was also higher, however, only a two-fold increase in contrast enhancement was observed over the higher intestinal tissue autofluorescence.

Here we investigate the use of Irinotecan as a tumor contrast agent in an *in vivo* Murine Mammary Cancer Model. There are currently only a handful of contrast agents approved by the FDA, and chemotherapeutic drugs exhibiting strong intrinsic fluorescence could prove instrumental in allowing the study drug metabolism, drug and metabolite localization, cellular uptake heterogeneity, and possibly drug resistance.

A.

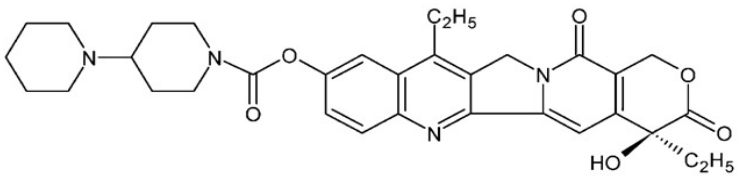

B.

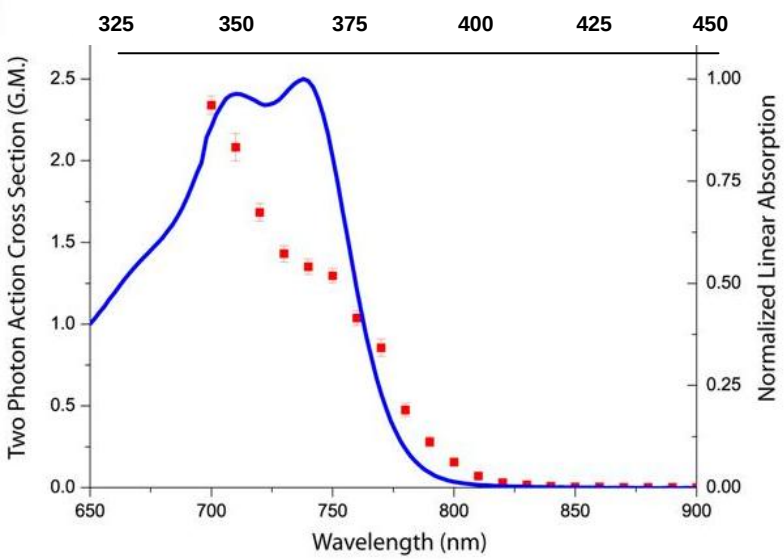

Figure 4.1. Irinotecan structure (A.) and action cross-section (B.). The two photon action cross section was measured across the wavelength range of the Ti:Sapphire laser for 10 μM Irinotecan in PBS, pH 7.4 (red squares, y-axis on left). The normalized linear absorption of Irinotecan at half the wavelength is plotted in blue for lineshape comparison (y-axis on right).

METHODS

MCN2 cell line. The MCN2 (Mammary Carcinoma cells established in Nikitin laboratory 2) cell line was generously donated by Dr. Alexander Nikitin (Cornell University). The MCN2 cell line is an immortalized mammary cancer epithelial cell line derived from mammary carcinomas resected from $p53^{ME-/-}$ $Rb^{ME-/-}$ mice as previously described (Cheng *et al.*, 2010). Cells were cultured in HAM's medium (Dulbecco's Modified Eagle's Medium/F12, 50/50 Mix; Cellgro) supplemented with 5% fetal bovine serum, 2 mM L-glutamine, 1 mM Na-pyruvate and 5 µg/ml insulin.

Generation of murine mammary cancer model. (Animal protocol: 2009-0101; Williams; "In vivo imaging of cell-mediated processes in mouse models of ovarian and mammary cancer"). Mammary fat pad tissue and lymph nodes were removed from the 4^{th} inguinal mammary glands of 3-4 week old female FVB/N mice (DeOme *et al.*, 2012) (Figure 4.2). Prior to tissue removal, blood vessels leading to the 3^{rd} thoracic and 5^{th} inguinal glands were cauterized (Figure 4.2B). MCN2 cells (10^5 – 10^6) were injected directly into the remaining fat pad tissue (Figure 4.2C). Surgical incisions were repaired using wound clips (Figure 4.2D) (Fisher Scientific, Atlanta, GA). All mice surgical procedures were performed under 2% isoflurane inhalation anesthesia.

Nonlinear (MPM and SHG) Imaging of Intrinsic Fluorescence. Multiphoton imaging was performed as previously described (Zipfel *et al.*, 2003; Williams

et al., 2001). A 780 nm beam from a mode-locked Ti:sapphire laser (Tsunami pumped with a Millenia Xs; Spectra Physics, Mountain View, CA) was directed through a Pockels Cell (350-80LA; Conoptics, Danbury, CT) with custom-built electronics for beam modulation and blanking during scan fly-back. The beam was directed into a modified scanhead (MRC-600, Hercules, CA) interfaced with a modified Olympus AX-70 upright microscope (Center Valley, PA).

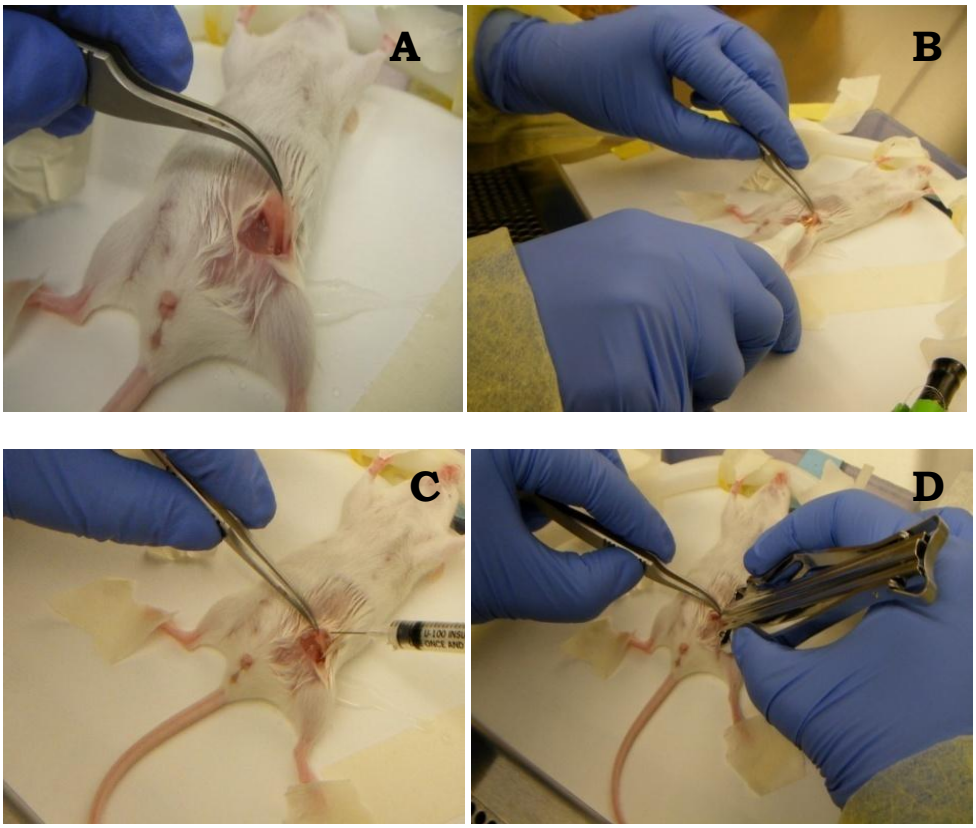

Figure 4.2 Mammary Gland Transplantation of MCN2 cells. (A.) Mammary gland is surgically exposed for blood vessel identification. (B.) Blood vessels are cauterized. (C.) MCN2 cells are injected into mammary tissue. (D.) Surgical area is repaired.

Mammary carcinomas and mammary glands were imaged with a 20x/0.95W water immersion objective (XLUNPlanFl, Olympus). Tissue sample emissions were separated from the excitation beam using a 670DCXRU long-pass dichroic filter (Chroma Technology Inc., Rockingham, VT) placed directly at the back of the aperture of the microscope objective. Tissue sample emissions were separated into two channels with a 440DCRXU long-pass dichroic and UV/Blue emission filters (Chroma Technology, Inc.). The first channel collected the second harmonic signal from collagen (360-390 nm) and the second channel collected intrinsic fluorescence associated with Irinotecan injection (450-550 nm). Signals in both channels were detected using bialkali photocathode photomultiplier tubes (HC125-02; Hamamatsu, Bridgewater, NJ).

Quantitative Analysis of Intrinsic Fluorescence. Data stacks acquired at each time point consisted of 50 images (kalman average of two scans), in 3 μm intervals for a total imaging depth of 150 μm per stack or time point. Average image intensities were measured for each time point. Due to increases in background fluorescence over time (presumably due to drug leaking into the media in the imaging region), the threshold for intensity measurements was determined to be the mean intensity plus a single standard deviation as previously described (Williams *et al.*, 2010). Pixel calculation routines were custom-written using the IDL data analysis program (ITT Visual Information Solutions, White Plains, NY). Average single cell intensities were calculated using the ImageJ platform.

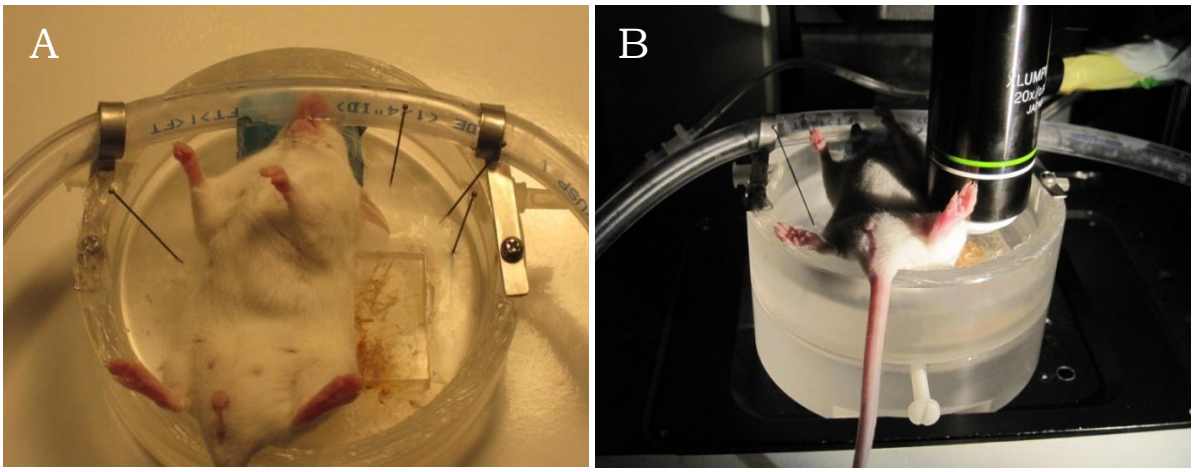

Figure 4.3 *In vivo* Imaging Chamber. (A.) Mouse is vivisected under 2% isoflurane inhalation. **(B.)** Imaging chamber with saline profusion system accommodates mouse and objective.

In vivo imaging. Each mouse was placed in an induction chamber and anesthetized with 3% isoflurane for 1-2 minutes and immediately moved to a custom-designed perfusion chamber outfitted with a 0.5 inch diameter tube with an opening large enough to accommodate the mouse's snout (Figure 4.3A). Gas concentration was adjusted to 2% in order to maintain respiration at ~60 breaths/min. as suggested (Flesken-Nikitin *et al.*, 2005). The mouse was vivisected while anesthetized to expose MCN2-derived carcinomas which were subsequently pinned to a small platform in the chamber. The chamber was moved to the imaging stage (Figure 4.3B) and the mouse and tissue to be imaged were perfused with saline (37°C) over the course of the imaging experiment. Images were acquired prior to drug injection and the mouse was subsequently injected intracardially with 100 µl of 20 mg/ml Irinotecan (Hospira, Inc., Lake Forest, IL). Images were

acquired over a 1-2 hour time period and mouse was subsequently sacrificed by decapitation.

In vitro MCN2 experiments. For imaging MCN2 cells were cultured to 80% confluency in 55 mm glass bottom dishes (MatTek Corp., Ashland, MA). Cells were incubated for 1 hour at 37°C with 1, 5, or 10 μM Irinotecan in DMEM/F12 without phenol red (Invitrogen, Grand Island, NY), washed to remove residual drug and imaged immediately. Fifteen focal planes through the cells Images were acquired in 2 μm intervals. In the *in vitro* experiments in which drug intrinsic fluorescence was measured over time, growth media was aspirated from the cell culture dish, 5 μM Irinotecan in DMEM/F12 without phenol red (Invitrogen, Grand Island, NY) was added and cells were imaged immediately. The first channel collected blue emission (380-480 nm) and the second channel collected green emission (500-600 nm). We used a green emission filter to determine whether a red shift in the average intrinsic fluorescence occurred. In a previous study by Williams *et al.*, (2010), tumor-derived cell masses exhibited a red shift in intrinsic fluorescence. Green emission was also monitored to look for the metabolized form of SN-38 which does not emit in the blue, but has a weak green (~550 nm peak) emission (Sano et al, 2003). Since 550 nm emission of SN-38 is ~100 times weaker than the 450 nm peak of irinotecan (Figure 4.4), it would not be detectable in the *in vivo* experiments above the background autofluorescence and we did not collect the green spectral region during the *in vivo* imaging.

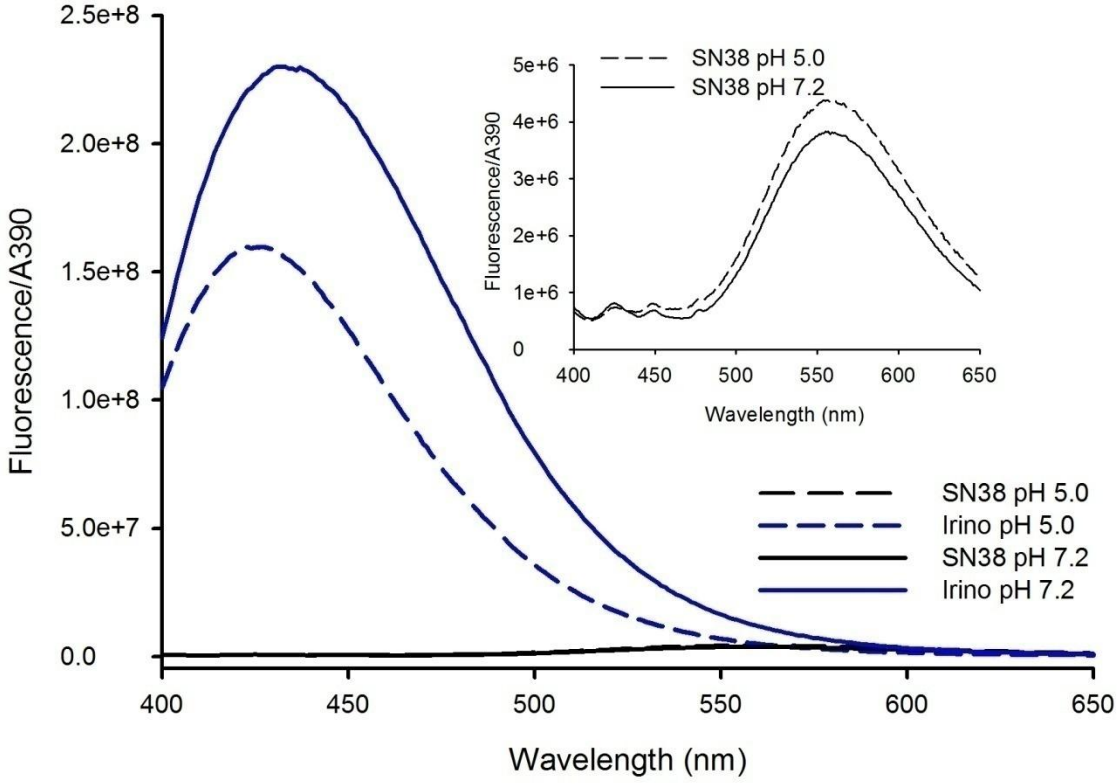

Figure 4.4 Absorption normalized fluorescence spectra of Irinotecan and SN-38 at low and high pH. Excitation was at 390 nm and fluorescence intensity plotted was normalized to the absorption at 390 nm for each sample. SN-38 emits at 550 nm (insert) at an intensity that is ~100 times weaker than irinotecan.

RESULTS

In vivo irinotecan intrinsic fluorescence. We evaluated the intrinsic fluorescence of Irinotecan in MCN2-derived carcinomas and mammary glands *in vivo* using MPM and SHG (Figures 4.5 and 4.6). Data were acquired over 5-23 time points for 5 animals that developed mammary carcinomas in the 9th ventrolateral mammary gland and 3 animals without tumors. Each time point of the raw data represents a stack of 50 images taken at 3 micron intervals. Autofluorescence was measured before Irinotecan administration and served as the (t = 0) intensity measurement.

Due to the nature of *in vivo* imaging, bleeding or other biologically associated secretions can interfere with signal intensities; we therefore collected SHG intensities simultaneously to be used as a reference signal (Figure 4.7). Irinotecan intrinsic fluorescence was evaluated by plotting the ratio of overall intensity (average pixel value from all regions of the image containing tissue) to SHG (collagen) intensity as a function of time. Mammary carcinoma intensities increased 2-fold over 60 minutes (Figure 4.8A) and mammary gland control fluorescence increased ~1.8-fold over 20 minutes (Figure 4.8B).

A visual examination of the data indicated a more significant increase in the fluorescence of the tumor cells after injection of Irinotecen so a more detailed analysis was carried out in which average single cell pixel intensities were measured in the *in vivo* mammary carcinomas and mammary gland control images (Figure 4.9). Single cells (n = 7 cells/time

point, 6 time points) were manually selected using ImageJ and average single cell intensities were computed for each time point. Cells selected were those that increased in intensity over time as a result of drug injection. Overall, tumor cells exhibited a 4-fold increase in intensity while mammary gland cells exhibited a ~2-fold increase in average intensity. Mammary cells increased 2-fold after ~20 min. while carcinoma cells increased 2-fold within ~32 min. and 4-fold after ~70 minutes.

In vitro Irinotecan intrinsic fluorescence. In order to evaluate intrinsic fluorescence of irinotecan *in vitro*, MCN2 cells were incubated for 1 hour at 37°C with several concentrations of Irinotecan (0-10 μM). Irinotecan intensity was concentration dependent and the average intensity increased ~1.5-fold with 5 μM Irinotecan and almost 3-fold with 10 μM Irinotecan (Figure 4.10). When Irinotecan intensity was monitored over time (Figure 4.11), a ~2-fold increase was observed after 2 minutes of drug application, and after 70 minutes a ~4-fold increase in intensity was observed.

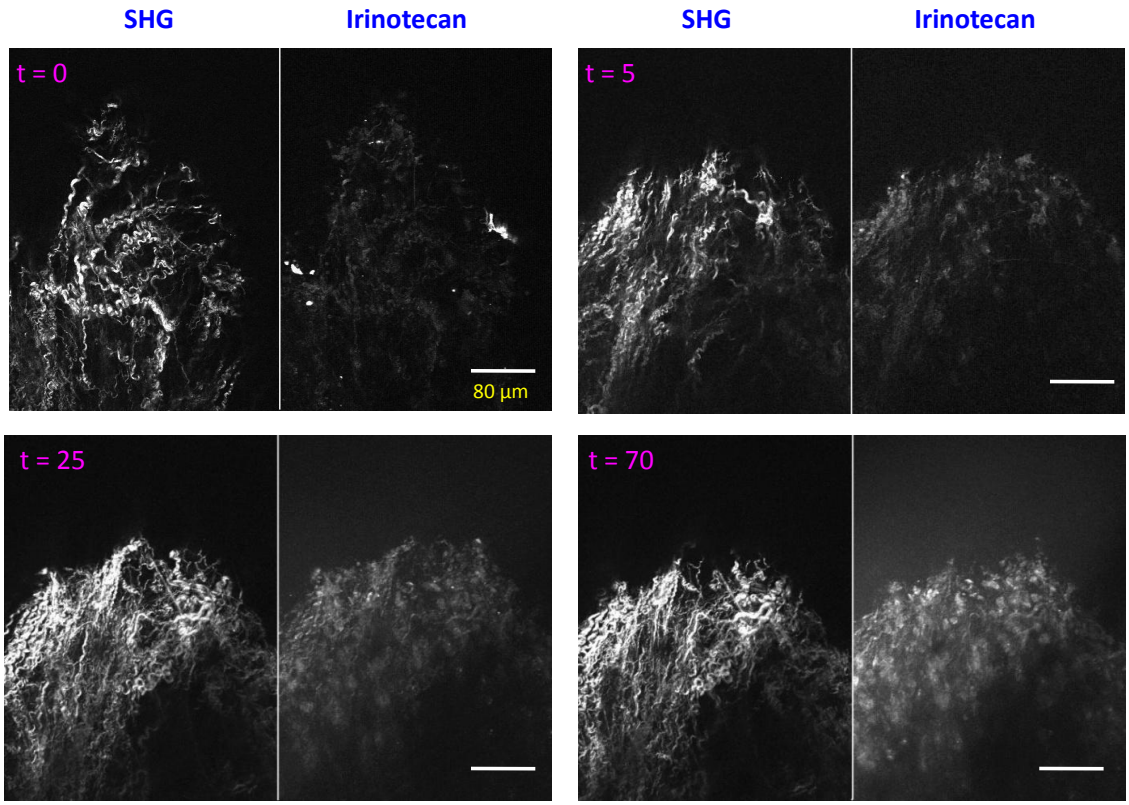

Figure 4.5. *In vivo* Irinotecan intrinsic fluorescence in an MCN2-derived carcinoma. Representative MPM/SHG images of intrinsic fluorescence of tumor tissue after Irinotecan injection at several time points (pink). The left panel of each time point image represents SHG fluorescence (355-425 nm) and the right panel represents fluorescence as a result of drug injection (450-475 nm). Scale bar: 80 µM.

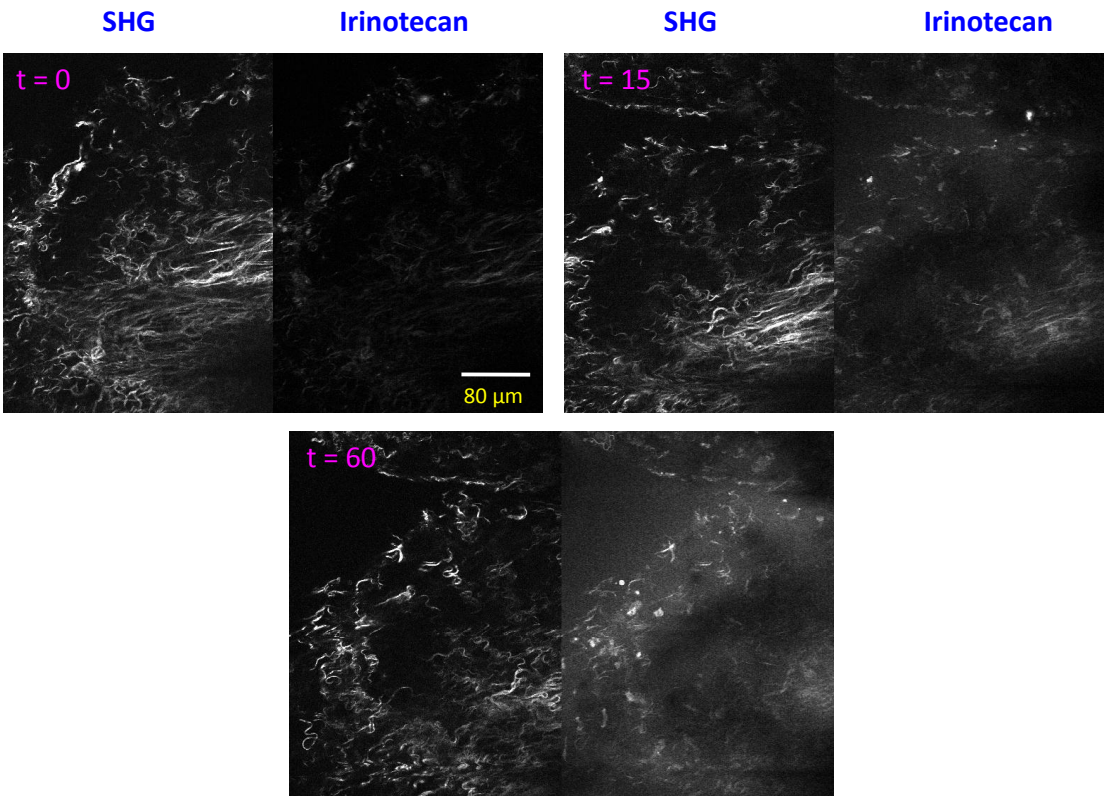

Figure 4.6. *In vivo* Irinotecan intrinsic fluorescence in a mammary gland control sample. Representative MPM/SHG images of intrinsic fluorescence of mammary gland after Irinotecan injection at several time points (pink). The left panel of each time point image represents SHG fluorescence (355-425 nm) and the right panel represents fluorescence as a result of drug injection (450-475 nm). Scale bar: 80 µM.

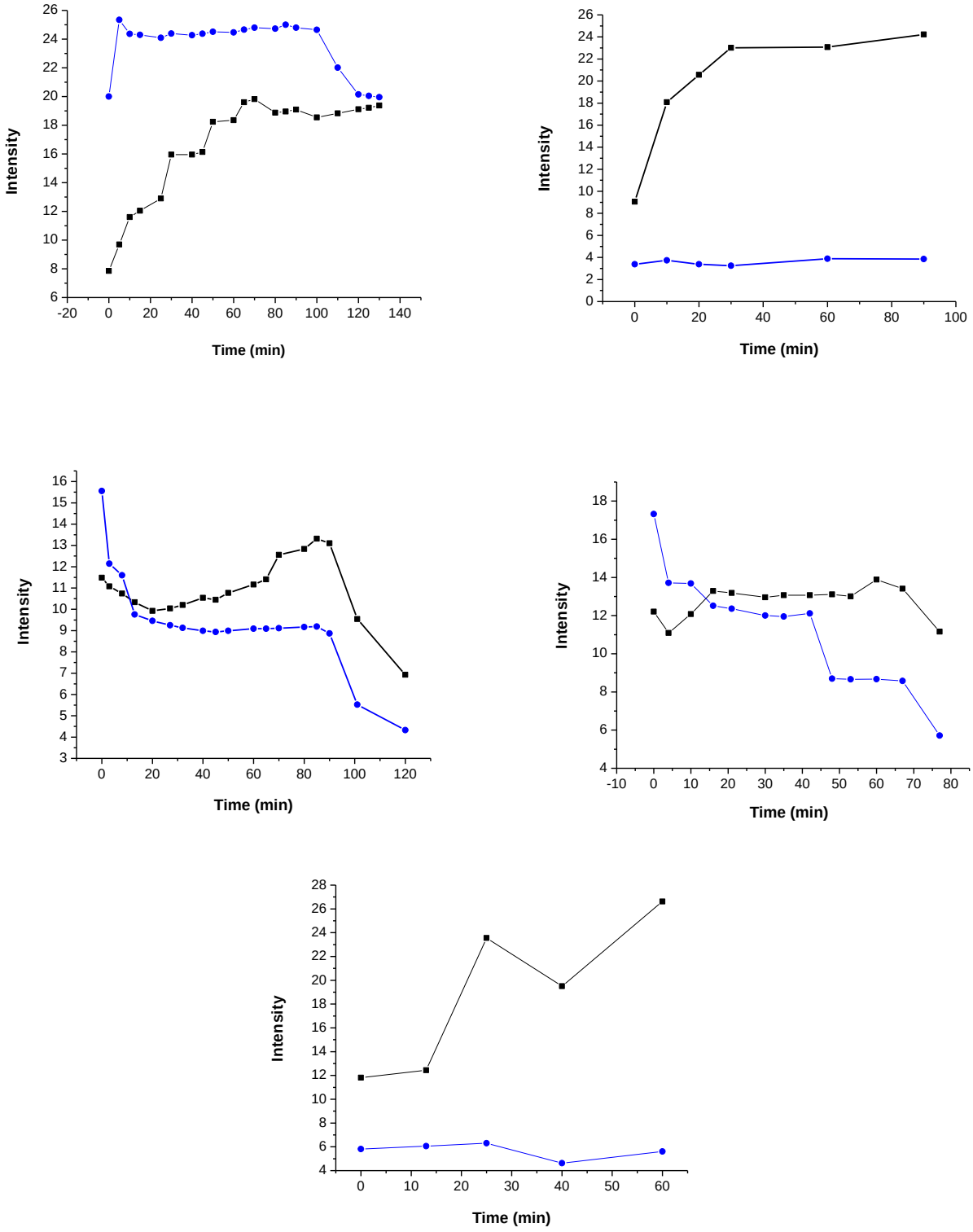

Figure 4.7. Raw Data for *in vivo* tumor imaging after irinotecan injection. SHG (blue trace) and Irinotecan (black trace) intensities are plotted as a function of time for each animal (n = 5).

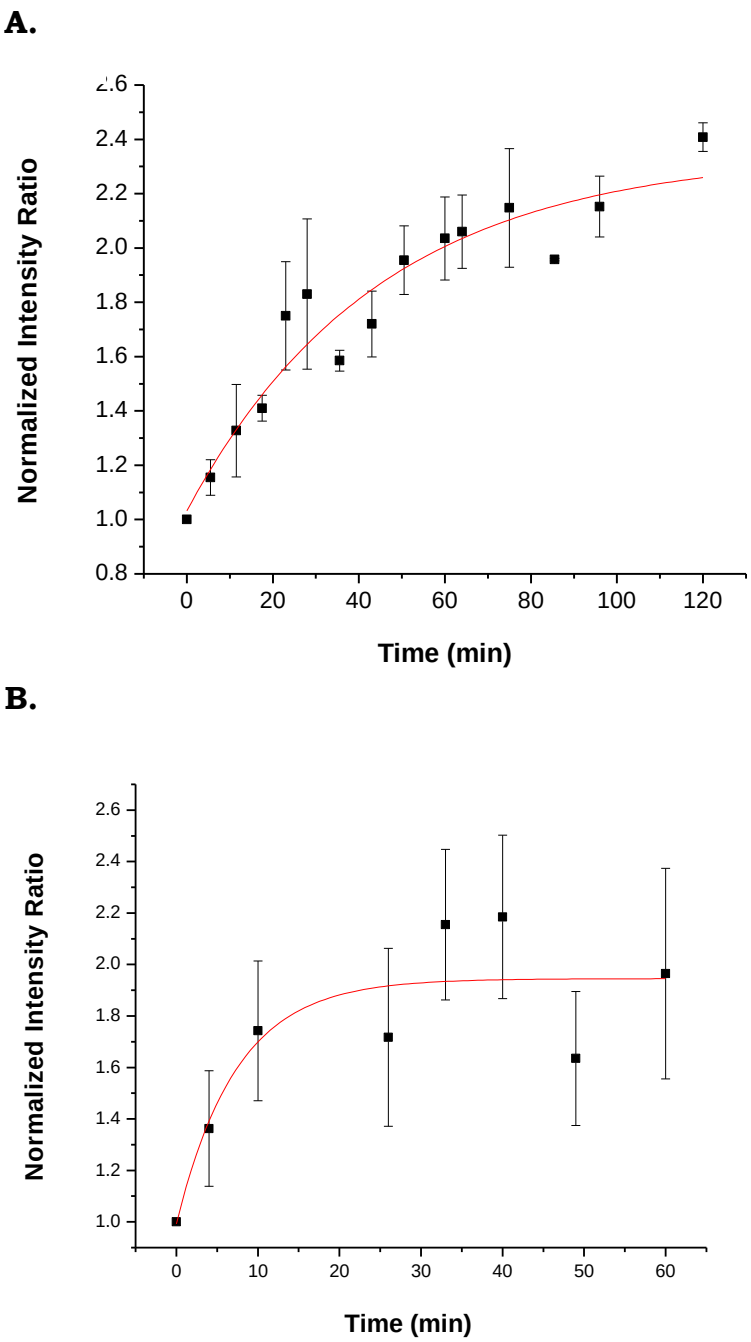

Figure 4.8. Irinotecan intrinsic fluorescence in mammary carcinomas (A.) and mammary gland controls (B.). Mammary carcinomas (n = 5 animals) (A.) and mammary gland controls (B.) (n = 3 animals) were imaged using MPM and SHG. Fluorescence intensity was measured over time (t = 0-120 min) in mammary carcinomas and (t = 0-60 min) in mammary glands and plotted as the normalized intensity ratio. The normalized intensity ratio was defined as the ratio of the average intensity due to intrinsic fluorescence of Irinotecan in both mammary carcinomas and mammary glands versus the average intensity due to SHG of collagen.

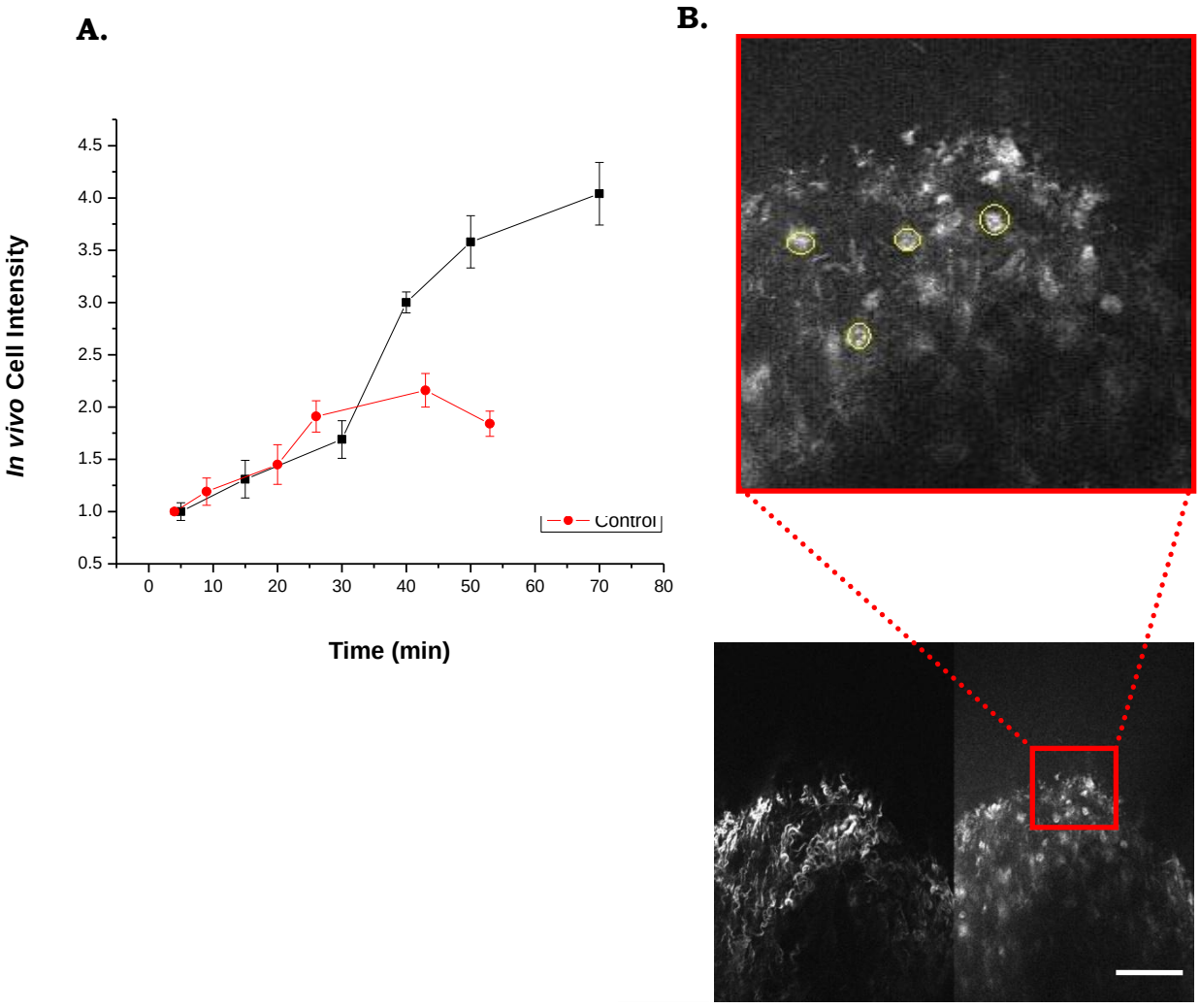

Figure 4.9. *In vivo* single cell intensity. (A.) Image of mammary gland control (left panel) and freshly excised tumor (right panel) from same animal. Scale bar: 80 μm (B.) The average single cell intensity was measured at each time point and normalized to the first intensity measurement after Irinotecan injection for mammary carcinomas (black trace) and mammary controls (red trace).

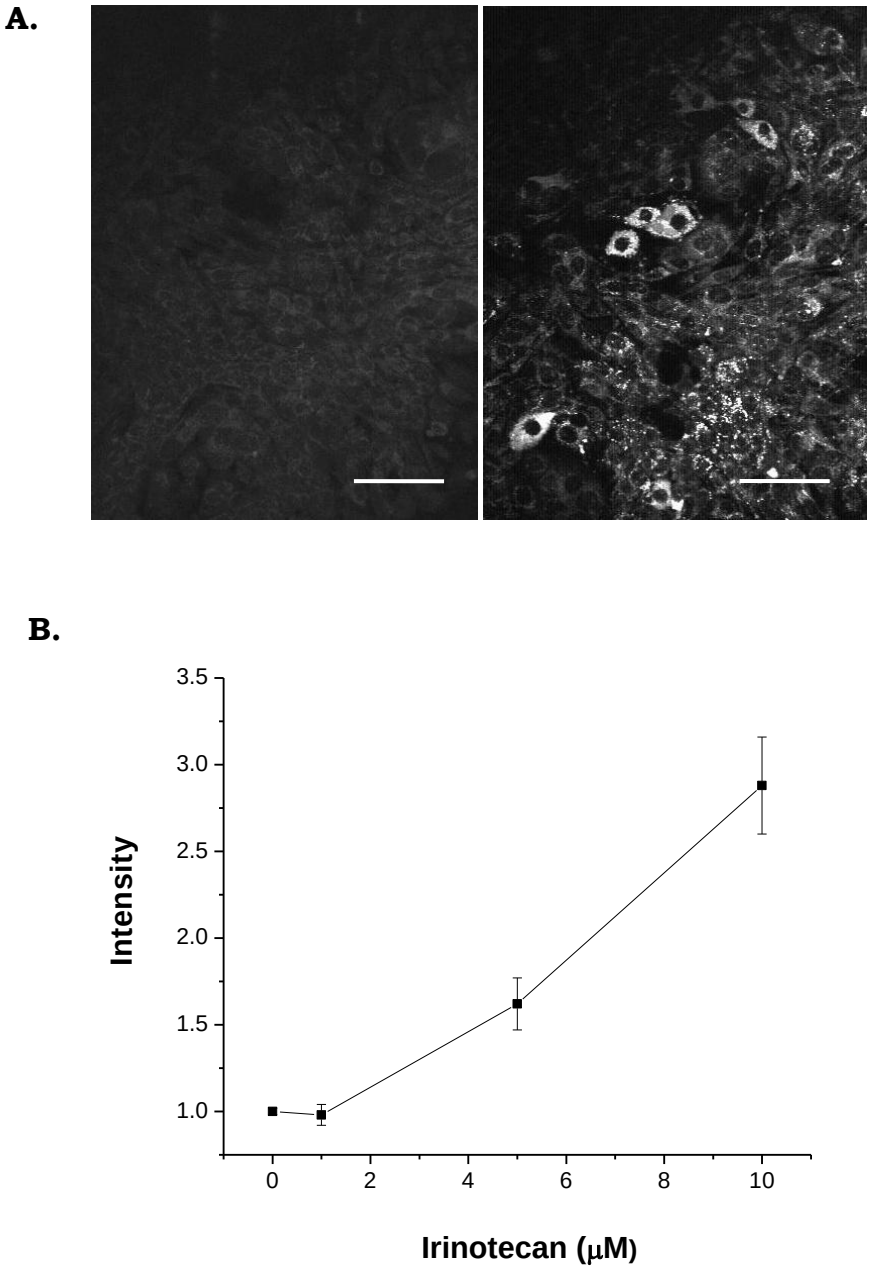

Figure 4.10. Irinotecan intensity is concentration dependent *in vitro*. (A.) MCN2 cells without Irinotecan (left image) and MCN2 cells incubated with 5 μM Irinotecan (right image). Image data shown were collected in the blue channel (450-475 nm). Scale bar: 80 μm (B.) The average intensity was measured for MCN2 cells incubated with 1, 5, or 10 μM Irinotecan for 1 hour at 37°C. Average intensities of Irinotecan intrinsic fluorescence were normalized to the average intensity of MCN2 cells without Irinotecan.

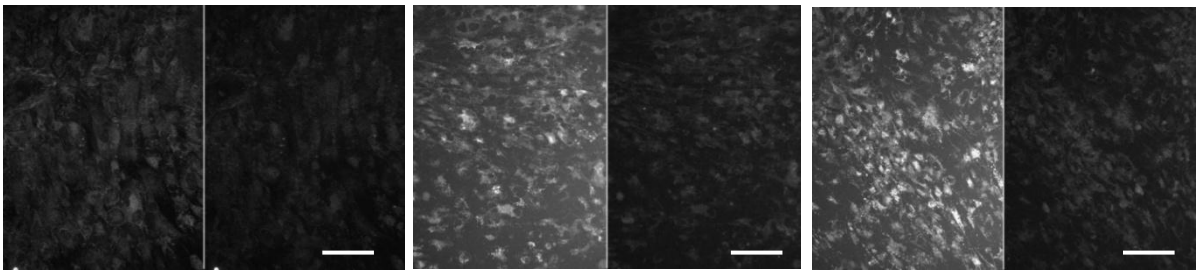

t = 0 min 23 min 61 min

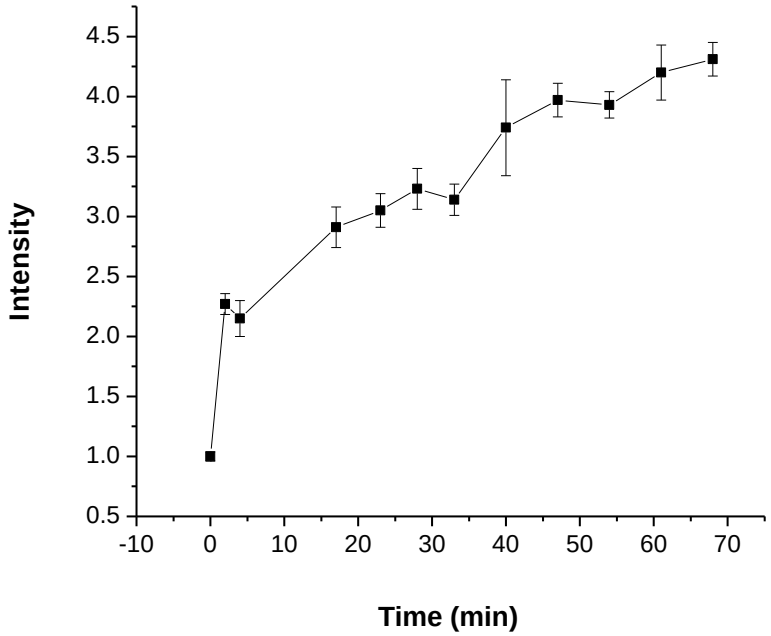

Figure 4.11. *In vitro* Irinotecan intrinsic fluorescence time series. (Top panel) Representative MPM images of MCN2 cells at t = 0 (no drug), t = 23 min., and t = 61 min. after 5 μM Irinotecan application. The left panel of each time point image represents intrinsic fluorescence emission from 450-475 nm and the right panel represents intrinsic fluorescence emission from 495-570 nm. Scale bar: 80 μm. Average intensity of MCN2 cells after Irinotecan application were normalized to the average intensity before drug application (t = 0) and measured over time.

DISCUSSION

Previously, it had been demonstrated that intraperitoneal (IP) injection of Irinotecan using an OSN3 ovarian cancer metastasis model led to a 4-fold increase in fluorescence in uterine tumors and a 2-fold increase in intestinal tumors (McMullen, 2010). Irinotecan also exhibited a preference for tumor cells versus non-tumor tissue. In this study employing the murine mammary cancer model we found that intracardial injection of Irinotecan led to a 2-fold increase in fluorescence in both mammary carcinomas and mammary tissue controls. Based on average intensity measurements of whole tumor or whole mammary gland, Irinotecan did not show preference for mammary carcinoma tissue. We did observe; however, diffuse fluorescence in mammary gland controls, while fluorescence in tumors was primarily localized to cell bodies within tumor tissue (Figures 4.5 and 4.6). When we evaluated the *in vivo* intrinsic fluorescence of single cells within those tissues, we found that Irinotecan produced a 4-fold increase in intensity in tumor cells and a 2-fold increase in single mammary cells. This indicated that the practical use of Irinotecan as a tumor contrast agent would require a multiphoton laparoscopic tool or perhaps a surgical microscope with UV excitation (*e.g.,* Zeiss OPMI VARIO 700) to provide single cell resolution.

An approximately equal (~2-fold) increase in overall mammary tumor and control gland intensity after Irinotecan injection was unexpected but may be explained by the structural components of the mammary gland.

Mammary glands consist of a system of branching ducts and alveoli composed of mammary epithelial ductal cells, myoepithelial cells, adipose cells and secretory cells (Rillema, 1994; Sapino *et al.*, 1990). Mammary glands are dynamic biological structures and epithelial cell proliferation is dependent upon hormone stimulation by estrogen, progestin, or prolactin (Sapino *et al.*, 1990). Moreover, mice were imaged between puberty and adulthood during which mitotic activity in the mammary gland can be very high (Medina, 1996). Irinotecan is a Topoisomerase I inhibitor targeting mitotically active cells (Sparreboom *et al.*, 1998) and there may be less intrinsic fluorescence due to Irinotecan uptake in older mice. The extensive duct network within mammary glands may also account for the earlier intensity increase observed in mammary gland controls. Mammary carcinomas are very heterogenous tissues composed of neoplastic cells, non-neoplastic in addition to normal mammary epithelial cells, immune cells such as fibroblasts, and blood vessels (Kelleher *et al.*, 2009). While the density of tumor tissue may contribute to slower uptake in tumor cells, other factors such as the branching and quality of vasculature, and tumor size may affect the time course of Irinotecan uptake and intrinsic fluorescence detection.

When we evaluated single cell intensity from *in vivo* data, we found a 4-fold increase in the intrinsic fluorescence of Irinotecan in tumor cells whereas the single cell intensity of mammary cells increased only 2-fold (Figure 4.9). Irinotecan functions *in vivo* as a prodrug of SN-38, and both

molecules act as Topoisomerase I inhibitors. Topoisomerase I relieves torsional strain in DNA during DNA synthesis by inducing reversible single-strand breaks. Irinotecan and SN-38 prevent religation of these single-strand breaks leading to irreversible double-strand DNA damage (Ikeguchi *et al.*, 2011). *In vivo* SN-38 is formed when the carbamate bond between the camptothecin moiety and the dipiperidino side chain of Irinotecan is cleaved by liver carboxylesterase 1 (Figure 4.12) (Sparreboom *et al.*, 1998; Mathijssen *et al.*, 2001). Liver carboxylesterase 1 was not present in our *in vitro* experiments and the intrinsic fluorescence we observe in the cytoplasm may be the result of Irinotecan binding to mitochondrial Topoisomerase I (top1mt) as the parent compound of Irinotecan, CPT, interacts with top1mt (Zhang *et al.*, 2001). Several Irinotecan metabolites have been identified, but their effects *in vivo* are unknown.

In our *in vitro* experiments we observed that MCN2 cells derived from $p53^{ME-/-}$ $Rb^{ME-/-}$ mice carcinomas Irinotecan uptake is heterogenous. This was observed in experiments where MCN2 cells were incubated with varying concentrations of Irinotecan for 1 hour (Figure 4.10B), as well as experiments in which Irinotecan was directly applied to cells and intensity was monitored over time (Figure 4.11). Differential uptake of Irinotecan in MCN2 cells may be due to genetic alterations, perhaps leading to drug resistance. Chemotherapeutic drug resistance has been a subject of intense study—in the treatment of colorectal cancer, patients respond differently to Irinotecan, and toxic doses range from 50-340 mg/kg (Clarke *et al.*, 2011).

Using MPM, it should be possible to use a single excitation wavelength to excite both Irinotecan and SN-38 intrinsic fluorescence and collect emission in different emission channels to learn more about Irinotecan metabolism *in vivo*. This may lead to an increased understanding of drug metabolism and to further optimization of drug treatment plans.

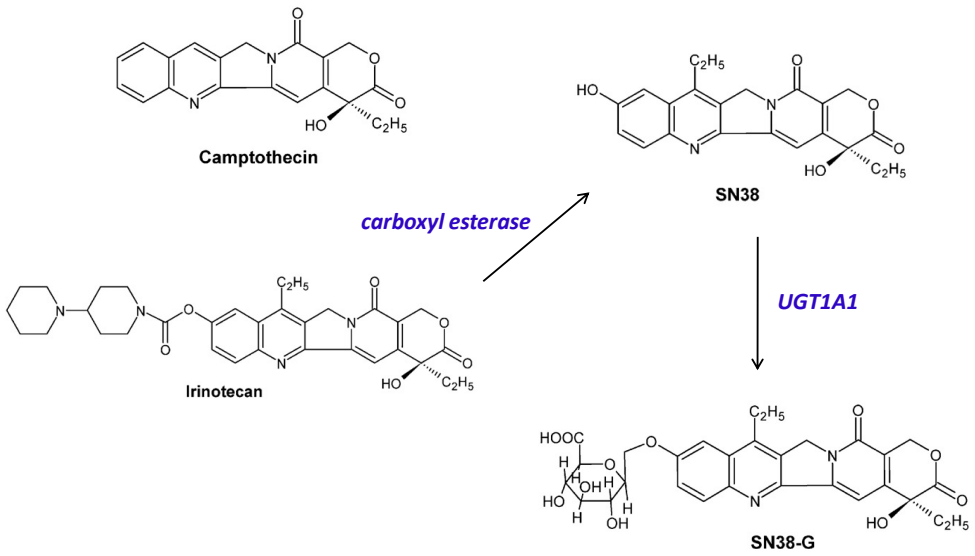

Figure 4.12. General Overview of Irinotecan Metabolism. Irinotecan is a semisynthetic derivative of Camptothecin which is metabolized by Liver carboxylesterase 1 to form SN-38 which is 2-20,000 times more potent in cytotoxicity assays *in vitro*. The active metabolite, SN-38, can be glucouronidated by UGT1A1 to form the inactive metabolite SN38-G which can in turn be deconjugated to SN-38. Both Irinotecan and SN-38 exist in an active lactone form and an inactive hydroxy acid anion form. A pH-dependent equilibrium exists between the two forms and acidic pH shifts the equilibrium towards the formation of the active lactone (Mathijssen *et al.*, 2001).

CONCLUSION

In vivo multiphoton microscopy and second harmonic generation has been used to identify cancer-associated morphological and cellular alterations using intrinsic tissue emissions alone (Kosaka *et al.*, 2009; Williams *et al.*, 2010). Although tissue imaging based solely on the intrinsic signals holds promise, increased contrast enhancement that provides an improved metric for tumor differentiation would be of great benefit. Chemotherapeutic drugs which exhibit intrinsic fluorescence may be used as tumor contrast agents to facilitate surgical resection. Direct MPM imaging of drug fluorescence *in vivo* would also be useful in studies of drug metabolism and pharmacokinetics. Tissue autofluorescence is several orders of magnitude weaker than conventional fluorophore fluorescence; therefore, chemotherapeutic drugs fluorescence must be several orders of magnitude greater than tissue autofluorescence in order to be used as contrast agents. In a mammary tumor model tumor cell intensities exhibited a 4-fold contrast enhancement providing details about drug localization *in vivo.* As multiphoton microscopy transitions from the lab to the clinic, the possibility of real time optical biopsies in the surgical suite using laparoscopic or endoscopic multiphoton instruments, may provide information about drug metabolism, and facilitate early detection in various types of cancer leading to improved prognoses.

REFERENCES

American Cancer Society, Breast Cancer Facts & Figures, 2010-2011. http://www.cancer.org/acs/groups/content/@epidemiologysurveilance/documents/document/acspc-030975.pdf

Cheng L, Zhou Z, Flesken-Nikitin A, Toshkov IA, Wang W, Camps J, Ried T, Nikitin AY. Rb inactivation accelerates neoplastic growth and substitutes for recurrent amplification of cIAP1, cIAP2 and Yap1 in sporadic mammary carcinoma associated with p53 deficiency. *Oncogene.* 2010 Oct 21; 29(42):5700-11.

Clarke SJ, Yip S, Brown C, van Hazel GA, Ransom DT, Goldstein D, Jeffrey GM, Tebbutt NC, Buck M, Lowenthal RM, Boland A, Gebski V, Zalcberg J, Simes RJ; Australasian Gastro-Intestinal Trials Group. Single-agent irinotecan or FOLFIRI as second-line chemotherapy for advanced colorectal cancer; results of a randomised phase II study (DaVINCI) and meta-analysis [corrected]. *Eur J Cancer.* 2011 Aug; 47(12):1826-36. Epub 2011 Jun 12. Erratum in: *Eur J Cancer.* 2012 Feb; 48(3):407.

DeOme KB, Miyamoto MJ, Osborn RC, Guzman RC, Lum K. Detection of inapparent nodule-transformed cells in the mammary gland tissues of virgin female BALB/cfC3H mice. *Cancer Res.* 1978 Jul; 38(7):2103-11.

Flesken-Nikitin A, Williams RM, Zipfel WR, Webb WW, Nikitin AY. Use of multiphoton imaging for studying cell migration in the mouse. *Methods Mol Biol.* 2005; 294:335-45.

Fukuoka M, Masuda N, Kusunoki Y, Matsui K, Takifuji N, Kudoh S, Negoro S, Nishioka M, Nakagawa K, Takada M. CPT-11: a new derivative of camptothecin for the treatment of refractory or relapsed small-cell lung cancer. *J Clin Oncol.* 1992 Aug; 10(8):1225-9.

Ikeguchi M, Arai Y, Maeta Y, Ashida K, Katano K, Wakatsuki T. Topoisomerase I expression in tumors as a biological marker for CPT-11 chemosensitivity in patients with colorectal cancer. *Surg Today.* 2011 Sep;41(9):1196-9. Epub 2011 Aug 26.

Kelleher SL, Lopez V, Lönnerdal B, Dufner-Beattie J, Andrews GK. Zip3 (Slc39a3) functions in zinc reuptake from the alveolar lumen in lactating mammary gland. *Am J Physiol Regul Integr Comp Physiol.* 2009 Jul; 297(1):R194-201. Epub 2009 May 20.

Kosaka N, Ogawa M, Longmire MR, Choyke PL, Kobayashi H. Multi-targeted multi-color in vivo optical imaging in a model of disseminated peritoneal ovarian cancer. *J Biomed Opt.* 2009 Jan-Feb; 14(1):014023.

Kunimoto T, Nitta K, Tanaka T, Uehara N, Baba H, Takeuchi M, Yokokura T, Sawada S, Miyasaka T, Mutai M. Antitumor activity of 7-ethyl-10-[4-(1-piperidino)-1-piperidino]carbonyloxy-camptothec in, a novel water-soluble derivative of camptothecin, against murine tumors. *Cancer Res.* 1987 Nov 15; 47(22):5944-7.

Lemasters JJ, Chacon E, Ohata H, Harper IS, Nieminen AL, Tesfai SA, Herman B. Measurement of electrical potential, pH, and free calcium ion concentration in mitochondria of living cells by laser scanning confocal microscopy. *Methods Enzymol.* 1995; 260:428-44.

Mathijssen RH, van Alphen RJ, Verweij J, Loos WJ, Nooter K, Stoter G, Sparreboom A. Clinical pharmacokinetics and metabolism of irinotecan (CPT-11). *Clin Cancer Res*. 2001 Aug; 7(8):2182-94. Review.

McMullen, J. Improving the Contrast Of Two-Photon Microscopy And The Application Of Fluorescence Methods To The Detection Of Tuberculosis. Cornell University PhD thesis. 2010.

Medina, D. The mammary gland: a unique organ for the study of development and tumorigenesis. *JMBNFU*. 1996; 1, 5-19.

Muggia FM, Creaven PJ, Hansen HH, Cohen MH, Selawry OS. Phase I clinical trial of weekly and daily treatment with camptothecin (NSC-100880): correlation with preclinical studies. *Cancer Chemother Rep.* 1972 Aug; 56(4):515-21.

Nitta K, Yokokura T, Sawada S, Kunimoto T, Tanaka T, Uehara N, Baba H, Takeuchi M, Miyasaka T, Mutai M. Antitumor activity of new derivatives of camptothecin. *Gan To Kagaku Ryoho*. 1987 Mar; 14(3 Pt 2):850-7. Japanese.

Ohno R, Okada K, Masaoka T, Kuramoto A, Arima T, Yoshida Y, Ariyoshi H, Ichimaru M, Sakai Y, Oguro M, et al. An early phase II study of CPT-11: a new derivative of camptothecin, for the treatment of leukemia and lymphoma. *J Clin Oncol.* 1990 Nov; 8(11):1907-12.

Rillema, J. Development of the mammary gland and lactation. *TEM*. 1994. 5, 149-153.

Sano K, Yoshikawa M, Hayasaka S, Satake K, Ikegami Y, Yoshida H, Ishikawa T, Sawada S, Tanabe S. Simple non-ion-paired high-performance liquid chromatographic method for simultaneous quantitation of carboxylate and lactone forms of 14 new camptothecin derivatives. *J Chromatogr B Analyt Technol Biomed Life Sci.* 2003 Sep 25; 795(1):25-34.

Sapino A, Macri L, Gugliotta P, Bussolati G. Evaluation of proliferating cell types in human and mouse mammary gland by a double immunostaining procedure. *Acta Histochem Suppl.* 1990; 40:81-4.

Shimada Y, Yoshino M, Wakui A, Nakao I, Futatsuki K, Sakata Y, Kambe M, Taguchi T, Ogawa N. Phase II study of CPT-11, a new camptothecin derivative, in metastatic colorectal cancer. CPT-11 Gastrointestinal Cancer Study Group. *J Clin Oncol.* 1993 May; 11(5):909-13.

Sparreboom A, de Bruijn P, de Jonge MJ, Loos WJ, Stoter G, Verweij J, Nooter K. Liquid chromatographic determination of irinotecan and three major metabolites in human plasma, urine and feces. *J Chromatogr B Biomed Sci Appl.* 1998 Aug 7; 712(1-2):225-35.

Wall, M. E., M. C. Wani, C. E. Cook, K. H. Palmer, A. T. McPhail and G. A. Sim, "Plant antitumor agents. 1. The isolation and structure of camptothecin, a novel alkaloidal leukemia and tumor inhibitor from *Camptotheca acuminata*." *Journal of the American Chemical Society.* 1966 88: 3888-3890.

Wall ME, Wani MC, Ronman PE, Lindley JT. Plant antitumor agents. 18. Synthesis and biological activity of camptothecin analogues. *J Med Chem.* 1980 May; 23(5):554-60.

Williams RM, Zipfel WR, Webb WW. Multiphoton microscopy in biological research. *Curr Opin Chem Biol.* 2001 Oct; 5(5):603-8. Review.

Williams RM, Flesken-Nikitin A, Ellenson LH, Connolly DC, Hamilton TC, Nikitin AY, Zipfel WR. Strategies for high-resolution imaging of epithelial ovarian cancer by laparoscopic nonlinear microscopy. *Transl Oncol.* 2010 Jun 1; 3(3):181-94.

Zipfel WR, Williams RM, Christie R, Nikitin AY, Hyman BT, Webb WW. Live tissue intrinsic emission microscopy using multiphoton-excited native fluorescence and second harmonic generation. *Proc Natl Acad Sci* U S A. 2003 Jun 10; 100(12):7075-80.

Zhang H, Barceló JM, Lee B, Kohlhagen G, Zimonjic DB, Popescu NC, Pommier Y. Human mitochondrial topoisomerase I. *Proc Natl Acad Sci* U S A. 2001 Sep 11; 98(19):10608-13.

Zivanovic O, Carter J, Kauff ND, Barakat RR. A review of the challenges faced in the conservative treatment of young women with endometrial carcinoma and risk of ovarian cancer. *Gynecol Oncol.* 2009 Dec; 115(3):504-9. Epub 2009 Sep 15. Review.

CHAPTER 5

Future Directions

The studies previously described were conducted to understand the underlying mechanisms of drug action in order to facilitate drug design for neurological disorders, drug addiction, and to facilitate the use of chemotherapy drugs as tumor contrast agents. In our glutamate receptor studies using knowing the relative contributions of each thermodynamic parameter in ligand binding is of practical significance. These experiments may provide fundamental knowledge necessary for structure-based drug design when we compare full agonist, antagonist and partial agonist thermodynamic binding parameters. While cocaine binds to several targets in the central nervous system, one of its major metabolites, benzoylecgonine, inhibits the neuronal nAChR subtype associated with nicotine addiction to a greater extent than cocaine. These studies highlight the importance of further investigating addictive drug metabolites in an effort to develop greatly needed pharmacological interventions. Our irinotecan studies were motivated but the drug's potential use as a tumor contrast agent. In the process we discovered that we may be able to image drug localization and learn more about the drug's pharmacokinetics *in vivo*. Lastly, these studies highlight the importance of investigating pharmacological interactions through multidisciplinary approaches—from molecular interactions to live animal studies.

5.1. Continuing studies of GluA2-s1s2.

Identifying thermodynamic driving forces of ligand binding can guide

us towards drug affinity optimization, and an understanding of how the energy of ligand binding translates to ion channel opening. Due to solubility difficulties with GluA2-s1s2 we were not successful in stabilizing the unbound state of the soluble ligand-binding domain to perform direct titration experiments. In addition to experimenting with buffer conditions, it would be very interesting to evaluate thermodynamic binding parameters of antagonists and partial agonists to GluA2-s1s2 dimers in solution since glutamate receptors exist as dimers *in vivo* (Armstrong and Gouaux, 2000). GluA2-s1s2 can sample a spectrum of lobe conformations which may represent several energetically favorable states of the receptor, and studies in which these states can be isolated may lead to a better understanding of the contribution of lobe closure stability to ion channel opening. In one such study, Ahmed *et al.* (2011) cleverly stabilized the closed lobe conformation to investigate the existence of the fully closed state when bound to partial agonists.

We did not have the opportunity to fully characterize the change in heat capacity upon ligand binding to GluA2-s1s2. Heat capacity changes are directly proportional to the amount of water-accessible surface area (Makhatadze *et al.* 1995; Makhatadze and Privalov 1995; Murphy and Freire 1992; Murphy and Gill 1991; Spolar *et al.* 1992) and can provide information about the exposure of polar and non-polar groups to solvent that were buried in the glutamate-bound state compared to antagonist and partial agonist-bound states. In addition to characterizing heat capacity

change, characterizing the strength of hydrogen bonds, electrostatic interactions, and non-covalent interactions between key residues in the binding pocket and the 5-substituted willardiines may help delineate the role of γ-substituents in partial agonist binding, as well as the contributions from these interactions to thermodynamic measurements of GluA2-s1s2.

Several thermodynamic parameters have yet to be resolved in antagonist and partial agonist binding to GluA2-s1s2. Individual contributions from the enthalpies of binding (ΔH^{bind}), enthalpies due to conformational changes (ΔH^{conf}), and enthalpies of ionization (ΔH^{ion}) will help us identify how solvent interactions contribute to antagonist and partial agonist binding relative to glutamate. Similarly, further characterization of the conformational (ΔS^{conf}), roto-translational ($\Delta S^{r,tr}$), and desolvation entropies (ΔS^{sol}) is needed and could be obtained through molecular dynamics studies. This would allow us to examine the relative contributions of each type of entropy to our net values. Knowing the relative contributions of each thermodynamic parameter is of practical significance since it may provide the fundamental knowledge necessary for structure-based drug design.

5.2. Future benzoylecgonine studies on neuronal nAChRs.

Nicotinic receptors are differentially expressed within the brain allowing us to investigate regional-specific behavior by characterizing the various subunit (subtype) combinations. The α4β2 subtype is widely

expressed in the brain and plays a critical role in nicotine addiction (Flores *et al.,* 1992). While several studies have been dedicated to rapid detection of benzoylecgonine (Munoz *et al.*, 2011; Teller *et al.*, 2008; Paula *et al.*, 2004) its biological target is still unknown. Based on our studies, benzoylecgonine is a more potent inhibitor of the neuronal α4β2 subtype more than cocaine, illustrating the importance of continued study.

We measured the effect of a single concentration of benzoylecgonine and a concentration-dependence curve would be the next step in characterizing its inhibition of α4β2. It is not evident whether benzoylecgonine acts as a competitive or non-competitive antagonist, and whether it inhibits other heteromeric receptor subtypes, or perhaps activates homomeric nicotinic receptors similar to cocaine methiodide (Francis *et al*, 2000). Since cocaine action is associated with inhibition of dopamine, serotonin and norepinephrine reuptake by blocking catecholamine transporters (Ritz *et al.*, 1987; Carroll *et al.,* 1999; Filip *et al.*, 2010; Ganapathy, 2011;), it may also be of interest to investigate the action of benzoylecgonine on catecholamine transporters.

5. 3. Future *in vitro* Irinotecan experiments.

Chemotherapeutic drugs exhibiting intrinsic fluorescence may prove very useful in studying *in vivo* drug metabolism and cellular localization of metabolites. Irinotecan only exhibited a two-fold increase in intensity in *in vivo* tumors unlike the four-fold increase in intensity seen in uterine horn and intestinal tumors. It may be of interest to evaluate mammary

carcinoma-specific drugs exhibiting intrinsic fluorescence. There are currently 43 chemotherapy drugs on the market to treat breast cancer and despite this, breast cancer associated deaths each year number in the tens of thousands (~40,000 in 2011) further highlighting the need to study *in vivo* metabolism of these drugs.

While we investigated the effects of Irinotecan on mammary gland controls, it may be advantageous to determine the effects of Irinotecan on a mammary epithelial cell line *in vitro.* Identifying mammary epithelial cells *in vivo* can be challenging because of the heterogeneity of mammary gland tissue. Further in vitro studies may also help us determine whether Irinotecan is binding to mitochondrial TopoI (Topoisomerase I). It may also be of interest to determine the binding affinities of Irinotecan and SN-38 to nuclear Topoisomerase I versus mitochondrial Topisomerase I. Lastly, Irinotecan has shown a wide spectrum of effectiveness in patients and some patients' tumors develop resistance to the drug. Further study of Irinotecan's metabolites may provide more information about how Irinotecan is differentially metabolized by cancer patients leading to more effective and personalized treatment modalities.

REFERENCES

Ahmed AH, Wang S, Chuang HH, Oswald RE. Mechanism of AMPA receptor activation by partial agonists: disulfide trapping of closed lobe conformations. *J Biol Chem.* 2011 Oct 7; 286 (40):35257-66.

Armstrong N, and Gouaux E. Mechanisms for activation and antagonism of an AMPA-sensitive glutamate receptor: crystal structures of the GluR2 ligand binding core. *Neuron.* 2000 Oct;28 (1):165-81.

Carroll FI, Howell LL, Kuhar MJ. Pharmacotherapies for treatment of cocaine abuse: preclinical aspects. J Med Chem. 1999 Jul 29;42(15):2721-36. Review. No abstract available.

Filip M, Alenina N, Bader M, Przegaliński E. Behavioral evidence for the significance of serotoninergic (5-HT) receptors in cocaine addiction. Addict Biol. 2010 Jul;15(3):227-49. Epub 2010 Apr 29. Review.

Flores CM, Rogers SW, Pabreza LA, Wolfe BB, Kellar KJ. A subtype of nicotinic cholinergic receptor in rat brain is composed of alpha 4 and beta 2 subunits and is up-regulated by chronic nicotine treatment. *Mol Pharmacol.* 1992 Jan;41(1):31-7.

Francis MM, Vazquez RW, Papke RL, Oswald RE. Subtype-selective inhibition of neuronal nicotinic acetylcholine receptors by cocaine is determined by the alpha4 and beta4 subunits. Mol Pharmacol. 2000 Jul;58(1):109-19.

Ganapathy V. Drugs of abuse and human placenta. Life Sci. 2011 May 23;88(21-22):926-30. doi: 10.1016/j.lfs.2010.09.015. Epub 2010 Oct 16. Review.

Makhatadze GI, Clore GM, Gronenborn AM. Solvent isotope effect and protein stability. Nat Struct Biol. 1995 Oct; 2(10):852-5.

Makhatadze GI, Privalov PL. Energetics of protein structure. *Adv Protein Chem.* 1995;47:307-425. Review.

Munoz EM, Lorenzo-Abalde S, González-Fernández A, Quintela O, Lopez-Rivadulla M, Riguera R. Direct surface plasmon resonance immunosensor for in situ detection of benzoylecgonine, the major cocaine metabolite. *Biosens Bioelectron.* 2011 Jul 15;26(11):4423-8. Epub 2011 May 6.

Murphy KP, Freire E. Thermodynamics of structural stability and cooperative folding behavior in proteins. *Adv Protein Chem.* 1992; 43:313-61. Review.

Murphy KP, Gill SJ. Solid model compounds and the thermodynamics of protein unfolding. *J Mol Biol*. 1991 Dec 5;222(3):699-709.

Loladze VV, Ermolenko DN, and George I. Makhatadze GI. Heat capacity changes upon burial of polar and nonpolar groups in proteins. *Protein Sci.* 2001 July; 10(7): 1343–1352.

Paula S, Tabet MR, Farr CD, Norman AB, Ball WJ Jr. Three-dimensional quantitative structure-activity relationship modeling of cocaine binding by a novel human monoclonal antibody. J Med Chem. 2004 Jan 1;47(1):133-42.

Perozzo R, Folkers G, and Scapozza, L. Thermodynamics of Protein–Ligand Interactions: History, Presence, and Future Aspects. *J. Receptors and Signal Trans.*Vol. 24, Nos. 1 & 2, pp. 1–52, 2004.

Ritz MC, Lamb RJ, Goldberg SR, Kuhar MJ. Cocaine receptors on dopamine transporters are related to self-administration of cocaine. *Science*. 1987 Sep 4;237(4819):1219-23.

Spolar RS, Livingstone JR, Record MT Jr. Use of liquid hydrocarbon and amide transfer data to estimate contributions to thermodynamic functions of protein folding from the removal of nonpolar and polar surface from water. *Biochemistry*. 1992 Apr 28; 31(16):3947-55.

Teller C, Halámek J, Zeravík J, Stöcklein WF, Scheller FW. Development of a bifunctional sensor using haptenized acetylcholinesterase and application for the detection of cocaine and organophosphates. Biosens Bioelectron. 2008 Sep 15;24(1):111-7. Epub 2008 Apr 1.